Aus dem Bereich der Molekularen Zellbiologie
Theoretische Medizin und Biowissenschaften
der Medizinischen Fakultät
der Universität des Saarlandes, Homburg/Saar

Calcium Signaling in Red Blood Cells

Dissertation zur Erlangung des Grades eines
Doktors der Naturwissenschaften

der Medizinischen Fakultät
der UNIVERSITÄT DES SAARLANDES
2013

vorgelegt von: Jue Wang
geb. am: 10.10.1981 in Zhuzhou, Hunan, China

Erklärung gemäß § 7 Abs. 1 Nr. 4

Ich erkläre hiermit an Eides statt, dass ich die vorliegende Arbeit ohne unzulässige HilfeDritter und ohne Benutzung anderer als der angegebenen Hilfsmittel angefertigt habe. Die ausanderen Quellen direkt oder indirekt übernommenen Daten und Konzepte sind unter Angabeder Quelle gekennzeichnet.

Weitere Personen waren an der inhaltlich-materiellen Erstellung der vorliegenden Arbeit nicht beteiligt. Insbesondere habe ich nicht die entgeltliche Hilfe von Vermittlungs- bzw. Beratungsdiensten (Promotionsberater/innen oder anderer Personen) in Anspruch genommen. Außer den Angegebenen hat niemand von mir unmittelbar oder mittelbar geldwerte Leistungen für Arbeiten erhalten, die im Zusammenhang mit dem Inhalt der vorgelegten Dissertation stehen.

Die Arbeit wurde bisher weder im Inland noch im Ausland in gleicher oder ähnlicher Form ineinem anderen Verfahren zur Erlangung des Doktorgrades einer anderen Prüfungsbehörde vorgelegt.

Ich versichere an Eides statt, dass ich nach bestem Wissen die Wahrheit gesagt und nichts verschwiegen habe.

Vor Aufnahme der vorstehenden Versicherung an Eides Statt wurde ich über die Bedeutungeiner eidesstattlichen Versicherung und die strafrechtlichen Folgen einer unrichtigen oderunvollständigen eidesstattlichen Versicherung belehrt.

Homburg, im Juni 2013

Jue Wang

Contents

Contents iii
Zusammenfassung vii
Abstract viii
List of Figures ix
List of Tables xi
List of Abbreviations xii

1. Introduction 1
1.1 Red blood cells (RBCs) 2
1.1.1 RBCs membrane lipids 3
1.1.2 RBCs channels 4
1.1.2.1 Voltage activated non-selective cation channel 8
1.1.2.2 Receptor activated non-selective cation channel 9
1.1.2.3 Gardos channel 10
1.1.2.4 Transient receptor potential channel C6 (TRPC6) 12
1.1.2.5 *N*-methyl-D-aspartate (NMDA) channel 12
1.1.2.6 Aquaporin (water channel) 13
1.1.3 RBCs cytoskeletal proteins 14
1.1.4 Ca^{2+} in RBCs: effects of elevated $[Ca^{2+}]_i$ 14
1.1.4.1 On Red Cell Homeostasis 14
1.1.4.2 Ca^{2+} and Red Cell Survival 15
1.2 Lysophosphatidic acid (LPA) 18
1.3 TRP channels 18
1.3.1 The transient receptor potential channel (TRP) family 18
1.3.2 Discovery of the “canonical” TRPCs: the Drosophila transient receptor potential channel 19
1.3.3 Properties of TRPC channels 19
1.3.4 TRPC6 regulation 20
1.4 Aggregation of RBCs 21
1.4.1 Active role of RBCs in aggregation 21

1.4.2 Effects of proteins in the blood plasma for RBCs aggregation 23
1.5 Sickle cell disease 24
2. Materials and methods 26
2.1 Materials 26
2.1.1 Chemicals and reagents 26
2.1.2 Main solutions used 28
2.1.3 Fluo-4/AM 28
2.2 Imaging devices 29
2.2.1 Video-imaging Set-up 29
2.2.2 Leica TSC SP5 confocal microscope 30
2.3 Methods 31
2.3.1 Red blood cell preparation 31
2.3.2 Intracellular Ca^{2+} measurements 36
2.3.3 Induction of reticulocytosis 36
2.3.4 Flow cytometry to measure intracellular Ca^{2+} 37
2.3.5 PKH26 labeling of RBCs 37
2.3.6 Immunoblotting and gel staining 40
2.3.7 Immunostaining 40
2.4 Data analysis 41
2.4.1 Image analysis 41
2.4.2 Single trace of Ca^{2+} influx analysis 41
2.4.3 Statistical Analysis 42
3. Results 43
3.1 Single cell analysis 43
3.1.1 LPA induces Ca^{2+} influx into human RBCs 43
3.1.2 Ca^{2+} influx induced by LPA is not homogenous among individual RBCs 45
3.1.3 Different parameters to characterize and analyze LPA-induced Ca^{2+} influx 47
3.1.4 Definition of “Responding cells” and analysis 49
3.1.5 Different RBCs cell age led to inhomogeneous Ca^{2+} influx 51

3.1.5.1 Percoll gradient centrifugation to separate young from old RBCs 51
3.1.5.2 Induction of reticulocytosis by phenylhydrazine injection 52
3.1.5.3 Retro-orbital repetitive bleeding 55
3.1.5.4 LPA induced Ca^{2+}-signals in reticulocytes from mice with reticulocytosis 57
3.1.5.5 Ca^{2+} influx in old RBCs 60
3.2 The signaling pathway from LPA to Ca^{2+} in RBCs 63
3.2.1 Characterization of TRPC6 knock out mice 63
3.2.2 TRPC6 contributes to LPA induced Ca^{2+} influx 64
3.2.3 Expression of LPA Receptor subtypes in RBCs 67
3.2.4 LPA receptor activation is through G_i protein both in human and mouse RBCs 69
3.2.5 PI_3K is involved in the LPA signal pathway in human and mouse RBCs 71
3.2.6 PKCα is involved in the LPA signal pathway in human and mouse RBCs 72
3.2.7 Wortmannin and Gö6976 in combination can fully inhibit LPA-evoked Ca^{2+} influx in human and mouse RBCs 75
3.2.8 MEK is involved in LPA signal pathway in human and mouse RBCs 77
3.2.9 Cav2.1 in LPA induced Ca^{2+} influx 79
3.3 LPA in sickle cell disease 81
3.3.1 Ca^{2+} in human sickle RBCs 81
3.3.2 LPA receptors in sickle cells 83
3.3.3 PTX inhibits LPA-induced Ca^{2+} influx in healthy RBCs and sickle cells 85
3.3.4 PI_3K-MAPK-Cav2.1 branch of LPA-induced signal pathway in healthy RBCs and sickle cells 86
3.3.5 Gö6976 inhibits LPA-induced Ca^{2+} influx in healthy RBCs and sickle cells 89

3.3.6 Gö6976 in combination with Wortmannin fully inhibit LPA-induced Ca^{2+} influx in healthy RBCs and sickle cells 90

4. Discussion 92

4.1 Single cell analysis discussion 93

4.1.1 Fluorescence indicator in RBCs 93

4.1.2 Ca^{2+} concentrations and changes are not homogenous amongst individual RBCs 94

4.1.3 Analysis protocols 96

4.1.4 Fe^{2+} and folate deficiency leads to abnormal Ca^{2+} influx in RBCs during repetitive bleeding induced reticulocytosis 100

4.1.5 The influence of cell age on LPA-induced Ca^{2+}-influx 101

4.1.6 Ca^{2+} balance in RBCs 104

4.2 Signal pathway induced by LPA in RBCs 106

4.2.1 Scheme showing the involving signal transduction pathway 106

4.2.2 Ca^{2+} free pretreatment induced Ca^{2+} influx 107

4.2.3 ω-agatoxin-TK could not fully inhibit PMA/LPA induced Ca^{2+} influx 108

4.3 Ca^{2+} homeostasis and LPA in sickle cell disease 111

4.4 Summary and perspective 112

5. References 114

6. Publications 135

7. Acknowledgment 137

8. Curriculum Vitae 139

9. Attachments 141

Zusammenfassung

Lysophosphatsäure (LPA) bewirkt einen signifikanten Anstieg der intrazellulären Kalziumkonzentration in Humanerythrozyten. Frühere Untersuchungen ergaben bereits Hinweise, dass der Kalziumeinstrom eher durch Kalziumkanäle als durch ein unspezifisches Kalzium-Leck zustande kommt. Die molekulare Identität der Kanäle konnte jedoch noch nicht geklärt werden. In dieser Arbeit wurde der durch LPA hervorgerufene Kalzium-Einstrom mittels Kalzium-Imaging untersucht. Auf Basis von Einzelzellen wurden pharmakologische Experimente zur Identifikation des zugehörigen Signalweges durchgeführt. Ich fand, dass der LPA induzierte Kalziumeinstrom zwischen individuellen Erythrozyten einer Population stark variiert. Eine solche Inhomogenität kann man mit traditionellen Untersuchungsmethoden (z.B. Flux Messungen) nicht detektieren. Daher entwickelte ich einen Analyseweg, der auf Einzelzellen beruht. Mit dieser Methode bestimmte ich die halb-maximale Wirkungskonzentration des LPA bezüglich der Kalziumzunahme in Erythrozyten auf etwa 5 µM. Desweiteren untersuchte ich die Beziehung zwischen dem LPA-Signalweg und TRPC6 Kanälen, welche in Erythrozyten nachgewiesen wurden. Der LPA induzierte Kalziumeinstrom war in TRPC6 "knock-out" Mäusen nicht vollständig blockiert, was auf die Koexistenz von wenigstens zwei Signalwegen hindeutet. Ich habe einen Satz pharmakologischer Experimente durchgeführt, um den LPA Signalweg sowohl in Erythrozyten gesunder Spender als auch in Erythrozyten von Sichelzellanämie Patienten zu untersuchen. In humanen Sichelzellen war die Expressiion des LPA Rezeptor Subtyp 4 (LPAR4) erhöht, aber der LPA induzierte Kalziumeinstrom folgte dem gleichen Signalweg wie in gesunden Humanerythrozyten. Diese Untersuchung erlaubte neue Einblicke in LPA induziertes Kalziumsignale sowohl in gesunden als auch in Sichelzell-Erythrozyten. Der gefundene Signalweg könnte sich im Kontext der Erythrozyten-assoziierten Blutgerinnung unter pathophysiologischen Bedingungen als bedeutend erweisen.

Abstract

Lysophosphatidic acid (LPA) induces a significant increase in the intracellular Ca^{2+} concentration in human red blood cells(RBCs). Previous experiments provided evidence that Ca^{2+} influx is mediated by Ca^{2+} channels rather than by a nonspecific Ca^{2+} leak. However, the molecular identity of the channels has not been resolved. In this thesis, Ca^{2+} imaging was used to investigate the LPA induced Ca^{2+} influx. Pharmacological experiments on single cells were performed to identify the related signal pathway. I found that in RBCs, Ca^{2+} influx induced by LPA varies betweenindividual cells of a population. Such an inhomogeneity cannot be revealed from traditional RBCs research methods (e.g., flux measurements). Thus, I developed a single cell based analysis procedure of RBCs. With this method, I determined the IC_{50} of LPA for Ca^{2+} increase in RBCs to be approximately 5 μM. Furthermore I probed the relationship between LPA induced signaling and TRPC6, which has been shown to be present in RBCs. LPA induced Ca^{2+} influx was not fully inhibited in TRPC6 knock out ($TRPC6^{(-/-)}$) mice, suggesting the coexistence of at least two signal pathways. I performed a set of pharmacological experiments to identify LPA signaling pathways both in RBCs from healthy donors and sickle cell disease patients. In human sickle RBCs, LPA receptor subtype 4 (LPAR4) was found to present an increased expression, but LPA-induced Ca^{2+} influx followed the same signal pathway as in human healthy RBCs. This study revealed novel insights into LPA induced Ca^{2+} signaling both in healthy and sickle RBCs. The identified signaling pathways might be important in the context of RBCs associated blood clotting under pathophysiological conditions.

List of Figures

Figure 1: TRPC channels structure. 20
Figure 2: Schematic cascades proposed for the aggregation of RBCs inactivated conditions. 23
Figure 3: Molecular structure and fluorescence emission spectra of Fluo-4 and Fluo-3. 29
Figure 4: The basic design of Imago-imaging setups. 30
Figure 5: Blood sample collection from mouse cheek. 33
Figure 6: Only inhibitors could not induce Ca^{2+} influx both in human and mouse RBCs 35
Figure 7: PKH26 background correction. 39
Figure 8: LPA induced Ca^{2+} influx in human RBCs. 44
Figure 9: LPA induced Ca^{2+} responses are heterogeneous amongst individual RBCs. 46
Figure 10: Characterization of single cell response. 48
Figure 11: Parameters of responding cells in LPA induced Ca^{2+} influx. 50
Figure 12: Separation of RBCs by Percoll gradient ultracentrifugation and SDS-Page of ghost membrane proteins of the different fractions. 52
Figure 13: Phenylhydrazine induced reticulocytosis. 54
Figure 14: Induction of reticulocytosis and staining of reticulocytes with New Methylene Blue. 56
Figure 15A: Reticulocytes shows lower sensitivity to LPA. 58
Figure 16: Response of old RBCs to LPA stimulation. 62
Figure 17: TRPC6 expression in mouse RBCs. 64
Figure 18: LPA and PGE_2 in wild type and $TRPC6^{(-/-)}$ mice and human RBCs… 66
Figure 19: LPA receptors in human RBCs. 68
Figure 20: LPA receptors activation through G_i protein both in human and mouse RBCs. 70
Figure 21: PI_3K is involved in LPA-induced Ca^{2+} influx. 72
Figure 22: PKCα is involved in LPA induced Ca^{2+} influx. 74
Figure 23: In combination with Wortmannin and Gö6976 could fully inhibit

Ca^{2+} influx induced by LPA in human and mouse RBCs. 76
Figure 24: MEK is involved in the LPA signal pathway in human and mouse RBCs. 78
Figure 25: Cav2.1 is involved in LPA induced Ca^{2+} influx. 81
Figure 26: Ca^{2+} distribution in sickle cells before stimulation. 82
Figure 27A: LPA receptor distributions and LPA induced Ca^{2+} influx in sickle cells. 84
Figure 28: PTX inhibited LPA-induced Ca^{2+} influx in human healthy RBCs and sickle RBCs. 86
Figure 29: PI_3K branch in LPA-induced Ca^{2+} influx in normal RBCs and sickle cells. 89
Figure 30: Gö6976 inhibits LPA-induced Ca^{2+} influx in healthy RBCs and sickle cells. 90
Figure 31: Gö6976 in combination with Wortmannin fully inhibited LPA-induced Ca^{2+} influx in normal RBCs and sickle cells. 91
Figure 32: Absorption spectrum of hemoglobin and autofluoresence excited by UV irradiation. 94
Figure 33: Protocols and handling of LPA-induced Ca^{2+} influx. 98
Figure 34: 3-steps protocol and handling of LPA-induced Ca^{2+} influx..... 99
Figure 35: $Fe^{2+}$and folate deficiency leads to abnormal Ca^{2+} increase..... 101
Figure 36: Schematic showing the involving signal transduction pathway... 107
Figure 37: Ca^{2+} free pretreatment induced Ca^{2+} influx in human RBCs..... 108
Figure 38: 1 μM ω-agatoxin-TK can partly but not fully inhibit 3 μM PMA induced Ca^{2+} influx in human RBCs. 110

List of Tables

Table 1: Molecular characteristic of major membrane proteins in human RBCs. 6

List of Abbreviations

Abbreviations

AA	Amino acid
ADP	Adenosine diphosphate
AFM	Atomic force microscope
ANOVA	Analysis of variance
APLT	Amino phospholipid translocase
APS	Ammonium persulfate
ATP	Adenosine triphosphate
BLAST	Basic local alignment search tool
CCD	Charge coupled device
CD	Cluster of differentiation
cDNA	Complementary deoxyribonucleic acid
DMSO	Dimethyl sulfoxide
EC	Endothelial cell
EDTA	Ethylenediaminetetraacetic acid
EGTA	Ethylene glycol tetraacetic acid
FACS	Fluorescence-activated cell sorter
FITC	Fluorescein isothiocyanate
G3PD	Glyceraldehyde-3-phosphate dedydrogenase
G6PD	Glucose-6-phosphate dehydrogenase
HEPES	4-(2-Hydroxyethyl)piperazine-1-ethanesulfonic acid, N-(2-Hydroxyethyl)piperazine-N′-(2-ethanesulfonic acid)

HUVEC	Human umbilical vein endothelial cells
IgG	Immunoglobulin G
Kd	Dissociation constant
kDa	Atomic mass unit (1000 dalton)
LPA	Lysophosphatidic acid
LSCM	Laser scanning confocal microscope
NADH	Nicotinamide adenine dinucleotide
NADPH	Nicotinamide adenine dinucleotide phosphate
NSVDC	Non selective voltage dependent cation channel
PE	Phosphatidylethanolamine
PGE_2	Prostaglandin E_2
PI	Phosphatidylinositol
PKC	Protein kinase C
PLSCR	Phospholipid scramblase
PMA	Phorbol 12-myristate 13-acetate
PMSF	Phenylmethanesulphonylfluoride
PS	Phosphatidylserine
RBC	Red blood cell
S.D.	Standard deviation
SDS	Sodium dodecylsulfate
SDS-PAGE	Sodium dodecyl sulfate polyacrylamide gel electrophoresis
SM	Sphingomyelin
SPM	Scanning probe microscope
TSP	Thrombospondin
AP	Action Potential

1. Introduction

Calcium (Ca^{2+}) is crucial in the physiology and biochemistry of the cell. It plays a very important role in signal transduction, because it acts as a second messenger. Many enzymes require Ca^{2+} ions as a cofactor, such as the blood-clotting cascade.

In the human body, Ca^{2+} is taken from food, stored in the bones, and then transported as dissolved ions or bound to proteins such as serum albumin. Intracellular Ca^{2+} levels are tightly regulated. Ca^{2+} stored in intracellular organelles, including mitochondria and endoplasmic reticulum, which can accumulate and release Ca^{2+} ions. However, for RBCs, which lack organelles and a nucleus, many questions about Ca^{2+} related functions are still not fully understood. Examples are the role of Ca^{2+} in blood clot formation, RBCs aging and their Ca^{2+} hemostasis in general. The mechanisms of these processes are still not resolved because the involvement of many factors generates a complex signaling system. This field is the focus of my research work.

Using fluorescent dyes, fluorescence microscopy, flow cytometry and further techniques, the main work of this thesis was focused on the relation between lysophosphatidic acid (LPA) induced intracellular Ca^{2+} increase and transient receptor potential channels C6 (TRPC6) activation in RBCs. Aspects related to RBCs aging and the interactions between Ca^{2+} and blood clot formation have also been included. These experiments clarified the relationship between LPA-induced Ca^{2+} influx and TRPC6 in RBCs. Additionally, LPAR4 was found to present an increased expression in human sickle RBCs. Furthermore, I also found LPA-induced Ca^{2+} influx in human sickle RBCs followed the same signal pathway as in human healthy RBCs. Thus, this dissertation comprises three parts: single cell analysis of Ca^{2+} influx in RBCs,

the signal pathway of LPA induced Ca^{2+} influx and LPA signal pathway in sickle RBCs.

1.1 Red blood cells (RBCs)

RBCs, also known as red cells, red blood corpuscles (an archaic term), haematids or erythrocytes (from Greek *erythros* for "red" and *cyte* translated as "cell" in modern usage), are the most abundant type of blood cell. Through a process named erythropoiesis, human erythroid cells are differentiated from stem cells in the bone marrow to become mature RBCs. This process takes about 7 days. The lifespan of matured human RBCs in the circulation is about 100 – 120 days. Furthermore, RBCs are thought to be the vertebrate organism's principal means of delivering oxygen (O_2) to the body tissues and transport carbon dioxide via the blood flow through the circulation system back to the lung.

Due to the lack of organelles and nucleus, RBCs seem to be relative simple cells. However, on a closer look they turn out to be much more complicated cells. Although RBCs have been intensively studied for many years, many questions are still not fully understood. For example, are all RBCs similar in structure and function? How do RBCs get mature and become old? What is the function of Ca^{2+} in the ageing process or how does apoptosis-like effects develop in RBCs and what is the role of RBCs in blood clot formation? The mechanisms of these processes still need to be elucidated - many of the involved factors are associated to the cell membrane.

The human RBC membrane shows unique features, which allow RBCs to endure great reversible deformations while maintaining structural integrity during the 120 days life span in the circulation system. RBCs are highly elastic and highly sensitive to fluid stresses [1-3]. These amazing properties are based on a composite structure in which a plasma membrane comprises cholesterol and phospholipids. A 2-dimensional elastic network is anchored to

cytoskeletal proteins through binding sites on cytoplasmic domains of transmembrane proteins inserted into the lipid bilayer [4]. Further attachments of the cytoskeletal network to the lipid bilayer comprise direct interactions between several cytoskeletal proteins and anionic phospholipids [5, 6].

1.1.1 RBCsmembrane lipids

The human red blood cell membrane contains lipids (41%), proteins (52%), and carbohydrates (7%) [7, 8]. Membrane lipids can be divided into three classes: neutral lipids (25.2%), phospholipids (62.7%) and glycosphingolipids (12.1%) [9].

Here phospholipids consist of sphingomyelin (SM, 26%) and glycerophospholipids (74%). Sphingomyelin ismainly distributed in the outer leaflet of the membrane [9, 10]. Glycerophospholipids also consist of 3 main groups: phosphatidylcholine (PC, 30%), phosphatidylethanolamine (PE, 27%), and phosphatidylserine (PS, 13%), and several minor fractions, such as phosphatidic acid, lyso PC, mono and disphosphates phosphatidylinositol (PI) [11-13]. In brief, these four phospholipidis are asymmetrically distributed, but cholesterol is thought to be uniformly disposed in the 2 leaflets. SM and PC are found mainly in the outer of the membrane while PS and PE, are located predominantly in the inner leaflet [14].

The asymmetry of lipid distribution was thought to be generated and maintained by different types of phospholipid transporter proteins [15, 16]. Actually, the distribution is adjusted by (1) “Flippases”, an inward-directed pump, specific for PS and PE, also known as aminophospholipid translocase (APTL), which moves phospholipids from the outer to the inner leaflet; (2) “Floppases”, an outward-directed pump, which performs in the opposite direction when compared to flippase; and (3) “scramblases”, which move phospholipids bi-directionally down their concentration gradients in an energy independent manner, thus promoting unspecific bidirectional redistribution

across the bilayer. Several additional membrane proteins have been reported to exert these different lipid transport activities in human RBCs. For example, in recent studies, specific proteins, such as flotillins, stomatin, G-proteins, and β-adrenegic receptors [17, 18] are found to associate to the specific membrane areas that are enriched in cholesterol and sphingolipids.

Additionally, emerging evidence suggests that the increase of cytosolic Ca^{2+} may activate scramblase and floppase but inhibit the flippase, which results in the lipid asymmetry collapse. In this procedure, PS exposure on the outer surface of the cell is the most important change in the lipid distribution [19]. The localization of PS and phosphoinositides at the inner leaflet has very important functional implications. For example, in the spleen, macrophages recognize and phagocytize RBCs according to the PS they present on the outer surface [20-22]. Furthermore, the adhesion of normal RBCs to vascular endothelial cells could also be activated by PS exposure in sickle cell disease [23]. One explanation of the PS regulation function of the lipid bilayer is their interactions with the cytoskeletal proteins, spectrin, and protein 4.1R [24, 25].

According to Manno and co-workers, binding of spectrin to PS increases membrane stability [25] and An and co-workers [26] found that PIP_2 may modulate the linkage of the bilayer to the membrane skeleton through enhancing the binding of 4.1R to glycophorin C but decreasing its interaction with band 3 protein.

1.1.2 RBCs channels

In the lipid bilayer membrane of RBCs, more than 150 transmembrane proteins have been identified by proteomic methods [27]. Table 1 shows the molecular characteristics of major membrane proteins in human RBCs [28]. According to various criteria, they can be divided into different groups.

Based on the connection properties, membrane proteins can be divided into 3 groups: (1) cytoskeletal proteins (containing α and β spectrins, protein 4.1, actin), which are located beneath the lipid bilayer; (2) integral membrane proteins (including band 3 and glycophorins); and (3) anchoring proteins (containing ankyrin and protein 4.2), which connect the cytoskeletal network with integral proteins.

Based on their relationship to lipids, membrane proteins can be divided into 2 groups: (1) peripheral proteins, which are loosely associated only at one side, exterior or interior of the membrane, and which can be easily removed by high or low salt or high pH extraction; and (2) integral proteins, which are inserted tightly into or through the lipid bilayer by hydrophobic domains within their amino acid sequences, and can only be extracted by harsh reagents (chaotropic solvents or detergents).

Based on the function, membrane proteins can be divided into 3 groups: (1) transport proteins, including the Na^+-K^+-ATPase, Ca^{2+} ATPase, Na^+-K^+-$2Cl^-$ cotransporter, Na^+-Cl^- cotransporter, Na^+-K^+ cotransporter, K^+-Cl^- cotransporter, Gardos Channel, band 3 (anion transporter), aquaporin 1 (water transporter), Glut1 (glucose and L-dehydroascorbic acid transporter), Kidd antigen protein (urea transporter) and RhAG (gas transporter, probably of carbon dioxide); (2) adhesion proteins involved in interactions with other blood cells and endothelial cells, such as ICAM-4 which interacts with integrins and Lu, the laminin-binding protein [29-31] and (3) signaling receptors, such as LPA receptor [32], and NMDA receptor (in reticulocytes) [29, 31, 33, 34].

Most transmembrane proteins determine the different blood group antigens [22]. Expression of the membrane proteins is under the control of genetic and epigenetic modification of their genes, for example gene phosphorylation, acetylation and methylation. The functions of these membrane proteins are also mainly regulated by the state of phosphorylation, methylation,

glycosylation, or lipid modification (myristylation, palmitylation, or farnesylation) [28, 35].

Band on SDS gel	Protein	Molecular mass (kDa)		Copy number ($\times 10^3$/cell)	Relative amount of total ghost proteins (%)	Localization on membrane
		On SDS gel	Calculated			
1	α-Spectrin	240	280	242 ± 20	14	SKL
2	β-Spectrin	220	246	242 ± 20	13	SKL
2.1	Ankyrin	210	206	124 + 11	5	ANC
2.9	α-Adducin	103	81	30	1	SKL
	β-Adducin	97	80	30	1	SKL
3	Anion exchanger 1 (AE-1): band 3	90~100	102	1200	26	INT
4.1	Protein 4.1	80, 78	66	200	5	SKL
4.2	Protein 4.2	72	77	250	5	ANC
4.9	Dematin	48, 52	43, 46	140	1	SKL
	p55	55	53	80	1	SKL
5	β-Actin	43	42	500	6	SKL
	Tropomodulin	43	41	30		SKL
6	Glyceraldehyde-3-phosphate dehydrogenase(G3PD)	35	36	500	5	SKL
7	Stomatin	31	32		4	INT
	Tropomyosin	27, 29	28	70	1	SKL
8	Protein 8	23	22	200	1	SKL
Glycoproteins:						
PAS-1	Glycophorin A	36	14	1000	1.6	INT
PAS-2	Glycophorin C	32	14	150	0.1	INT
PAS-3	Glycophorin B	20	8	150	0.2	INT
	Glycophorin D	23	11	82	0.02	INT
	Glycophorin E	–	6	(not expressed)		

SDS-gel: sodium dodecylsulfate polyacrylamide gel electrophoresis,
SKL: skeletal protein, ANC: anchor protein, INT: integral protein.

Table 1: Molecular characteristic of major membrane proteins in human RBCs

(This table is a reprint from [28] with kind permission from Elsevier)

RBCs exchange molecules and ions with the surrounding environment, namely the blood plasma. This continuous transport of molecules and ions, such as glucose, Na^+ and Ca^{2+}, in and out of the cell requires their passage through the plasma membrane. In eukaryotic cells, additionally to the ion and molecule exchange through the plasma membrane, there are transport processes involving internal stores such asthe endoplasmic reticulum and mitochondria. For example, proteins, Ca^{2+} and ATP are exchanged through the plasma membrane in eukaryotic cells. For the exchange of ions, three important factors need tobe considered: (1) their relative concentrations, (2) their permeability and (3) the membrane potential. Considering aspect (1), molecules and ions build up a gradient facilitating diffusion from higher to lower concentration. However, active transport mechanisms, which require energy (usually in from of ATP), can also pump against concentration gradients. In aspect (2), the lipid bilayer is permeable to water and a few other small, uncharged molecules, such as oxygen (O_2) and carbon dioxide (CO_2). These diffuse freely into and out of the cell. In summary, lipid bilayers themselves are not permeable to: ions such as K^+, Na^+, Ca^{2+} (cations), Cl^-, HCO_3^- (anions), small hydrophilic molecules, e.g., glucose and macromolecules, e.g., proteins and RNA.

Ion pumps are transmembrane proteins that use energy in form of ATP, to move ions across the plasma membrane against their concentration gradient. In contrast, ion channels, which belong to the group of passive transporters, only allow the flow of ions down their electrochemical gradient. According to different transport modes, ion transporter in the RBCs membrane can be subdivided into channels (passive transport), carriers (passive or secondary active transport), pumps (active transport), and residual transport (also called “leak” transport). The latter one subsumises unknown transport mechanisms and in the past the portion of residual transport in RBCs decreased with the discovery of novel transport entities [36].

Cation channels are transporters, which can modulate the resting membrane potential in most cells, induce the action potential in excitable cells and are also responsible for the transmembrane transduction of many signaling cascades and ion exchange. In RBCs numerous cation channels exist, such as (1) the Gardos channel; (2) the voltage activated non-selective cation channel; (3) the receptor activated non-selective cation channel; (4) the Transient receptor potential channel C6 (TRPC6); and (5) the *N*-methyl-D-aspartate (NMDA) channel [37]. Different kinds of techniques are used to characterize these transporters including radioactive tracers (flux measurements), fluorescent dyes and electrophysiological approaches, such as the patch-clamp technique.

1.1.2.1 Voltage activated non-selective cation channel

Voltage activated non-selective cation channels are transmembrane proteins that are activated by changes of the electrical potential near the channel. They play a crucial role in electrically excitable cells, and also exist in RBCs [38-40]. Voltage activated cation channels, such as voltage-gated sodium channels and Ca^{2+} channels, are composed of several subunits, which form a central poreto allow ions to travel along their electrochemical gradients. Changes of the membrane potential are sensed by specific channel subdomains and transduced into conformational changes of the protein resulting in altered ion permeability. Such abehavior subsequently generates an electrical current [41, 42].

A property of RBCs now attributed to the voltage-activated non-selective cation channel was initially identified by Donlon and Rothstein [43] in their flux measurements in 1969. They found a three-phasic increase in the salt efflux from RBCs after a continuous decrease of the extracellular NaCl concentration. They already considered the contribution of a channel in this process. In 1989, Halperin and co-workers provided further evidence for the existence of a voltage-activated cation channel in RBCs. Below voltages of

+40 mV, the cell membrane was permeable for Na^+, K^+ and Ca^{2+} and this permeability could be inhibited by ruthenium red in flux measurements [44]. The membrane potential was adjusted by either changing the K^+ concentration gradient in the presence of valinomycin or by changing the concentration gradient of anion nitrate in the presence of 4,4‘-diisothiocyanostilbene-2,2‘-disulfonic acid (DIDS). The electrophysiological features of the non-selective cation channel were firstly identified by Christophersen and Bennekou in 1991 [45]. They reported that the channels open probability increased between -30mV and +30mV from 0 to 100%, and Bennekou further showed that the channel was acetylcholine sensitive [38]. Besides activation with acetylcholine, the voltage-activated non-selective cation channel could also be activated by clotrimazole and analogues, and inhibited by La^{3+}, ruthenium red, N-ethyl-maleimide, iodoacetamide, 2,4‘-dibromoacetophenone and bypH values down to 6.0 [39, 46, 47]. The electrophysiological characterization of the non-selective cation channel under physiological conditions has been investigated by Kaestner and co-workers in 2000 [48]. Additionally, the hysteretic behavior of the open probability also has been investigated by Bennekou and co-workers in 2004 [40]. Furthermore, there is also some evidence suggesting the presence of Cav2.1 in RBCs [49]. However, there are still open questions about the non-selective cation voltage activated channel in RBCs that need to be resolved.

1.1.2.2 Receptor activated non-selective cation channel

In RBCs, receptor activated non-selective cation channels open or close in response to binding of a small signaling molecule, the so-called "ligand". Some channels response to extracellular ligands, such as NMDA, LPA and PGE_2, and some to intracellular ligands, such as “second messengers" in RBCs, e.g. cyclic AMP (cAMP) and cyclic GMP (cGMP). In both cases, the ligand is not the substance that is transported when the channel opens.

In RBCs, the presence of receptor activated non-selective cation channels was first identified by flux measurements [50]. In the following decades, many substances were found to be able to open cation channel in RBCs. For example, lysophosphatidic acid (LPA) and prostaglandin E_2 (PGE_2) have been proven to induce Ca^{2+} influx in RBCs [32, 51].

There is also some evidence, suggesting that receptor gated channels can be activated by osmotic shock and oxidative stress [52, 53]. Ethylisopropylamiloride (EPMI) and erythropoietin (EPO) have been shown to inhibit the receptor activated nonselective cation channel [54, 55].

1.1.2.3 Gardos channel

The Gardos channel, the intermediate-conductance Ca^{2+}-activated K^+ channel (IK1 channel), also known as $K_{Ca}3.1$, was originally characterized by Gardos in RBCs [56]. The Gardos channel consists of 6 transmembrane domains, like most K^+ channels, with the pore region (S5-S6 transmembrane domains) containing amino acid sequence GYG responsible for its K^+ selectivity [57]. The N-terminus contains an endoplasmic retention signal, which is important for intracellular packaging and trafficking of the channel. The C-terminus contains the calmodulin-binding domain, which is a Ca^{2+} sensor, and has been proposed to be responsible for the sensitivity of $K_{Ca}3.1$ to submicromolar (100-300 nM) Ca^{2+} concentrations [57, 58]. However, there are still some controversial reports, proposing that the C-terminus is not responsible for Ca^{2+} dependence of the channel [59]. The C-terminus also has a leucine zipper motif as well as numerous consensus sites for PKA, PKC, and PKG phosphorylation. Interestingly, the C-terminus also contains a consensus sequence for tyrosine phosphorylation (RLLQEAWMY), suggesting that $K_{Ca}3.1$ could directly be activated by a tyrosine kinase receptor, e.g., growth factor receptors [57]. It is noteworthy that $K_{Ca}3.1$ lacks a series of arginine residues, which form the voltage sensor for voltage-gated K^+ channels, consistent with its lack of voltage dependence [57].

George Gardos found the mechanism that intracellular Ca^{2+} led to potassium efflux [56, 60]. Although these measurements in RBCs where not based on electrophysiological measurements, the channel causing this effect was named after Gardos. After the introduction of the patch-clamp technique, inside-out patches, revealed numerous features of the Gardos channel. For example, itsselectivity of K^+ over Na^+ of Gardos channel is measured as (17:1), which is also temperature dependent. Its whole cell conductance was noninactivating and inward rectifying for K^+ [50, 61, 62], inhibited by charybdotoxin (IC_{50}=28 nM), clotrimazole (IC_{50}=153 nM), nitrendipine (IC_{50}=27 nM), Stychodactyla toxin (IC_{50}=291 nM), margatoxin (IC_{50}=459 nM), miconazole (IC_{50}=785nM), econazole (IC_{50}=2.4 μM), cetiedil (IC_{50}=79 μM); and activated by 1-ethyl-2-benzimidazolinone (EC_{50}=74 μM) [63].

Within the last 40 years, the role of the Gardos channel in RBCs became more and more clear. In normal RBCs, the K^+ permeability is 100 times lower than the one for Cl^- [64, 65]. After full activation of the Gardos channels, the K^+ permeability is increased and at least 10 times higher than that of Cl^- [66]. This also induced Cl^- flowing out of the cells. The Cl^- loss results in a net loss of K^+, whose rate depends on the Cl^- permeability. The loss of KCl leads to an osmotic loss of cell water, which caused progressively dehydration of the cells. This leads to an increase inthe $[Cl^-]_o/[Cl^-]_i$ concentration ratio and drives a H^+ flux into the cells [67], causing cell acidification [68-70]. Afterwards, hemoglobin is also concentrated as the cells dehydrating and forces water to stay within the cells, thus limiting the extent of dehydration. The dehydration procedure results in the loss of an alkaline. In this condition, the cell is greatly dehydrated and the pH inside the cell is highly increased [71]. The whole procedure can be accelerated by changing Cl^- into more permeant anions, such as thiocyanate or nitrate [72] and blocked by specific Gardos channel inhibitors (described above).

1.1.2.4 Transient receptor potential channel C6 (TRPC6)

The transient receptor potential channel C6 (TRPC6) is expressed in RBCs shown by Western blot analysis [73].In human RBCs ghosts, TRPC6 was found to contribute to the Ca^{2+} leak of human RBCs [73].

Because of the lack of high affinity and selective ligands for activation and inhibition of TRPC6, the channel properties could not be comprehensively investigated. But in CHO-k1 cells transfected with TRPC6, diacylglycerol (DAG) showed direct activation of human TRPC6 channels [74]. Phospholipase C may also be involved in the TRPC6 activation signal pathways [75]. More detailed information about TRPC6 will be provided in section 1.3.1.

1.1.2.5 *N*-methyl-D-aspartate (NMDA) channel

In the central nervous system (CNS), the NMDA receptor (NR), a glutamate receptor, is a ligand-gated channel that mediates synaptic transmission and plasticity and is regulated by tyrosine phosphorylation. Activation of the NR opens the channel that is nonselective cations. A unique property of the NR is its voltage-dependent activation, a result of ion channel block by extracellular Mg^{2+} ions. This allows the voltage-dependent flow of Na^{+} and small amounts of Ca^{2+} into and K^{+} out of the cell [76-79].

Although NRs are nonselective ligand-gated cation channels, the selectivity of NR channels for Ca^{2+} exceeds that for Na^{+} 10-fold and thus ligand-mediated activation of the receptors typically results in an induction of a transient inward Ca^{2+} current. Thus, both activation and inactivation of NRs are modulated by the changes of intracellular Ca^{2+} levels. Such changes in intracellular Ca^{2+} have been reported to be involved in the proliferation of vascular smooth muscle cells and endothelia cells through NR activation [80, 81]. The interaction of noncompetitive and competitive NR antagonists, [^{3}H] MK-801 and [^{3}H] CGS-19755, has previously been reported [82]. The presence of NRs in RBCs

was recently shown by Bogdanova and co-workers [83]. Furthermore, in sickle cell patients, the expression of activated NRs is highly increased suggesting that NRs play a role in sickle cell disease [83]. In rat RBCs, the NMDA channel is mainly present in reticulocytes and young RBCs, suggesting that NMDA channels might be involved in the process of erythropoiesis [83].

1.1.2.6 Aquaporin (water channel)

In 1985, Bengaand co-workers firstly identified water channel protein, now called aquaporin 1, *in situ* in the human RBCs membrane [84]. And in 1988, it was re-discovered by Agre and co-workers and they characterized its main featurein 1992 [85, 86]. Aquaporins are integral membrane proteins belonging to a larger family of major intrinsic proteins that form pores in the membrane of biological cells. The three-dimensional structure of aquaporin 1 and the pathway by which water is transported through the channel (but not other small solutes) were described by Agre and co-workers [85]. Aquaporin is a hydrophilic channel formed by transmembrane proteins. Water is able to pass through the lipid bilayer of the plasma membrane although it is a polar molecule, but aquaporin can greatly accelerate the process. In brief, the extracellular vestibule and the intracellular vestibule of aquaporin channel are connected by a 20-Å span where water molecules pass through. A single water molecule could form hydrogen bonds with the side chains of the channel protein. The orientation of the two α-helices of the channel provide positive charges and make the water molecule enter but not entirely span the bilayer [85]. Of course, even without these, water is still able to pass through plasma membranes, but the aquaporin increases membrane permeability to water and makes this procedure adjustable.

1.1.3 RBCs cytoskeletal proteins

Many studies of RBCs cytoskeleton indicate that it is a network of spectrin polymers connected by junctional complexes [87-90]. The 2-dimensional spectrin-based membrane cytoskeletal network consists of α- and β-spectrin, actin, protein 4.1R, adducin, dematin, tropomyosin, and tropomodulin [91]. In RBCs, a large number of triple-helical repeats of 106 amino acids, 20 in α-spectrin and 16 in β-spectrin forma unique structure of the long filamentous spectrin [92]. These triple-helical repeats contain a spectrin super family of proteins that includes dystrophin, actinin, and utrophin [93]. Through a strong interaction between repeats 19 and 20 near the C-terminus of α-spectrin with repeats 1 and 2 near the N terminus of β-spectrin, they form an antiparallel heterodimer [94]. The spectrin tetramer is the main structural component of the 2-dimensional cytoskeletal network [95-97]. The other end of the long spectrin dimer is connected with F-actin and protein 4.1R to form a stable junction complex [24, 98]. Actually, actin forms only a weak contact with the α-spectrin N-terminus, but the existence of protein 4.1R greatly enhances this interaction [99]. Adducin and tropomodulin cap actin filaments at opposite ends. Their function has yet not been fully understood [100-103]. The spectrin dimer-dimer interaction and the spectrin-actin-protein 4.1R junction complex form the most important structure to maintain the membrane stability and prevent the deformation and fragmentation when the cells encounter high shear stress in the blood circulation system [104].

1.1.4 Ca^{2+} in RBCs: effects of elevated $[Ca^{2+}]_i$

1.1.4.1 On Red Cell Homeostasis

Mature RBCs lack organelles, which makes its Ca^{2+} equilibrium appears to be deceptively simple. The intracellular Ca^{2+} ($[Ca^{2+}]_i$) concentration and the membrane Ca^{2+} permeability (P_{Ca}) of RBCs are extremely low when compared to other cells, but it appears reasonable to assume that the

physiological intracellular Ca^{2+} level in human RBCs to be approximately within the range of 30 to 60 nM [105]. The cytosolic $[Ca^{2+}]_i$ is the result of the balance between Ca^{2+} influx and Ca^{2+} extrusion. Ca^{2+} influx might be mediated through ion channels [106]. Active Ca^{2+} extrusion is mediated by P-type pumps (PMCA) expressed in isoforms 1 and 4 [107-109]. There have been reports that $[Ca^{2+}]_i$ may transiently increase in physiological conditions in response to shear stress in the microcirculation [110], or terminally, as part of the programmed death [111, 112]. Increases in total Ca^{2+} wereonly reported in rather specific pathological conditions: in malaria, sickle cell anemia and thalassemia. Many abnormalities of RBCs have been attributed to increased $[Ca^{2+}]_i$. Such abnormalities cause large alterations of the cell's metabolism, volume and ion content. The $[Ca^{2+}]_i$ increase is associated with the activation of the Gardos channels and the PMCA. Depending on the experimental conditions, Gardos channel activation has profound effects on the homeostasis, while Ca^{2+} pump activation is affected by the ATP metabolism of the cells [56]. The PMCA activity and properties may be modulated by dimerization and intracellular factors, such as calmodulin binding or calpain activity [109]. Furthermore, the elevated $[Ca^{2+}]_i$ will activate Ca^{2+}-sensitive proteases [113], cytoskeletal cross-linking [114, 115], thyroid hormones [114], haem radicals [116, 117]. Thus, Ca^{2+}-homeostasis is an integrated function and all of the components regulating $[Ca^{2+}]_i$, and their interaction need to be considered when referring to RBC Ca^{2+} handling.

1.1.4.2 Ca^{2+} and Red Cell Survival

In human beings, the circulating RBCs originate from a differentiation process. In the bone marrow, stem cells undergo a series of differentiation steps stimulated by hormones, such as erythropoietin, to form erythroblasts, basophilic, polychromatophilic, orthochromatic normoblasts and reticulocytes. In this process, cell size decreases, the nucleus condensates and the hemoglobin synthesis rate increases. Finally, the nucleus is extruded, RNA production is terminated, and the reticulocyte is released into the blood

circulation system. In this erythroid cell maturation procedure, the morphology of RBCs greatly changed [118]. In addition to such structure changes, the functional properties of the RBC's membrane are also markedly altered. These characteristics include lipid composition and distribution as well as altered transport of amino acids, sugars and ions (Ca^{2+}, Na^{+} and K^{+}) [119].

Many methods, such as Percoll gradient centrifugation and filtration, which are based on the density difference between old and young cells, have been applied to separate populations of young and old RBC [120]. There are also separation methods using further differences between young and old RBCs including changes in geometry [121], reduced activity of the Gardos channel [122], enzymatic changes [123] and alterations of vitamin content [124]. Kinases such as galactokinase, alter their activity when young RBCs mature [125]. The activities of 6 enzymes, including glucose-6-phosphate dehydrogenase (G-6-PD), 6-phosphogluconate dehydrogenase (6-PGD), hexokinase (Hx), glutamate oxaloacetate transminase (GOT), lactate dehydrogenase (LDH) and acetylcholinesterase (AChE), were assayed in the RBCs of different ages. The results showed that activities of Hx, AChE and GOT were considerably increased in younger RBCs compared to older ones. Consequently, these enzymes may be used as an indicator of the RBC's age [126].

Ca^{2+} is often thought to be involved in RBCs ageing and removal from the circulation [112]. Romero and Romero [127] suggested a progressive increase in Ca^{2+} permeability during RBCs ageing, resulting in $[Ca^{2+}]_i$ increases associated with activation of Gardos channels and proteases. This alters cell homeostasis and causes Ca^{2+} pump proteolysis increasing $[Ca^{2+}]_i$ even further. This results in erypotosis of old cells and cleavage by macrophages in the spleen. The main problem with the above hypothesis is the absence of any *in vivo* evidence. The effect of elevated $[Ca^{2+}]_i$ on RBC survival *in vivo* was tested direct on rabbits [112]. Like human RBCs, rabbit RBCs have a powerful Ca^{2+} pump and Ca^{2+} - sensitive K^{+} channels capable of dehydrating

the cells rapidly when fully activated. In contrast to the above, rabbit RBCs showed normal survival *in vivo* following *in vitro* Ca^{2+}-loading dehydration and ATP depletion.

Commonly, quantitative measurement of intracellular Ca^{2+} is performed with Fura-2. However, a strong spectra interference between hemoglobin and Fura-2 prevents Fura-2 measurements in RBCs [128]. Fluo-4 seems to be the better indicator for fluorescent measurements because its excitation and emission properties are less influenced by hemoglobin and in contrast to UV-light (Fura-2), the excitation light for Fluo-4 does not induce auto-fluorescence in RBCs [128].

Early studies [111, 120] have shown a two-fold increase in the Ca^{2+} content of the dense fraction (old cells) compared with the light fraction (young cells) of human RBCs after centrifugation in Percoll gradients. It is also reported that the heaviest (old) cells take up more Ca^{2+} after being exposed to relatively high Ca^{2+} levels [120]. These results suggest that the Ca^{2+} in RBCs rises during ageing *in vivo*.

Simultaneously, it is widely accepted that the ATP concentration and several enzyme activities decrease while human RBCs age [120]. Because the intracellular Ca^{2+} level is directly related to the activity of the ATP-dependent PMCA, it can be expected that the decreased ATP content will augment the intracellular Ca^{2+} increase [129]. However, there are some controversial reports. For example, Kirkpatrick and co-workers found that the ATP content in old cells decreased compared with young cells in the circulation system, but if considering the smaller size of the old cell, the ATP concentration was the same between old and young RBCs [130]. Taken all data together, there is no coherent picture between the intracellular Ca^{2+} content in young and old RBCs.

1.2 Lysophosphatidic acid (LPA)

Lysophosphatidic acid (LPA) is a water-soluble lipid second messenger released in copious amounts from activated platelets, fibroblasts, adipocytes, and cancer cells [38, 131, 132]. LPA produced by stimulated platelets, recruits cells to assist in blood clot formation and wound healing [133]. LPA can also activate resting platelets [133], decreases endothelial permeability by narrowing of intercellular gaps [134], alter cerebral microcirculation [135], induce proliferation of cultured vascular smooth muscle cells and fibroblasts [136, 137], modulate the cell surface fibronectin assemble [138] and induce monocytes, lymphocyte, and neutrophil mobilization [139-141]. Lu and co-workers discovered that LPA can open a Ca^{2+} channel in human RBCs when compared to ionophore-treated cells, only approximately 25% of the RBCs exhibited a Ca^{2+} influx induced by 5 μM LPA, while the remaining population displayed only a slight fluorescence increase [32]. $[Ca^{2+}]_i$ increase in RBCs can activate the scramblase and the Gardos channel, led to cell shrinkage and phosphatidylserine exposure. Thus, it is reasonable to consider LPA as an important player in RBC's Ca^{2+} signaling and possible role in blood clot formation.

1.3 TRP channels

1.3.1 The transient receptor potential channel (TRP) family

The transient receptor potential (TRP) channels family often contribute to $[Ca^{2+}]_i$ changes in general by providing Ca^{2+} entry pathways for the Ca^{2+} entry. In many cell types TRP channels might also provide pathways for Ca^{2+} release from intracellular Ca^{2+} stores, such as the endoplasmic reticulum [142] or mitochondria [143]. Because the expression of TRPC6 in RBCs has been supported by Western blots [73], it appears appropriate to study and discuss their putative role for Ca^{2+}-handling in RBCs.

1.3.2 Discovery of the "canonical" TRPCs: the Drosophila transient receptor potential channel

TRP channels were firstly discovered in *Drosophila* in 1969. *A Drosophila* mutant exhibited a transient instead of sustained response to light. These channels were named *trp* (transient receptor potential) channels [144], and the gene of the channel was cloned in 1989 [145]. Two additional homologous channels, TRP-like (TRPL) and TRPγ, were also found to be involved in thesetransient response [146]. Consequently, TRP and TRPL double mutants are totally blind, suggesting that TRPγ may function together with TRPL [147].

1.3.3 Properties of TRPC channels

TRPC, the first subgroup in the TRP family, was cloned in 1995 from human beings [148] and can be divided into four subfamilies according to their function and structure: TRPC1, TRPC2, TRPC3/6/7 and TRPC4/5. These TRPC channels have the same sequence in the C terminal named TRP box (EWKFAR), and 3–4 NH_2-terminal ankyrin repeats. TRPC channels are non-selective Ca^{2+} permeable cation channels, although the selectivity between Ca^{2+} and Na^{+} varies considerably between different family members [149]. The TRPC channels are expressed in many cell types, and different members can co-exist in one cell type. TRPCs also form homotetrameters and heterotetramers. For example, TRPC1 can form heteromers with TRPC4, even though TRPC1 and TRPC4 are in a different subgroup; TRPC4 and TRPC5 can also form heteromers, but they are in the same subgroup [149]. Their properties are significantly different from the homotetramers [150, 151]. These features greatly increased the research complexity of the TRPC channel function and structure.

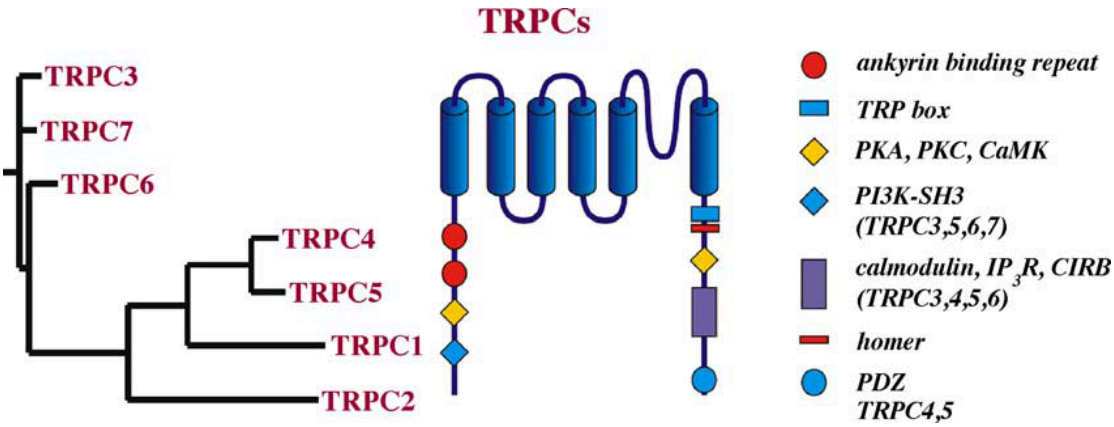

Figure 1: TRPC channels structure.

TRPC family members and proposed membrane topology. The legends represent the putative sites important for the channel regulation and protein–protein interactions (details in the text). This figure is a reprint from [149] with kind permission from Elsevier.

1.3.4 TRPC6 regulation

TRPC channels are activated by stimulation of receptors that activate multiple isoforms of PLC, for example, PLCβ following activation of G-protein coupled receptors (GPCRs), and PLCγ after activation of receptor tyrosine kinases (RTKs) [152]. Generally speaking, TRPC3/6/7 can also be activated by diacylglycerol (DAG) [153], indicating that DAG is the PLC-derived product mediating their activation. In contrast, TRPC1, 4 and 5, which are also stimulated by receptor mediated PLC activation, are totally insensitive to DAG [74]. Thus, the mechanism of PLC-mediated TRPC activation is still controversial.

Store-operated Ca^{2+} entry channels (SOCs) are also considered as regulators of TRPC channels [152], but there is also evidence that TRPC1, TRPC4/5 and TRPC3/6/7 show receptor-operated channel features that are insensitive to store depletion [152]. The relationship between stromal interaction molecule STIM1 and the store-operated Ca^{2+} entry suggests a connection of SOCs with TRP channels [154]. All TRPCs show binding sites for CaM and the inositol

(1,4,5) trisphosphate (IP_3) receptor named CIRB [155]. Research on TRPC3 showed a potential interconnection to the ryanodine receptor (RyR) [156].

TRPC6 mainly occurs in lung and brain [157], but still has other expression patterns [158]. In smooth muscle cells, TRPC6 is an essential part of the vascular α_1-adrenoreceptor-activated Ca^{2+}- permeable cation channel [159], and can be activated by flufenamate and AlF_4^- [160]. It also plays an essential role in thrombin induced Ca^{2+} entry in platelets [161]. TRPC6 has a slight selectivity for Ca^{2+} over Na^+, and can be activated by DAG [73, 160], eicosanoid and 20-hydroxyeicosatetraenoic acid (20-HETE) [162]. Some reports show that TRPC6 might be regulated by both intra- and extracellular Ca^{2+} in a complex manner: its activation is potentiation by $[Ca^{2+}]_e$ from 0.1 to 1 mM and $[Ca^{2+}]_i$ from 20 to 200 nM, yet inhibited at higher concentrations [163]. The SRC tyrosine kinase Fyn is believed to activate TRPC6 directly [164]. The muscarinic receptor and the MxA protein were also shown to be associated with TRPC6 [165]. Figure 1 summarizes important structural properties and protein–protein interaction sites of TRPC channels.

1.4 Aggregation of RBCs

1.4.1 Active role of RBCs in aggregation

Although RBCs aggregation has been intensively studied for decades [166], many questions still remain to be elucidated, for example: What is the relationship between the Ca^{2+} increase and aggregation in RBCs? According to the traditional view, coagulation is a result of interplay between endothelial cells, platelets, and soluble coagulation factors. In this process, platelets are the crucial players and RBCs are considered as innocent bystanders, just passively entrapped in a thrombus as they flow through the vasculature. In 1999 Andrews and Low summarized arguments for a much more active role of RBCs in blood clot formation [167]. Duke and co-workers [168] reported that an increased hematocrit in thrombocytopenic patients showed improved

bleeding frequency after transfusion, even though their platelet counts remained very low [169]. It is also reported that thrombocytopenic disease related animal models were accompanied with shorter bleeding time after RBC transfusion [170]. When studying anemic patients with bleeding deficiencies, Hellem and co-workers [171] reported improved bleeding times following injection of washed-RBCs. Because of the decreased platelet numberin these patients, the RBC was assumed to be the reason of this phenomenon.

It was suggested that PS exposure at the outer leaflet of the plasma membrane of the platelets might form a catalytic surface for the binding of coagulation factors. Therefore, platelets can initiate the coagulation cascade [172]. Kaestner and co-workers sproposed a signaling cascade in which RBCs actively contribute to clot formation [51]. Under specific circumstances (e.g. injury), the platelets will be activated, which led to LPA and PGE_2 release to the blood. These substances activate the non-selective voltage dependent cation (NSVDC) channel. This results in a rapid increase of intracellular Ca^{2+}, stimulating the Gardos channel and the scramblase. The activation of the Gardos channel induces an efflux of intracellular KCl and then causes cell shrinkage (see above). Combined with the activity of the scramblase, the consequences of the cascade are cell shrinkage and aggregation. Therefore, RBCs may play an active role in clot formation.

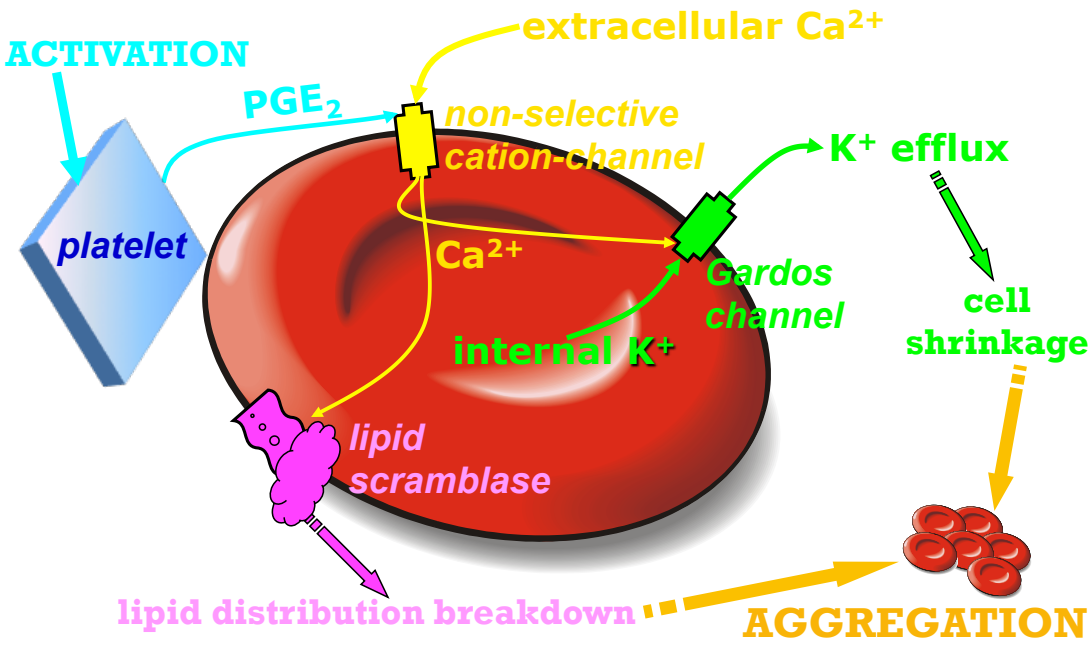

Figure 2: Schematic cascades proposed for the aggregation of RBCs in activated conditions.

(This figure is kindly provided by Dr. Lars Kaestner; proposed in [51])

1.4.2 Effects of proteins in the blood plasmafor RBCs aggregation

In blood plasma, human RBCs have a tendency to form rouleaux, which are linear aggregates and looks like a stack of coins. The number of RBCs per rouleaux varies in different conditions, and branching between two rouleaux could occur. Because of the relatively weak force between RBCs in rouleaux, it is possible to separate rouleaux into smaller fractions or even into single cells by applying sufficient shear forces [173]. Therefore, the rouleaux formation of RBCs is thought as a reversible process, while blood coagulation is irreversible. Macromolecules in blood plasma, such as fibrinogen, are assumed to play the main role in both the coagulation and aggregation procedure [174]. For example, suspending RBCs in solutions containing dextran (DEX), a neutral macromolecule, can also induce rouleaux formation [175]. Furthermore, without the presence of macromolecules, such as RBCs in Tyrode or saline solution, aggregation could not be observed.

However, different macromolecules play a different role in aggregation. For example, the fibrinogen mediated aggregation of RBCs increases with fibrinogen concentration [175], whereas the dextran-mediated aggregation of RBCs reaches a maximum at a certain dextran concentration. Furthermore, the molecular weight of the dextran also influences the aggregation [175].

In summary, until now, the mechanism of RBC aggregation is still not completely resolved. Two models were proposed to explain the rouleaux formation of RBCs: the bridging model and the depletion model. In the bridging model, it is proposed that fibrinogen or dextran molecules unspecifically stick to the cell membrane and form a “bridge" to connect cells [176]. The aggregation occurs when the bridging forces exceed the disaggregation forces such as electrostatic repulsion and shearing stress [177]. In the depletion model, when the cells approach each other in solution containing macromolecules, the concentration of macromolecules near the cell surface is depleted compared to the concentration of the environment, resulting in a net “depletion" force. Both of these two theories were supported by studies in the past. For example, non-specific binding [178, 179] and specific binding mechanism [180] were proposed for the bridging model, whereas several studies supporting the depletion model have also been published [181, 182]. Nevertheless, the aggregation of RBCs is a very complicated process and needs to be further investigated in the future.

1.5 Sickle cell disease

Sickle-cell disease (SCD) was first described by James B.Herrick in 1910 [183], characterized by RBCs which show an abnormal, rigid, sickle shape. SCD results in many types of anemia and crises, such as the vaso-occlusive crisis, aplastic crisis, and hemolytic crisis. The vaso-occlusive crisis is caused by the sickle RBCs-induced obstruction of capillaries and restriction of blood flow to organ, resulting in ischemia, pain, and necrosis [184]. The spleen is also frequently affected because of the narrow vessels and its function in clearing

defective RBCs, which causes the aplastic crisis [185-187]. Furthermore, these sickle-shaped cells are more fragile compared with normal RBCs, which trigger chronic hemolysis and the following inflammatory response [188, 189].

Almost a century after SCD was first described, it has already been proved a genetic hemoglobin disorder in RBCs [190]. The mutant sickle hemoglobin (Hb S) differed from normal hemoglobin A by a glutamine-to-valine substitution at the sixth residue of the β-globin polypeptide [191, 192], which followed by the formation of long intracellular polymers upon deoxygenation [193]. The abnormal hemoglobin polymers, on one hand, disrupt the RBC cytoskeleton and form protrusions, showing the characteristic sickle appearance, decrease the cells' flexibility and increase the fragility [194]. On the other hand, the polymers can also influence the RBC plasma membrane, resulting in the extracellular exposure of proteins and glycolipids that are normally found inside the cell, notably of phosphatidylserine (PS) [195]. These changes likely explain the increased adherence of sickle RBC to vascular endothelium and the higher risks of thrombosis of SCD patients [196, 197]. Most of the adhesion pathways was found involved in the interactions between sickle cells and endothelial cells, containing integrins [198-200], immunoglobulins [201, 202], selectins [203, 204], thrombospondin [205], fibrinogen [206], fibronectin [207] and some exposed membrane components such as Band 3 and sulfated glycolipids [208, 209]. Therefore, considering the presence of so many target proteins, the mechanism of increased sickle cell adhesion was an enormous challenge and still needs further investigation.

As described above, LPA can recruit cells to assist in blood clot formation [133] and induce Ca^{2+} influx in RBCs, which followed by PS exposure [210]. Meanwhile, sickle RBCs also show an increased PS exposure and adhesion potency [195]. Therefore, I investigated the function of LPA and its receptors in sickle RBCs in this thesis.

2. Materials and methods

2.1 Materials

2.1.1 Chemicals and reagents

The used substances and reagents are listed below:

Name	Supplier	Stock-solution
2-APB	Sigma-Aldrich	1 mM in methanol
Ca^{2+} ionophore A23187	Sigma-Aldrich	1 mM in ethanol
DMSO	Roth	
Ethanol	Sigma-Aldrich	
Ethylendiamintetraacetat-Na (EDTA)	Sigma-Aldrich	
Ethylenglycoltetraacetat-Na (EGTA)	Sigma-Aldrich	
Fibrinogen	Sigma-Aldrich	
Fluo-4, AM	Molecular Probes	1 mM in Pluronic
Glucose	Sigma-Aldrich	
Gö6983	TOCRIS	1 mM in DMSO
Gö6976	TOCRIS	1 mM in DMSO
Heparin	Sigma-Aldrich	
HEPES	Roth	
Inorganic salts (NaCl, $CaCl_2$, KCl, $FeCl_2$, $FeCl_3$, $FeSO_4.7H_2O$…)	Sigma-Aldrich/ Roth	
Lysophosphatidic acid (LPA)	Sigma-Aldrich	5 mM in PBS

Methanol	Sigma-Aldrich	
m-3M3FBS	Sigma-Aldrich	50 mM in DMSO
MK-801	Sigma-Aldrich	50 mM in DMSO
NaOH	Roth	
Neuron growth factor (NGF)	Sigma-Aldrich	10 µg/ml in H_2O
New methylene blue (NMB)	Sigma-Aldrich	
o-3M3FBS	Sigma-Aldrich	50 mM in DMSO
ω-agatoxin-TK	Peptanova	100 µM in H_2O
Pertussis toxin (PTX)	Sigma-Aldrich	250 µg/ml in H_2O
PGE_2	Sigma-Aldrich	1 mg/ml in H_2O
Pluronic F-127, 20% in DMSO	Molecular Probes	
PKH26 Red Fluorescent Cell Linker Mini Kit	Sigma-Aldrich	
PMA	Sigma-Aldrich	1 mM in DMSO
Poly-L-Lysin	Sigma-Aldrich	250 µg/ml in H_2O
Sodium orthovanadate	Sigma-Aldrich	100 mM in H_2O, pH=10
Tetramethylethylenediamine (TEMED)	Roth	
Tris (hydroxymethyl) aminomethane	Roth	
U0126	Sigma-Aldrich	10 mM in DMSO
U73122	Sigma-Aldrich	1 mM in ethanol
U73343	Sigma-Aldrich	1 mM in ethanol

VPC32183		1 mM in PBS with 3% BSA
Wortmannin	Sigma-Aldrich	10 mM in DMSO

2.1.2 Main solutions used

Tyrode solution (mM): NaCl 135, KCl 5.4, glucose 10, $MgCl_2$ 1, $CaCl_2$ 1.8, and HEPES 10. The pH was adjusted to 7.35 using NaOH.

PBS buffer (mM): NaCl 140, KCl 3.0, Na_2HPO_4 7.5, and KH_2PO_4 1.5. The pH was adjusted to 7.4 using NaOH.

2.1.3 Fluo-4/AM

Fluo-4/AM is a fluorescent dye to measure cellular Ca^{2+} concentrations from 100 nM to 1 µM, and its K_d (Ca^{2+}) is 345 nM [211]. Fluo-4 is similar in structure and spectral properties to it's precursor, Fluo-3, but due to its greater absorption near 488 nm and the emission at 520 nm, Fluo-4 offers much brighter fluorescence emission when using a 488 nm laser or other white light sources in conjunction with the standard FITC-fluorescence filter sets. The structure and fluorescence emission spectra of Fluo-4 and Fluo-3 are shown in Figure 3.

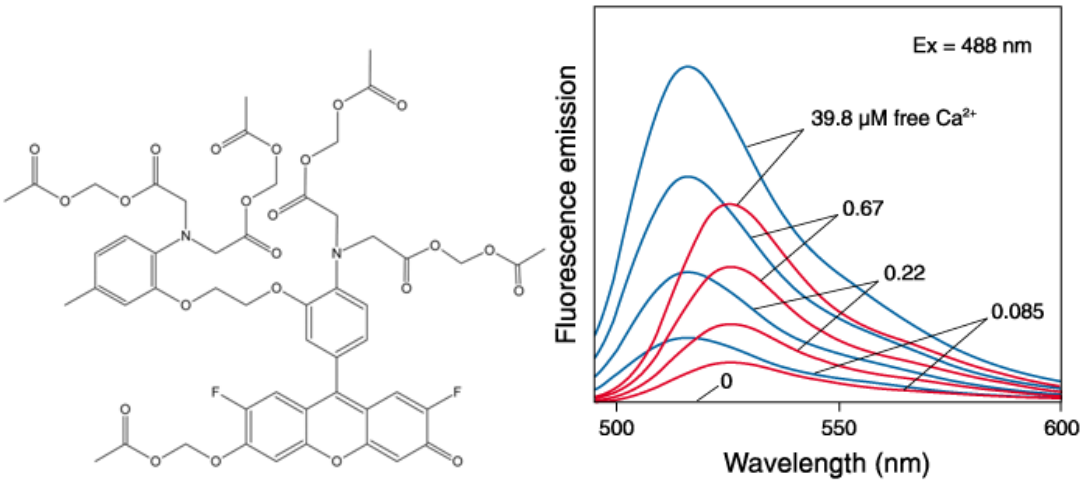

Figure 3: Molecular structure and fluorescence emission spectra of Fluo-4 and Fluo-3.

Left: molecular structure of Fluo-4. Right: fluorescence emission spectra of Fluo-4 and Fluo-3. The blue curves correspond to Fluo-4, the red ones to Fluo-3 for depicted Ca^{2+} concentrations. Fluo-4 and Fluo-3 were simultaneously excited at 488 nm, in solutions containing 0–39.8 µM free Ca^{2+} (Cited from the Handbook of fluorescent probes and research chemicals [212]).

2.2 Imaging devices

2.2.1 Video-imaging Set-up

A video-imaging microscope was used to measure intracellular free Ca^{2+} and kinetics. The set-up was based on an inverted microscope (TE-2000, Nikon, Tokyo, Japan), combined with a CCD camera (Imago-QE, TILL Photonics GmbH, Gräfelfing, Germany), as illustrated in Figure 4. A monochromator (Polychrome IV, TILL Photonics GmbH, Gräfelfing, Germany) was used to obtain the desired excitation wavelength (480 nm and 550 nm) that was reflected by a dichroic mirror (splitting edge at 505 nm) and focused onto the cells with a 60 × oil objective (CFI Plan Fluor, Nikon, Tokyo, Japan). For Fluo-4 measurements, the emission was collected by the same objective, filtered with a 535/40 bandpass filter nm long pass filter and recorded with a CCD camera. Both the camera and the monochromator were controlled by the Digital Signal Processor (DSP)-driven Imaging Controlling Unit (ICU, TILL

Photonics GmbH, Gräfelfing, Germany), which was connected to a computer and operated with TILLvisION v4.0 software.

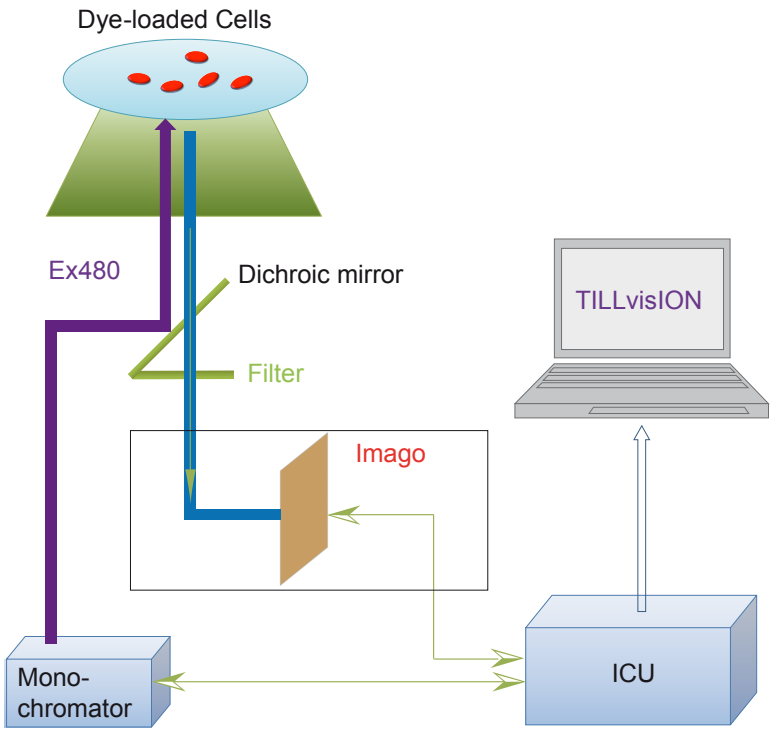

Figure 4: The basic design of Imago-imaging setups.

The system consists of a Polychrome IV, a Nikon TE-2000 inverted microscope and an ICU (central controlling unit).

2.2.2 Leica TSC SP5 confocal microscope

The Leica TCS SP5 II (Leica Microsystems GmbH, Wetzlar, Germany) was based on inverted epifluorescence microscope, with build in high-speed laser scanning head (8000 lines per second). For excitation of fluorescent immunostaining and Fluo-4, the 488 nm line of an Argon gas laser was used. The primary dichroic was substituted by an acusto-optical beam splitter (AOBS) and detection was achieved with a highly sensitive, two-channel prism spectrometer. Control of the experiments as well as the microscope was performed with Leica Application Suite software (ver. 2.4). High-resolution images were acquired using a Plan Apo 63 x oil immersion

objective. For image acquisition in Leica, xy (image resolution) depends on emission wavelenght, numerical aperture of the objective, immersion medium, stability of the system, brightness/contrast-settings and pixel size. Z (optical section thickness) depends on pinhole size, coverglass thickness and immersion medium. The section thickness (Z) in combination with the xy-pixel dimension defined the “voxel” size (volume element size), which is the smallest unit of the sampled three-dimensional (3D) volume. In our experiment, the physical size of xy-pixel was 100.5 nm, the z-pixel was 750 nm and the resolution was settled as 1024*768. The volume of RBCs samples was defined through setting the z-values for begin & end of the sample. Then the distance between two slices (197.6 nm) and number of optical sections within the volume (60 slices) were also defined and scanned to obtain z-stack images of the sample. Z-stack images were used to obtain two-dimensional (2D) images by z-projection.

2.3 Methods

2.3.1 Red blood cell preparation

Experiments with human RBCs were authorized by the ethics committee of the medical association of the Saarland underregistration number 132/08. Blood donors provided their written informed consent to participate in this study. This consent procedure was approved by the ethics committee of the medical association of the Saarland under the above mentioned study registration number. For the experiments, we used RBCs from healthy adult donors. Blood was drawn from a vein into heparinized syringes. Experiments with mice were carried out in strict accordance with the recommendations in the Guide for the Care and Use of Laboratory Animals of the National Institutes of Health. The protocol was approved by the State Office for Health and Consumer Protection (Permit Number: C1–2.4.3.4). All efforts were made to minimize suffering. Blood samples were collected from the cheeks of the mice by lancet puncture and were collected into heparinized Eppendorf tubes.

Mouse blood samples were taken from the cheek of the mouse, located the submandibular area, which is behind the jawbone (Figure 5). This area is rich of vascular micro-vessels and provided a convenient and consistent source of blood. After collecting the blood sample, the injury spot needed to be pressed and the mouse will self-groom and be virtually unaffected. The blood harvest can be done daily, but for safety and healthy reasons, it can not exceed the total volume recommended for that size of animal. 10-15% of total blood volume or 1% of body weight was the maximum amount of blood that could be collected at one time, and removal of up to 1% of total blood volume daily over time was permitted. On average, the total blood volume in the mouse is 6-8% of its body weight, or 6-8 ml of blood per 100 g of body weight. Therefore, I removed not more than 15~20 μl from a typical mouse (25g) per day [213].

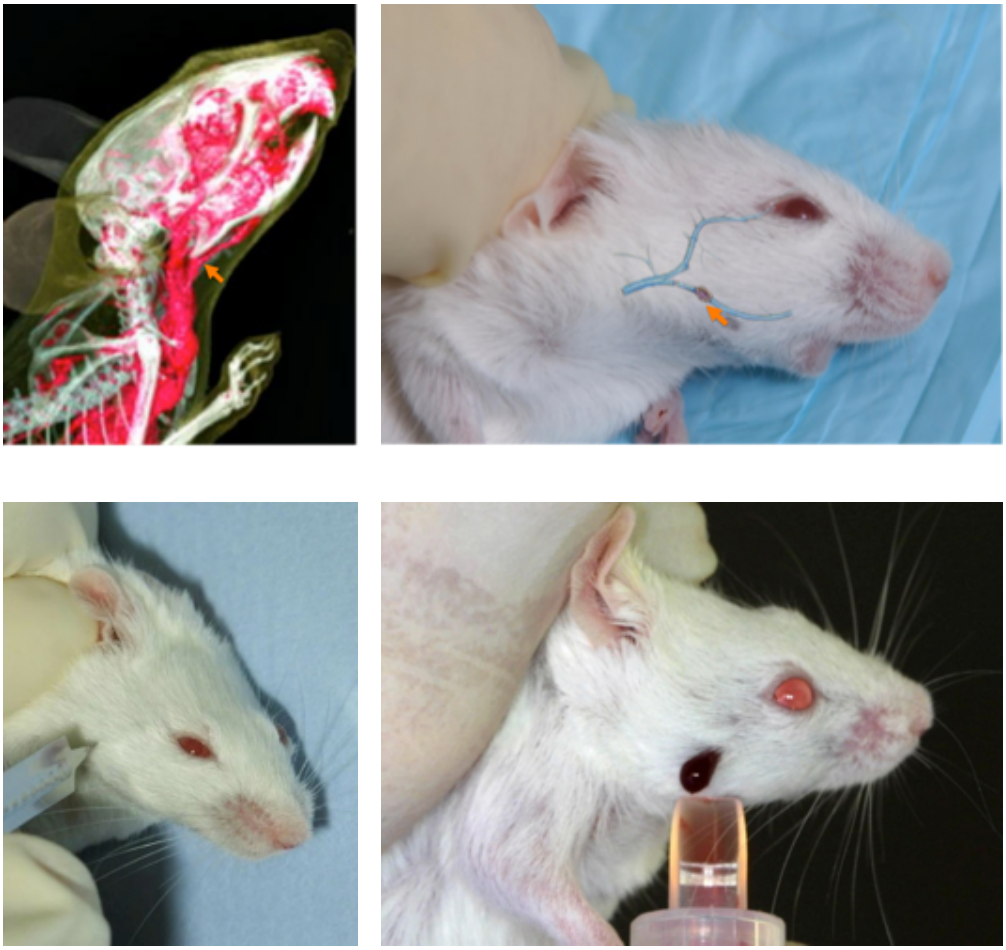

Figure 5: Blood sample collection from mouse cheek.

The submandibular area (orange arrow), which is in the back of the jawbone, was chosento collect blood samples. After collecting blood sample, the injury was pressed and the mouse will self-groom and be unaffected. (Cited from http://www.medipoint.com/html/directions_for_use1.html)

Human blood samples were drawn from healthy donors. Heparin was used as anticoagulant. The blood bank samples were obtained from the Institute of Clinical Hematology and Transfusion Medicine of Saarland University Hospital.

Sickle cell anemia blood samples were kindly provided by Prof. Anna Bogdanova & Dr. Jeroen Goede (Zürich Center for Integrative Human Physiology,

University of Zürich, Zürich, Switzerland). Experiments on SCD blood samples were operated within 48 h after withdraw from donor.

Blood was washed with Tyrode by centrifugation at 5,000× g for 3 min at room temperature for 3 times. In between the centrifugations supernatant (plasma after the initial centrifugation) was removed. Finally, RBCs were re-suspended in Tyrode solution to start the experimental procedure.

Before the application of inhibitors and LPA on cells, to exclude the possibility of inhibitors-induced Ca^{2+} influx, I treated cells with only inhibitors. All RBCs were loaded with Fluo-4 as described above and the application of blockers were also as described in the experiments in this work. In brief, PTX, Wortmannin, U0126, ω-agatoxin-TK, Gö6983 and Gö6976 were applied on cells at the same concentrations and times as used in the experiments, respectively. The fluorescence intensity change during the application time (F/F_0) was measured to analyze whether these inhibitors themselves could induce Ca^{2+} influx or not. The fluorescence intensity measured in Tyrode was still used as control. Figure 6 shows the results of all used inhibitors both in human and mouse RBCs. This figure indicates that these inhibitors, containing PTX, Wortmannin, U0126, ω-agatoxin-TK, Gö6983 and Gö6976, could not change Ca^{2+} influx both in human (Figure 6A) and mouse (Figure 6B) RBCs.

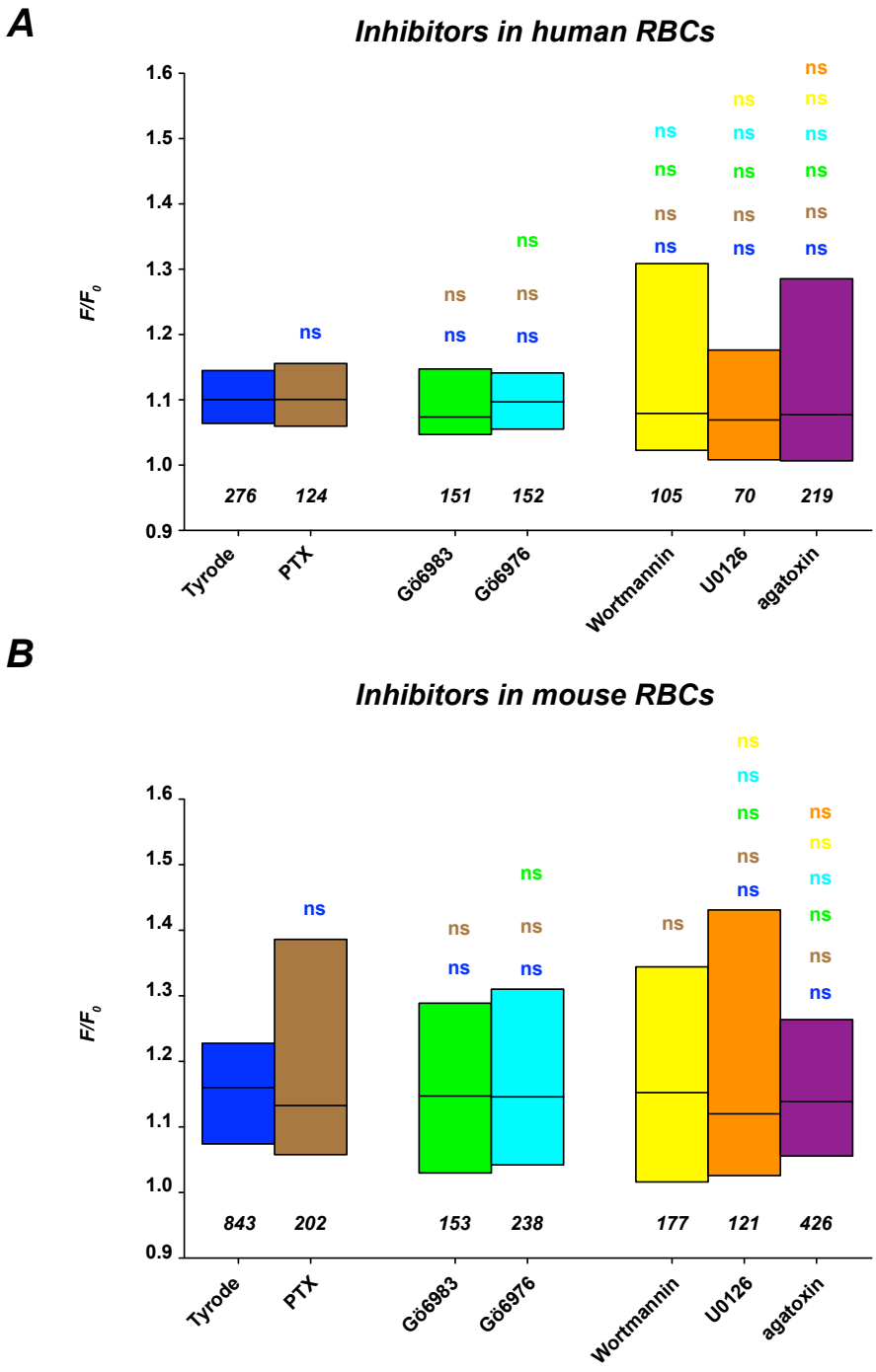

Figure 6: Only inhibitors could not induce Ca^{2+} influx both in human and mouse RBCs.

*All the inhibitors used in this thesis, containing PTX, Wortmannin, U0126, ω-agatoxin-TK, Gö6983 and Gö6976, could not induce Ca^{2+} influx both in human (**A**) and mouse (**B**) RBCs. Every experiment was repeated at least three times.*

2.3.2 Intracellular Ca^{2+}measurements

Fluo-4/AM was used as the indicator to measure intracellular Ca^{2+}. Live cell imaging was performed to monitor intracellular Ca^{2+} kinetics in individual cells when exposed to LPA (Sigma). For this experiment I used RBCs from healthy adult donors, sickle cell disease patients, wild type mice and TRPC6 $^{(-/-)}$ mice. After the RBCs were prepared as described in chapter 2.3.1, 20,000,000 RBCs in 1 ml Tyrode were loaded with Fluo-4/AM at a concentration of 5 µM for 1 hour at 37°C. Then cells were washed in Tyrode for 3 times at room temperature. 1,000,000 cells were plated on a coverslip in Tyrode solution. I waited 15 min for the cells to settle down and for dye de-esterification. Images were collected every 5 seconds for a total period of 15 minutes. A 505 nm long pass dichroic mirror separated the emission light from the excitation light and a 535/40-band pass filter was used to further clean up the emission. A local perfusion gravity-based system was utilized to quickly exchange solutions in the field of view and to apply the desired concentration of substances. For the experiments with LPA, PGE_2 or other "activation" substances, the samples were prepared like described above. For experiments with PTX, Wortmannin or other inhibitors, cells were pretreated with these substances for a given time before LPA stimulation. For the control, the fluorescence intensity of Fluo-4 was measured in Tyrode in the presence of 1.8 mM extracellular Ca^{2+}. Every experiment was carried out with at least three different blood samples and repeated at least three times. Images were processed in ImageJ (Wayne Rasband, National Institute of Mental Health, Bethesda, USA) and traces handled by Igor Pro software (WaveMetrics, Inc.).

2.3.3 Induction of reticulocytosis

Populations with a high reticulocyte count were prepared from BALB/c mice by repetitive bleeding according the protocol previously described by Joiner and co-workers [214] with slight modifications. On day 1, mice were treated with

an intraperitoneal injection of 2 ml saline, and then lightly anesthetized with Xylazin 17.5 mg/kg body weight (*Rompun*®) and Ketamin 85 mg/kg body weight (*Ursotamin*®) mixture. 500 µl of blood was then drawn by retro-orbital puncture. The procedure was repeated on day 3. During this period, drinking water was supplemented with iron (3 mg Fe^{2+}/100 ml) and folate (20 µg/100 ml) to compensate for iron loss by the haemoglobin in the withdrawn RBCs. Reticulocyte counts were determined on smears stained with new methylene blue (NMB). On day 5, the ratio of NMB positive cells in pooled blood samples reached ~30%. Approximately 0.5 ml of whole reticulocytes-rich blood was drawn by retro-orbital puncture for intracellular Ca^{2+} measurements and PKH26 staining.

2.3.4 Flow cytometry to measure intracellular Ca^{2+}

Flow cytometric measurements were performed as described by Nguyen and co-workers [210]. In brief, Fluo-4 loaded RBCs were analyzed using a flow cytometer (FACSCalibur, Becton Dickinson Biosciences, San Jose, USA). Fluo-4 was excited at 488 nm, and emission was collected at a center wavelength of 530 nm. Each experiment was performed in triplicate (3 blood samples) and for each measurement 30,000 RBCs were analyzed. The data were processed using BD Cell Quest ProSoftware (Becton Dickinson Biosciences, San Jose, USA).

2.3.5 PKH26 labeling of RBCs

After induction of reticulocytosis, 500 µl of blood was drawn by retro-orbital puncture on day 5, and then stained with PKH26 according to the manufacturers protocol: 50 µl of RBCs (prepared for experiments) were mixed with 450 µl Diluent C from the PKH26 Cell Linker kit, and then incubated with 2 µM PKH26 dye for 5 min at room temperature. The staining reaction was stopped by addition of 500 µl 1% BSA for 1 min followed by dilution of the

BSA with 1 ml saline. Cells were centrifuged at 400 x g for 10 minutes at room temperature for 3 times to remove staining solution from cells. The final volume of stained cells was adjusted to 300 µl, and injected back to mice through tail vein injection. Because PKH26 can also be excited by 480 nm, a background correction procedure was utilized in imaging analysis (Figure 7). A TRITC filter-set was used to get fluorescence from PKH26 (excitation: 550 nm). Cells, collected 43 days after the re-injection, were screened by FACS. PKH26 positive cells were in the circulation for at least 43 days and therefore represented an exclusive fraction of old RBCs.

Because PKH26 could also be excited at 480 nm, a background correction procedure was employed before data analysis. Prior to Fluo-4 loading, the cells were observed under the microscope and images of PKH^+ cells were taken at 480 nm and 550 nm excitation. The ratio ($R_{480/550}$) was calculated from the fluorescence at 480 nm before loading (F_{480b}) and the fluorescence at 550 nm before loading (F_{550b}). Cells were then loaded with Fluo-4. After loading, the real fluorescence (F_{480R}) from Fluo-4 was equal to the fluorescence at 480 nm after loading (F_{480a}) subtracted by the fluorescence at 550 nm after loading (F_{550a}) multiplied by the ratio ($R_{480/550}$). So the equation is: $F_{480R}= F_{480a}-F_{550a}*(F_{480b}/ F_{550b})$.

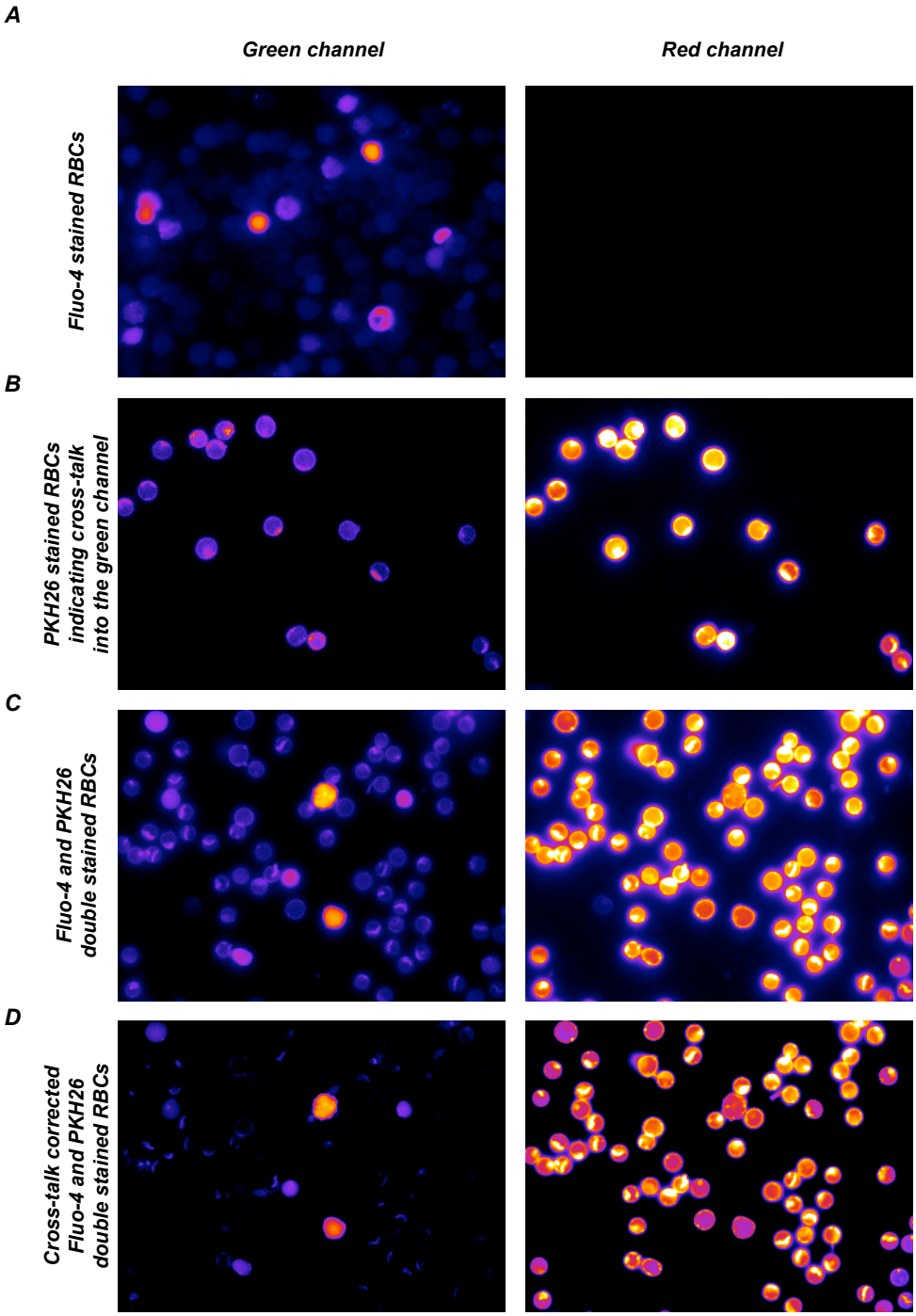

Figure 7: PKH26 background correction.

Double staining of mouse RBCs with Fluo-4 and PKH26. ***A****, Fluo-4-loaded cells do not show fluorescence bleed-through into the "red" recording channel.* ***B****, PKH26-stained cell recorded in the "red channel" depicted cross talk of 15% into the "green channel".* ***C****, Double-stained "raw images" in the green and red recording channels.* ***D,*** *Double-stained images [same as in (****C****)] after cross talk correction for the PKH26 crosstalk.*

2.3.6 Immunoblotting and gel staining

RBCs, HeLa and HEK293 cells were treated with desired stimulation protocol for 15 minutes, washed in Tyrode and lysed by EP Extraction Buffer (100 mM Tris-HCl, 100 mM NaCl, pH 7.5) supplemented with 0.5% Triton X-100, 20 mM DTT, Complete Protease Inhibitor cocktail and Phspho Stop (Roche Applied Science) on ice for 30 minutes. Then the whole cell lysates were centrifuged at 5,000 g for 10 minutes, and the supernant (membrane fragment) and precipitant (cytosol fragment) were individually separated on 12% polyacrylamide gels. For Western blotting, the proteins were transferred onto Nitrocellulose Transfer membranes (Protran, Whatman). Blots were incubated with goatpolyclonal anti-GAPDH (1:15,000, Santa Cruz Biotechnology, Inc., Dallas, Texas, U.S.A), rabbit polyclonal anti-Actin (1:10,000, LifeSpan BioScience, Inc., Seattle, WA), anti-LPAR 1 (1:2,000, LifeSpan BioScience, Inc., Seattle, WA), anti-LPAR 2 (1:1,000, LifeSpan BioScience, Inc., Seattle, WA), anti-LPAR 3 (1:1,000, LifeSpan BioScience, Inc., Seattle, WA), anti-LPAR 4 (1:1,000, Aviva Systems Biology, Corp. San Diego, CA) or anti-LPAR 5 (1:1,000, Aviva Systems Biology, Corp. San Diego, CA). Afterwards, blots were washed with phosphate buffered saline with 0.1% tween-20 (PBS-T) and incubated with horseradish peroxidase (HRP)-conjugated antibodies (1:5,000). Enhanced chemiluminescence (ECL) was used for detection of the bands. For gel staining, the gel was directly stained by Coomassie Brilliant Blue R250 overnight at room temperature and de-stained with acetic acid.

2.3.7 Immunostaining

For LPA receptors detection, RBCs were fixed with 2% PFA plus 0.0075% glutaraldehyde in Tyrode for 30minutes. Then cells were permeabilized with 0.3% Triton X-100 in Tyrode for 10 minutes, followed by centrifugationat 3700

g for 5 minutes. After blocking (5% BSA in Tyrode for 20 minutes), cells were incubated with the primary antibody, such as LPAR1-5 (1:50), in blocking buffer (5% BSA in Tyrode) for 4h in room temperature. Following 3 × washing Tyrode for 3 times, the cells were incubated with Alexa Fluor 488 goat anti-rabbit IgG (1:400; Molecular Probes, Eugene, OR) in Tyrode for 2h. Images were acquired with the Leica TSC SP5 confocal microscope.

For actin staining, human RBCs were treated either with 5 μM LPA for 15 minutes, or with CytoD at different concentration for 1 hour, and then fixed, permeabilized and blocked as described above. Cells were then stained with 50 nM Phalloidin for 15 minutes. Fluorescence images were acquired with the Leica TSC SP5 confocal microscope.

2.4 Data analysis

2.4.1 Image analysis

All images acquired with TillVision were analyzed with ImageJ (Wayne Rasband, NIH, Bethesda, USA) and custom-made macros (included in the supplementary CD-ROM). Each cell was marked as an individual "Region of Interest" (ROI) of which integrated/mean densities over time were extracted and stored. For RBCs and reticulocytes size quantification, each cell was also marked as an individual ROI, and the "area" value of each ROI were extracted and stored. The background correction of PKH26 images was described in chapter 2.3.5 and Figure 7.

2.4.2 Single trace of Ca^{2+} influx analysis

In this thesis, all Ca^{2+} signals measured with Fluo-4 were converted into self-ratios (F/F_0) before further analysis. Single fluorescence over time data from ROI was extracted in ImageJ. This output was further analyzed in Igor Pro (WaveMetrics Inc., Oregon, USA) running on custom-made macros. All

macros are included on the supplementary CD-ROM.

2.4.3 Statistical Analysis

All data are mean values of more than 100 cells from at least 3 independent experiments and 3 different animals and are presented as mean±SEM if not stated otherwise. The comparison between the experimental groups was performed using a normality test followed by the two-tailed Student's t-test, frequency distribution and one-way ANOVA for paired or unpaired samples (GraphPad Prism V5.0b, Inc., La Jolla, CA, USA). The level of statistical significance was set at $p<0.05$ (*), $p<0.01$ (**) or $p<0.001$ (***).

3. Results

RBCs are among the most intensively studied cells in natural history, elucidating numerous principles and groundbreaking knowledge in cell biology. Morphologically, RBCs are largely homogeneous, and most of the functional studies have been performed on large populations of cells, masking putative cellular variations. Therefore, we studied human and mouse RBCs by live-cell video imaging, which allowed single cells to be followed over time. We analyzed functional responses to hormonal stimulation with lysophosphatidic acid with the calcium sensor Fluo-4. Additionally, we developed an approach for analyzing the Ca^{2+} responses of RBCs that allowed the quantitative characterization of single-cell signals. Furthermore, using this method, we investigated the LPA induced Ca^{2+} signaling pathway, cytoskeleton change in RBCs and Ca^{2+} mediated aggregation of RBCs.

3.1 Single cell analysis

3.1.1 LPA induces Ca^{2+} influx into human RBCs

In blood serum LPA concentrations range from 1 to 10 µM [131, 132, 215, 216] while in the clot of RBCs levels as high as 20 µM have been reported [216].

In FACS experiments, LPA-stimulation of Fluo-4 loaded RBCs induced an increase in the intracellular $[Ca^{2+}]_i$ concentration (Figure 8A). In addition to the increase in the averaged Ca^{2+} concentration, the fraction of responding cells also increased as depicted in the right panel of Figure 8A. In video-imaging experiments, stimulation of cells with 1 µM LPA resulted in a slow increase in the intracellular $[Ca^{2+}]_i$ of individual RBCs (Figure 8B). This response reached a maximal plateau 15 minutes after LPA stimulation. To investigate the LPA responses further, I challenged RBCs with Tyrode, 1, 5, and 25 µM LPA and analyzed their responses. In Tyrode, no change in RBCs Fluo-4 fluorescence could be detected, while 5 and 25 µM LPA induce higher Ca^{2+} response than

1 µM LPA. Furthermore, to confirm the Ca^{2+} was not from Ca^{2+} pools inside the cell but from extracellular environment, I investigated LPA function in Ca^{2+} free condition (Figure 8C). Under this circumstance, LPA can not induce Ca^{2+} increase in RBCs. Taken together, these data demonstrate that LPA promotes the influx of extracellular Ca^{2+} into RBCs in a concentration dependent way.

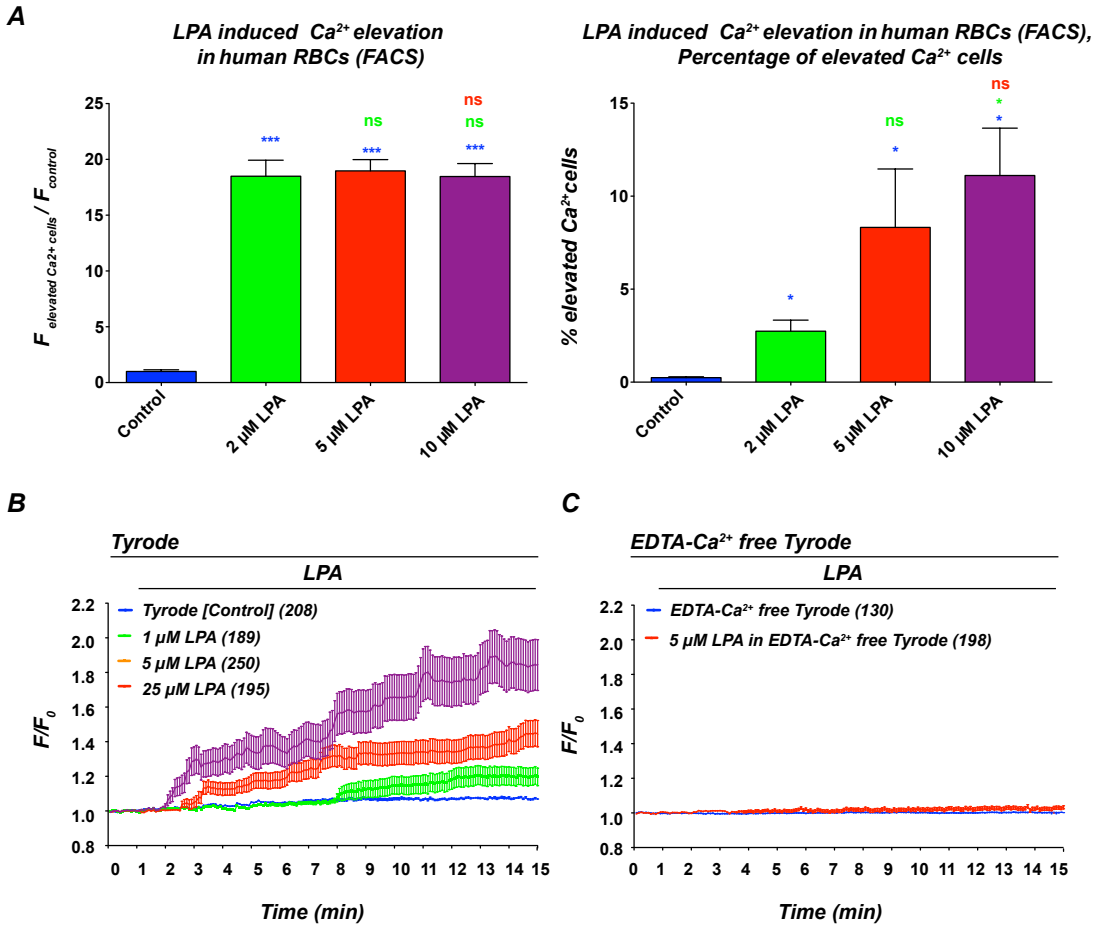

Figure 8: LPA induced Ca^{2+} influx in human RBCs.

A, *Flow cytometric analysis of the fraction of RBCs that respond to stimulation with LPA in 15 min.* ***B,*** *Effect of different concentrations of LPA on the kinetics of Ca^{2+} increase in human RBCs.* ***C****, Effect of LPA in Ca^{2+} free condition in human RBCs.*

3.1.2 Ca^{2+} influx induced by LPA is not homogenous among individual RBCs

Theanalysis of Ca^{2+} influx depicted in Figure 8 only presented the average response of all the RBCs in the experiment, but did not allow appreciation of single cell responses. In fact, although LPA can induce Ca^{2+} influx in RBCs from different donors (Figure 9A), single RBCs displayed individual responses (Figure 9B). Furthermore, even in Tyrode alone, there were few cells (~1%) showing Ca^{2+} influx (Figure 9C). In addition, on the level of individual cells the LPA response was not an all-or-none response, instead individual cells reacted with different delays, time courses and amplitudes (Figure 9D).

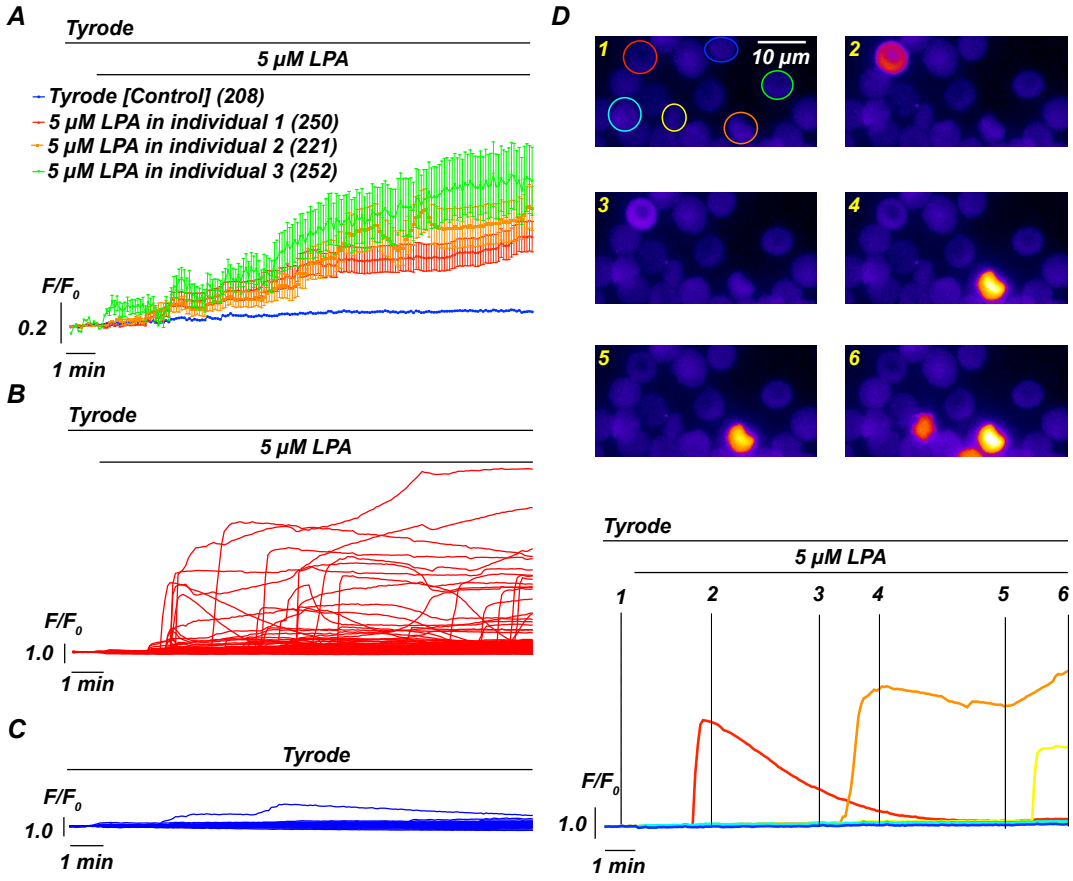

Figure 9: LPA induced Ca^{2+} responses are heterogeneous amongst individual RBCs.

A, *LPA induced Ca^{2+} responses in RBCs from 3 individual healthy donors indicating inter-individual variability.* ***B,*** *Original recordings of intracellular Ca^{2+} levels in Fluo4-loaded RBCsin response to 5 µM LPA. Time of incubation with LPA is shown. Cells are marked as regions of interest with colored circles. Changes in the normalized fluorescent intensity (F/F_0) are plotted below in the corresponding colors.* ***C,*** *Effect of Tyrode on human RBCs. Very few cells (~1%) showed Ca^{2+} influx signals.* ***D,*** *Single cell responses were very diverse. This panel depicts exemplified responses to LPA stimulation, ranging from no responses (blue and green traces) over delayed Ca transients with a plateau phase (yellow and orange traces) to fast and transient Ca responses (red trace).*

3.1.3 Different parameters to characterize and analyze LPA-induced Ca^{2+} influx

As depicted in Figure 9, LPA induced responses in RBCs show a great variability and thus analysis and characterization of such responses ought to be analyzed on a cell-to-cell basis. To foster analysis I standardized the responses and described their properties by fitting them applying the following equation:

$$y = 1 + (Amp - 1)\frac{x^{S_H}}{1 + x^{S_H} + (X_{half})^{S_H}}$$

From such a formular the following parameters could be deducted:

-) Amp: described the maximal amplitude of the Ca^{2+} response

-) X_{half}: depicted the time point at which half of the amplitude was reached

-) S_H: characterized the steepness of the Ca^{2+} increase

In addition to these parameters originating from the fitting process, I also deducted the following properties:

-) Max response: maximal $[Ca^{2+}]_i$ increase during the 15 minutes recording period

-) Reaction time: time from start of the stimulation to the onset of the $[Ca^{2+}]_i$ increase. For this parameter, the “onset” must be defined at first. As shown in in Figure 9A and Figure 11A, I calculated the mean value (Mean) and stand deviation (SD) for the entire control (Tyrode) trace, and used the value of meanplus 3 times SD as threshold. When the “F/F_0” value of single cell trace exceeds the threshold, this time point was considered asthe “onset” time point.

Taken together the collection of variables enumerated above offered a sufficient number of parameters to quantitatively describe and compare responses from RBCs under various conditions. To illustrate this, the various parameters are depicted on top of a typical RBCs response to LPA stimulation (Figure 10A).

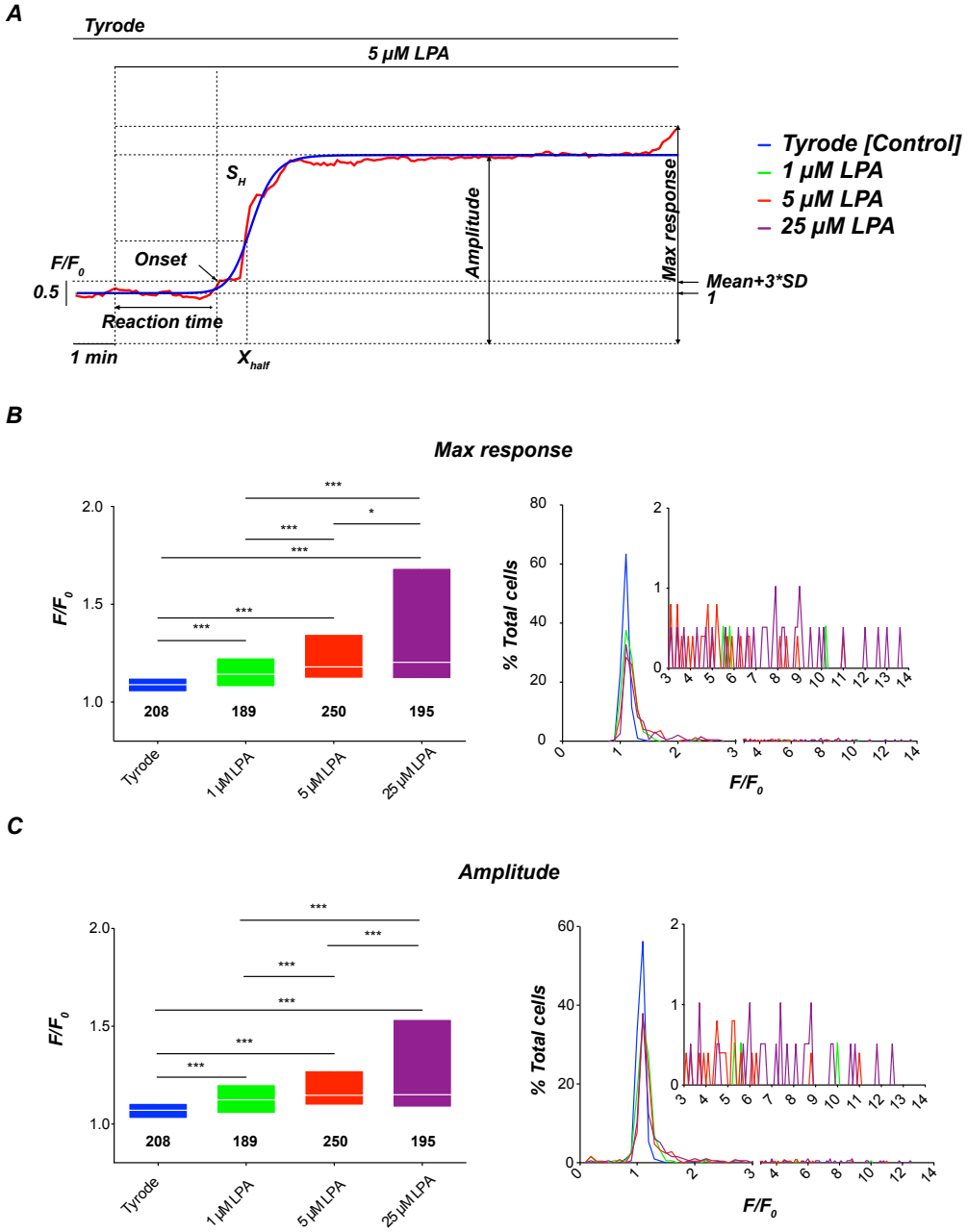

Figure 10: Characterization of single cell response.

***A**, Definition of different parameters. **B-C,** Statistical analysis of the parameters defined in **A**; the color-code for all diagrams is given in the right part of the panel. To avoid interindividual differences (see Figure 9A), all measurements were performed with freshly prepared samples from a single healthy donor. **B**, Maximal intensity of the cellular response within the period of measurement (max response). **C**, Value of the main plateau or the major peak of the Ca^{2+} response (amplitude). Parameters in **B** and **C** are derived from the total number of cells. The numbers below the boxes give the cell numbers taken from three blood samples.*

3.1.4 Definition of “Responding cells” and analysis

Because not all cells responded to LPA stimulation, a definition of “responding cells” is required. As shown in Figure 11A, I calculated the mean value (Mean) and stand deviation (SD) for the entire control (Tyrode) trace, and used the maximal value of mean plus 3 times SD as a threshold. If the “Amplitude” of a single cell trace exceeds the threshold, this cell was considered as a “responding cell” (red line), or otherwise, was considered as “non-responding cell” (green line). According to this criterion, the percentage of “responding cells” in 1, 5 and 25 μM LPA was 7%, 22% and 33%, respectively (Figure 11Ba). What needs to be pointed out is, that even in Tyrode, there are some cells showing Ca^{2+} influx (about 1%, Figure 9B). However, the reason is still unclear and it needs further investigation.

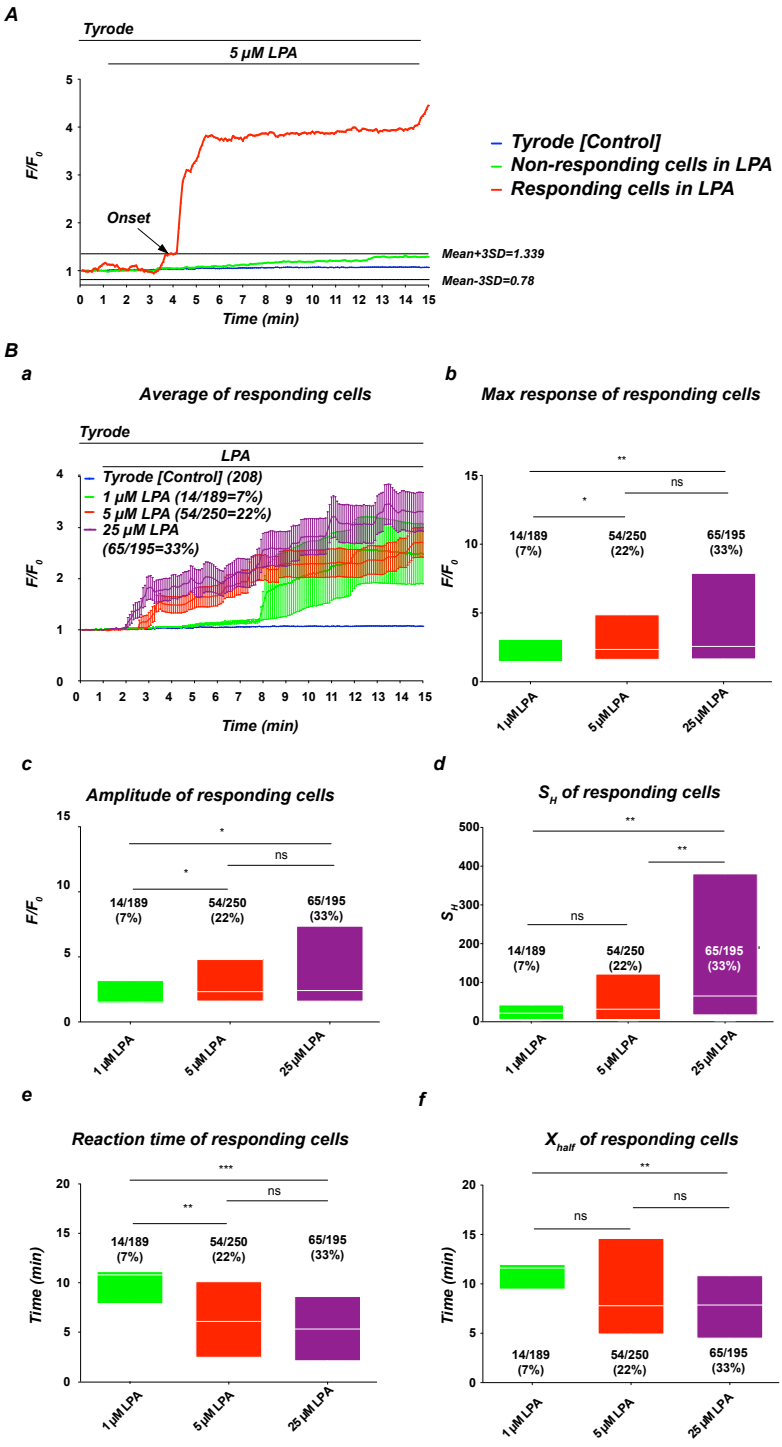

Figure 11: Parameters of responding cells in LPA induced Ca^{2+} influx.

***A**, Definition of responding cells in LPA stimulated RBCs. Responding cells: Amplitude of cell >Mean+3SD of Tyrode. **B**, Average of responding cells. According to the definition, there is 1% of cells that fall under "responders" even in Tyrode and ~7%, 23%, 33% in 1 µM, 5 µM, 25 µM LPA, respectively. **C**, Max response, Amplitude, S_H and X_{half} of responding cells in LPA and Tyrode did not show significant differences.*

3.1.5 Different RBCs cell age led to inhomogeneous Ca^{2+} influx

I already showed that Ca^{2+} influx induced by LPA in RBCs was inhomogeneous among individual cells, which cannot be extracted from traditional RBCs research methods, such as flux measurements. The mechanism is still unclear. In humans, RBCs are developing from committed stem cells, passed through a process named erythropoiesis, to get mature in about 7 days. When matured, these cells live in the blood circulation for about 100 to 120 days, and are removed from the circulation at the end of their lifespan. Therefore, I investigated the possibility that the inhomogeneous Ca^{2+} influx among individual cells might originate from differences in cell age.

To verify this hypothesis, the first step was to obtain RBCs populations of the same age. There are 2 principle ways to achieve this: 1) separation of RBCs of different age, by Percoll gradient centrifugation; or 2) induction of reticulocytosis to create a population of young cells, which can be followed in the aging process.

3.1.5.1 Percoll gradient centrifugation to separate young from old RBCs

Percoll is a kind of inert, polyvinyl propylene-coated colloidal silica particle. Under centrifugation force, it forms a gradient in which the different dense RBCs distribute [217]. Figure 12 showed a typical image of a centrifuge tube after centrifugation of RBCs in a Percoll gradient. Fraction 1 and 5 contained the youngest and oldest cells, respectively. Other fractions contained cells at various ages. The proteins from fractions were isolated from ghost cell membranes. According to Lutz and co-workers [120], the ratio of band 4.1a/4.1b could be used to distinguish the young and old cells. Young cells contain more band 4.1a; old cells contain more band 4.1b. On the SDS-PAGE, human RBC protein 4.1 could be resolved as two polypeptides 4.1a and 4.1b with 2 kDa difference in the C-terminal domain [218]. According to Inaba and co-workers [218], the molecular weights of band 4.1a and 4.1b are

81 and 79 kDa, respectively. However, some results indicate that percoll may activate receptors in RBCs, e.g. NMDA receptor, leading to perturbations in the ion equilibrium followed by volume and thus density changes that will interfere with the age separation process described above (Prof.Dr.Anna Bogdanova, personal communication). Therefore, I focused on the second method, induction of reticulocytosis and labeling of old RBCs.

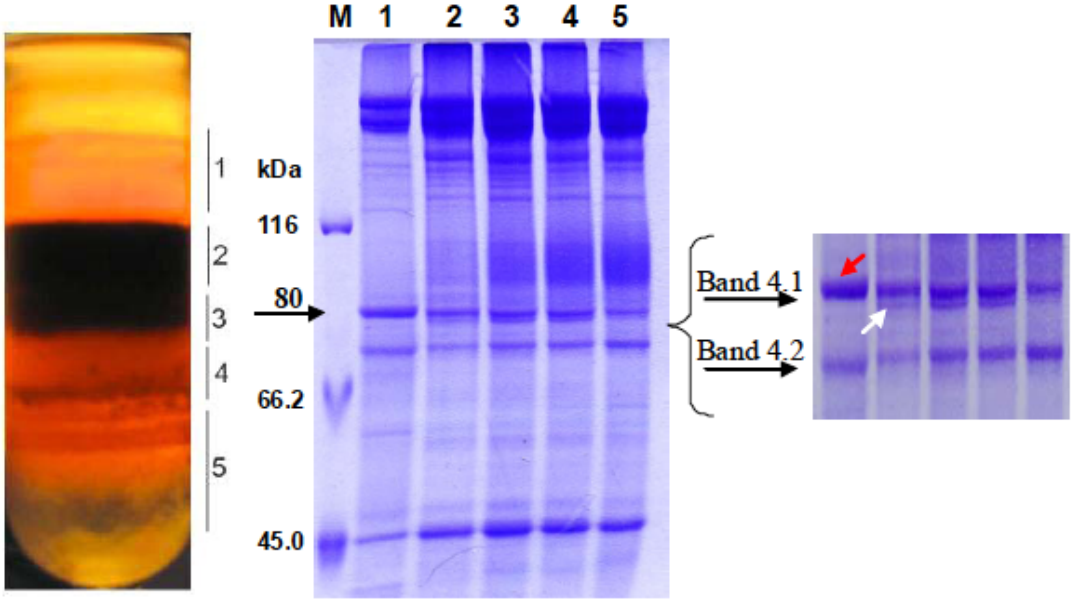

Figure 12: Separation of RBCs by Percoll gradient ultracentrifugation and SDS-Page of ghost membrane proteins of the different fractions.

Fractions (1-5) Left: A typical image of the centrifugation with 5 fractions containing cells at different age from 1-5: from the lightest to the heaviest cells (supposingthe youngest and the oldest cells). Middle: SDS-PAGE of proteins isolated from ghost cell membranes of different fractions. Right: A section of SDS-PAGE containing band 4.1a and 4.1b. The red arrow indicates band 4.1a; the white arrow indicates band 4.1b. Taken from thesis of Dr. Duc Bach Nguyen, 2010 with permission.

3.1.5.2 Induction of reticulocytosis by phenylhydrazine injection

The notion behind approach (2) was to use reticulocytosis to generate a population of young RBCs and follow the young cells over time. There are several options to achieve reticulocytosis: (A) pharmacological manipulation, such as erythropoietin injection or phenylhydrazine injection. The

erythropoietin can both increase the production of RBCs and promote survival of RBCs progenitors and precursors through protecting these cells from apoptosis [219-221]. The mechanismof phenylhydrazine is to cause hemolysis in mice to induce generation of new RBCs by the hematopoietic system [222-224]. (B) Physical interventions, such as repetitive bleeding.

Because erythropoietin itself can cause Ca^{2+} influx in RBCs [225], I investigated phenylhydrazine injection. But I found phenylhydrazine injection will lead to abnormal RBCs generation. The generated cells showed extremely inhomogeneous shape and size (Figure 13A). Furthermore, these cells were very fragile under LPA stimulation (Figure 13Ba, green arrows) and showed abnormal Ca^{2+} influx under control conditions (Figure 13Ba, Tyrode).

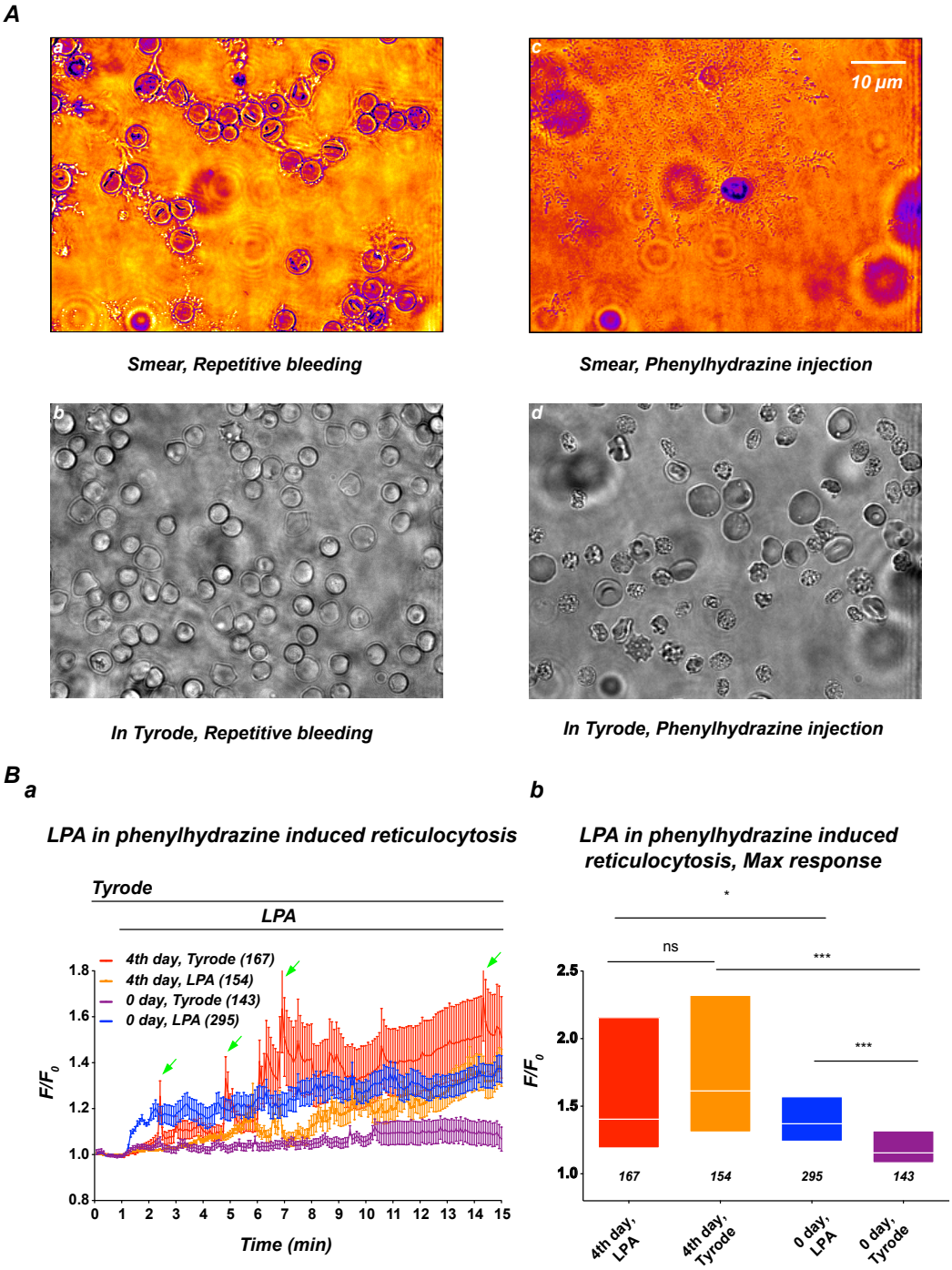

Figure 13: Phenylhydrazine induced reticulocytosis.

***A**, RBCs from phenylhydrazine-treatedmice (a, b) are more fragile in NMB stained smear and show abnormal cell shape in Tyrode compared with RBCs induced by repetitive bleeding(c, d). **B**, Mouse RBCs treated with phenylhydrazine showed abnormal Ca^{2+} influx. Cells from mice 4 days after phenylhydrazine injection (4^{th} Day) were fragile and easily broke, which led to abnormal peaks in the curve (green arrows). These cells also show abnormal Ca^{2+} influx even under control conditions (in Tyrode).*

3.1.5.3 Retro-orbital repetitive bleeding

Because of the results described above, I used retro-orbital repetitive bleeding to induce reticulocytosis. The method is described in detail above (In Materials and Methods). Reticulocytes contain a mesh-like reticular network of ribosomal RNA, which can be visualized by staining with new methylene blue (NMB). Furthermore, reticulocytes are slightly bigger than RBCs (Figure 14A). 5 days after bleeding, reticulocyte counts were determined on smears stained with NMB and revealed a ~32% rate of reticulocyte-positive cells**.** Blood samples from the same mouse before bleeding served as controls. Cell size difference between reticulocytes and RBCs are also quantified in Figure 14B.

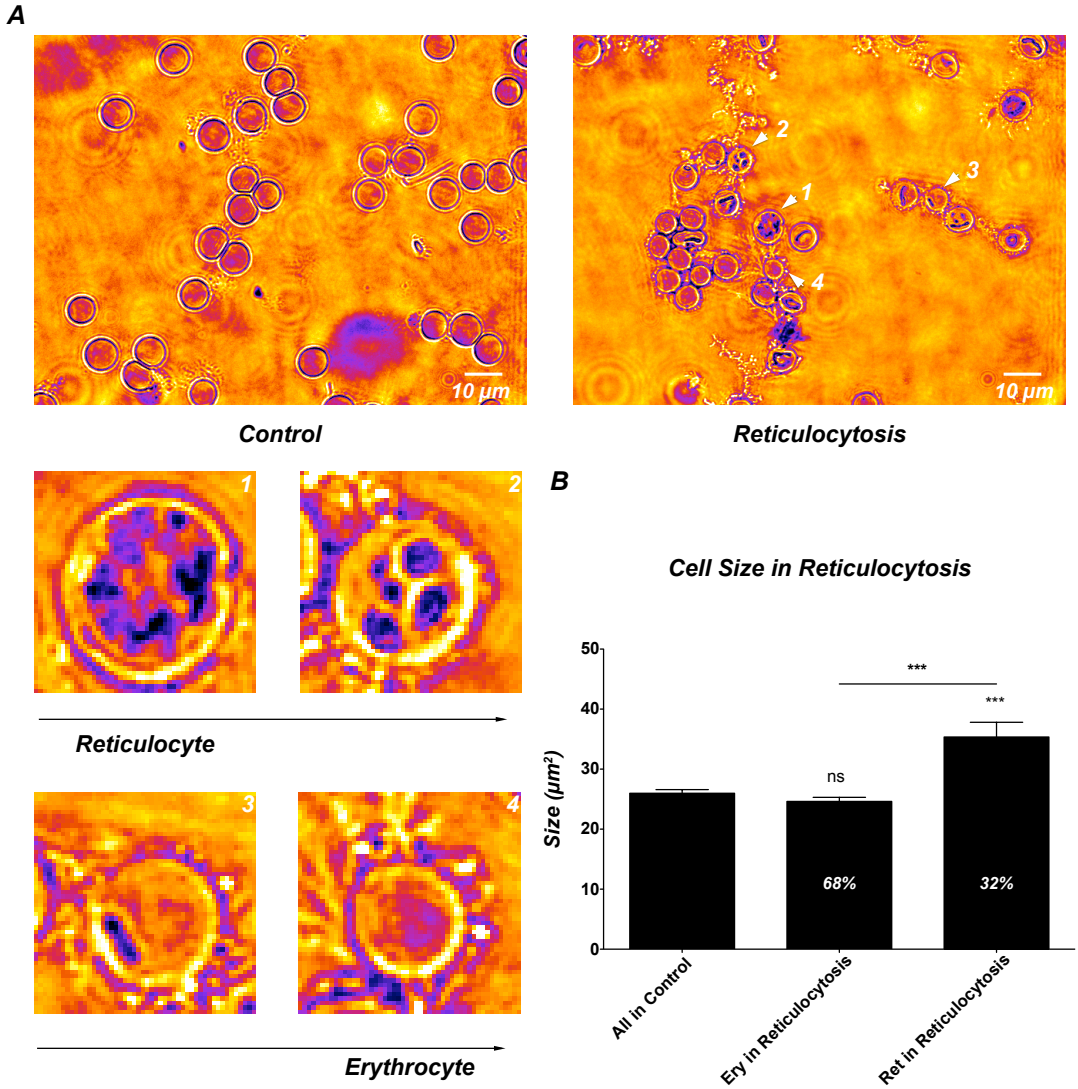

Figure 14: Induction of reticulocytosis and staining of reticulocytes with New Methylene Blue.

A, *The images depict typical samples of blood smear stains under control conditions (left image) and after induction of a reticulocytosis (right image). The cells marked 1-4 (enlargements of the cells marked with arrows in* ***A****) show the developmental stages fromreticulocytes to adult RBCs.* ***B****, The cell size difference between reticulocytes and RBCs was also quantified by ImagJ software.*

3.1.5.4 LPA induced Ca^{2+}-signals inreticulocytes from mice with reticulocytosis

In blood samples from mice receiving iron and folate supplement, NMB staining indicated that around one third (32%) of all blood cells were reticulocytes as measured 5 days after the initial bleeding (Figure 14B). Figure 15A depicts that LPA induced lower Ca^{2+} influx in RBCs at the day 3 after bleeding than at the day 1 (before bleeding). At day 5, RBCs even showed a much lower Ca^{2+} influx compared with day 3 (Figure 15Ba). Both the max response and the amplitude showed significance between RBCs from day 1, day 3 and day 5 (Figure 15Bb and Bc). In brief, during the 5 days, the percentage of reticulocytes in RBCs increased, but the average, max response and amplitude value of Ca^{2+} influx decreased. These results suggest that reticulocytes are less sensitive to LPA stimulation.

To verify this, I used NMB to stain RBCs after LPA stimulation to identify reticulocytes. In Figure 15C, it can be seen that upon LPA stimulation NMB positive RBCs (reticulocytes) showed no Ca^{2+} influx, but the NMB negative RBCs showed high Ca^{2+} influx. From these data I concluded that reticulocytes were apparently less sensitive towards LPA stimulation than more mature RBCs.

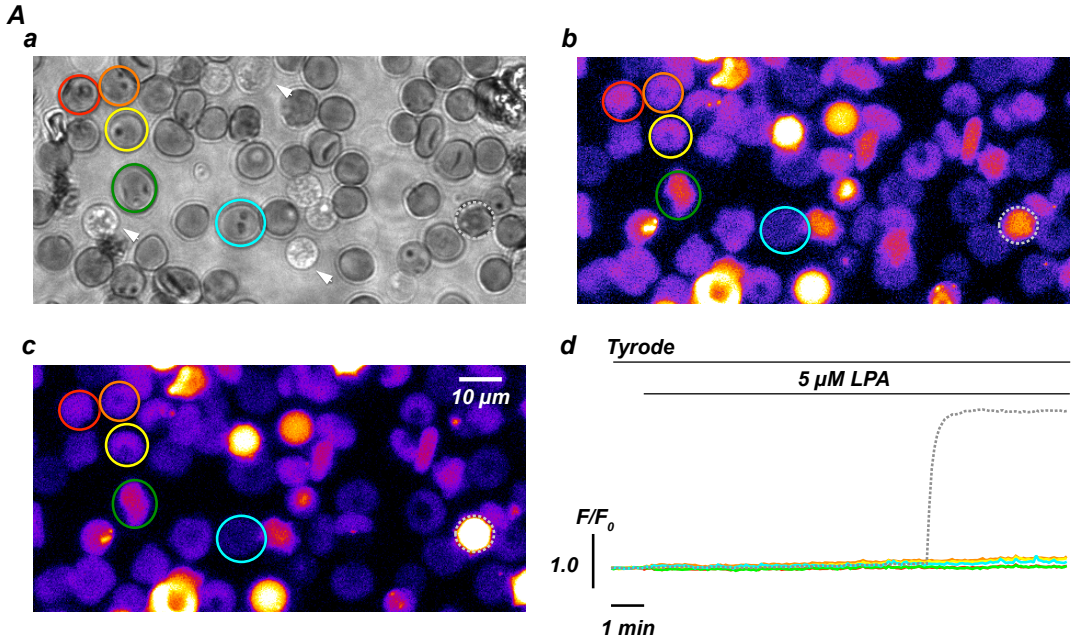

Figure 15A: Reticulocytes shows lower sensitivity to LPA.

A, *(a) shows NMB stained cells in bright field after LPA stimulation. The colored regions depict reticulocytes analyzed in (d) and the arrowheads point to lysed RBCs. (b) and (c) show the cells before and after the LPA stimulation, respectively. In (d), one can see there was no* Ca^{2+} *increase by LPA stimulation in labeled reticulocytes.*

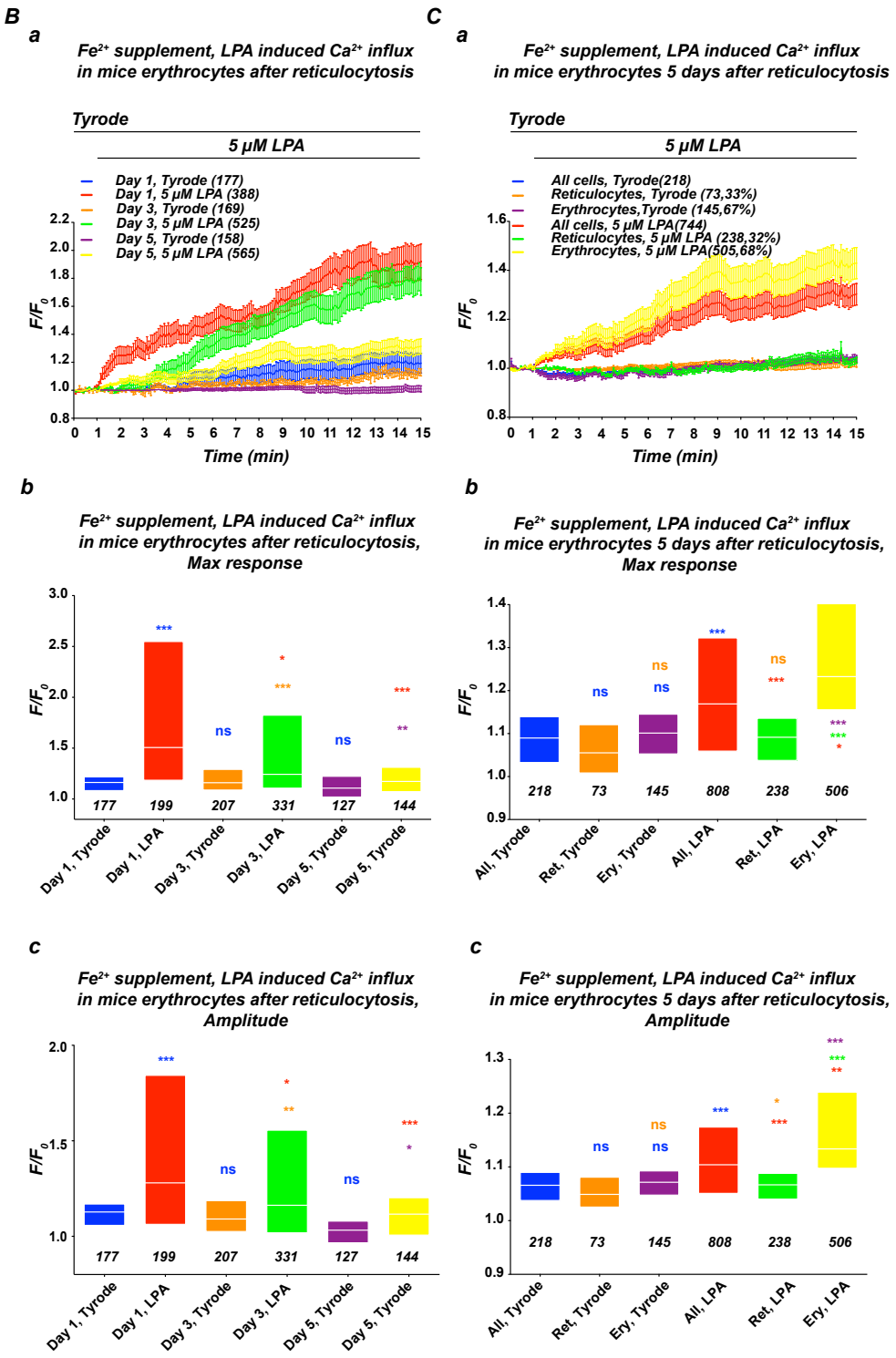

Figure 15B-C: Reticulocytes shows lower sensitivity to LPA.

B, *With supplement of Fe^{2+} and folate, counts of reticulocytes increased to 32% at day 5 and lead to a decrease of the Ca^{2+} influx compared with samples from day 3 and control (day 1, before reticulocytosis).* ***C,*** *Reticulocytes were not sensitive to LPA.*

3.1.5.5 Ca^{2+} influx in old RBCs

As described above, separation of old RBCs by centrifugation with percoll gradient diaplayed significant disadvantages, thus I introduced an additional protocol to obtain old RBCs. PKH26 is a dye for general cell membrane labeling and has been characterized in a number of model systems, such as *in vitro* cell labeling, *in vitro* proliferation studies and long term, *in vivo* cell tracking [226]. The half-life of PKH26 labeled rabbit RBCs is greater than 100 days [227]. PKH26 is a red fluorochrome, with an excitation maxium at 551 nm and an emission maxium at 567 nm [228]. It could thus be used together with Fluo-4. However, PKH26 could also be excited by the 480 nm laser line and has crosstalk into the Fluo-4 recording channel. Therefore, a background correction was made to remove the crosstalk (in Materials and Methods, Figure 7).

To identify old RBCs at the verge of clearance, we drew blood from mice to induce reticulocytosis. At day 5, blood was drawn from the reticulocytosis mice and RBCs were stained with the plasma membrane stain PKH26 [229]. And then these cells were re-injected into the same mouse. Analyzed by flow cytometry, at least 67.9% of the cells were stained with PKH26 (Figure 16Ab). The fluorescence of the cells was analyzed again after 7 and 43 days (Figure 16A, lower panels). After 7 days in circulation, 5.7% of cells were PKH26-stained; after 43 days, this portion was reduced to less than 1%, indicating that the rest of the PKH26 positive RBCs were cleared in the mouse body. Because the average lifetime of RBCs in BALB/c mice was reported to be 46 days [230], we waited for 43 days until we isolated PKH26-stained RBCs by fluorescence activated cell sorting (region R2 in Figure 16A). Those cells were regarded as old cells close to clearance. Ca^{2+} signals were compared to non-stained RBCs representing cells of all ages. Figure 17 B-D summarizes the results obtained with these two cell populations. PKH26-negative cells responded only with a very small but significant increase when stimulated with 5 µM LPA (green box in Figure 16B). In contrast, the PKH26-positive cells

that were manually selected from the original blood sample (purple box in Figure 16B) and the PKH26-positive cells enriched by FACS (red box in Figure 16B) both displayed a substantially augmented Ca^{2+} response. Nevertheless, neither visually identified PKH^{+} cells (VIS) nor FACS sorted cells showed LPA responses that were uniform. Instead, both populations of responders still displayed a substantial heterogeneity, as observed in the response histograms in Figure 16C and in the representative traces in Figure 16D.

In summary, the age of RBCs appeared to be an important factor responsible for the heterogeneity of LPA-induced responses. However, our data also indicate that the age of RBCs is not the only characteristic responsible for the observed variability.

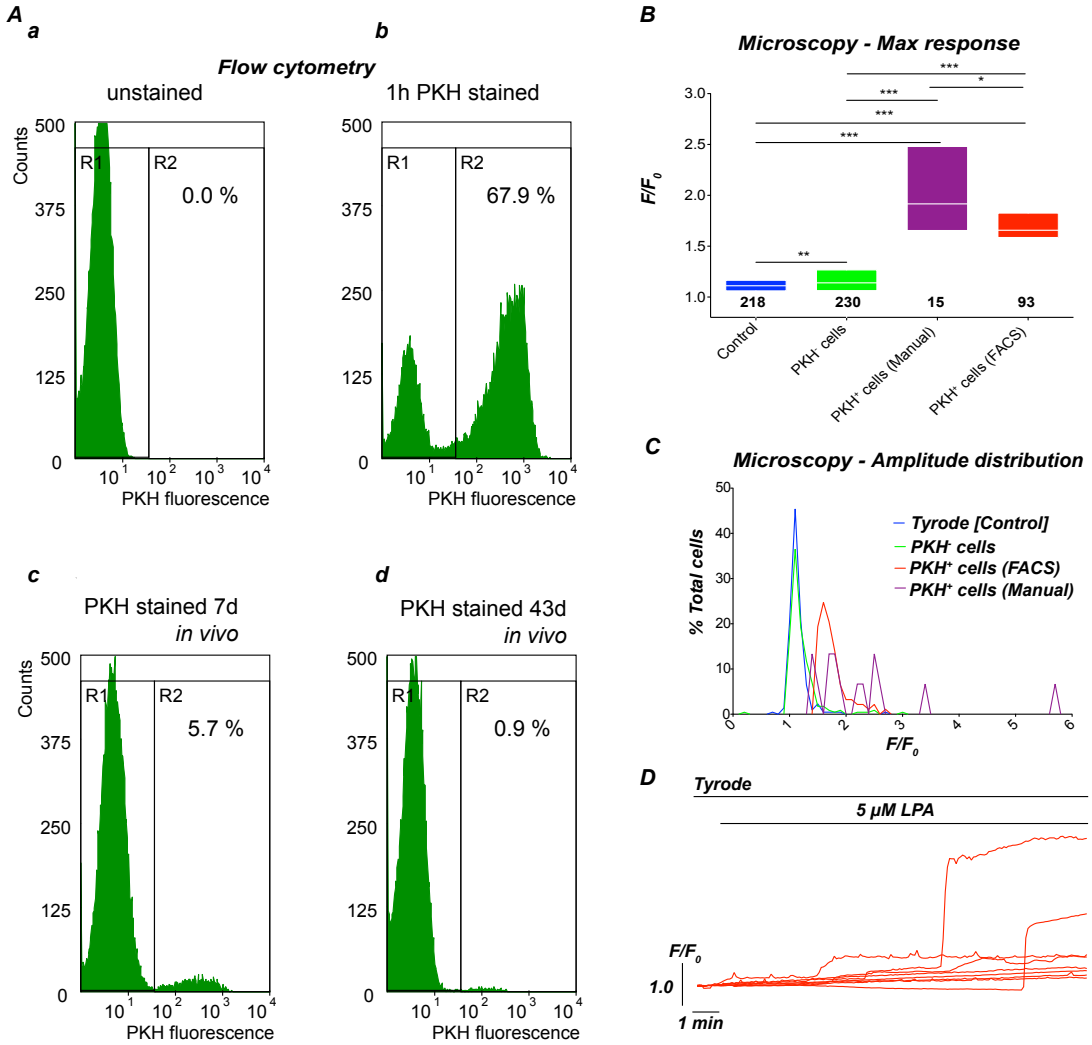

Figure 16: Response of old RBCs to LPA stimulation.

A, *Analysis of PKH26 fluorescence of 20,000 RBCs by flow cytometry before (a) and 1 hour after staining with PKH26 (b). After the staining procedure, the cells were re-injected into the same mice and analyzed 7 days (c) and 43 days (d) later. The percentage of PKH26 labeled cells (PKH(+), region R2) is indicated.* ***B,*** *Control and LPA stimulation experiments were performed on PKH26-positive (+) and PKH26-negative (-) RBCs. The maximal response under the different conditions is given. We discriminated between PKH(+) cells identified directly under the microscope (VIS, low in number) and RBCs sorted by FACS. The numbers below the boxes give the cell numbers taken from three mice.* ***C,*** *Amplitude histogram of the RBC treated under the conditions mentioned in* ***B****.* ***D,*** *Representative intensity traces of PKH(+) cells stimulated with 5 µM LPA revealing a high heterogeneity also in old RBCs.*

3.2 The signaling pathway from LPA to Ca^{2+} in RBCs

In chapter 3.1, we already concluded that LPA could induce Ca^{2+} influx in human RBCs. The next question is, how LPA induces the Ca^{2+} influx? For this, according to the literature, LPA opens a Ca^{2+} channel in human RBCs [32], while TRPC6 is thought as a Ca^{2+} permeable non-selective cation channel [149]. Furthermore, TRPC6 also contributes to the Ca^{2+} leak in human RBCs [73]. Another clue is that LPA stimulates Ca^{2+} entry through channels with characteristics similar to TRPC3 in B-lymphoblasts [231]. Therefore, TRPC6 appeared as a good candidate for RBCs cation channel in which the LPA-induced Ca^{2+} influx is involved. Because there is no TRPC6 deficiency model available in human RBCs, I investigated LPA-induced Ca^{2+} influx in RBCs from TRPC6 knock out mice.

3.2.1 Characterization of TRPC6 knock out mice

TRPC6 knock out mice were kindly provided by Prof. Marc Freichel (Ruprecht-Karls University of Heidelberg, Institute for Pharmacology, Heidelberg) and Prof. Veit Flockerzi (Saarland University, Institute for Pharmacology, Homburg). TRPC6 KO was established from the first generation offspring between C57Bl6/N and 129Svj mice because these mice had a genetic background that could be used as control for the TRPC deficient mouse lines available in the laboratory of Prof. Marc Freichel. To explore whether TRPC6 channels were expressed in mouse RBCs, Western blot was used as the method of choice in knock out (KO) and wild type (WT) mice. TRPC6 protein was detected in RBCs from $TRPC6^{(+/+)}$ but not from $TRPC6^{(-/-)}$ mice by Western blot using the mTRPC6-specific antibody 861 (Figure 17, cited from [73] and with kind permission from Karger).

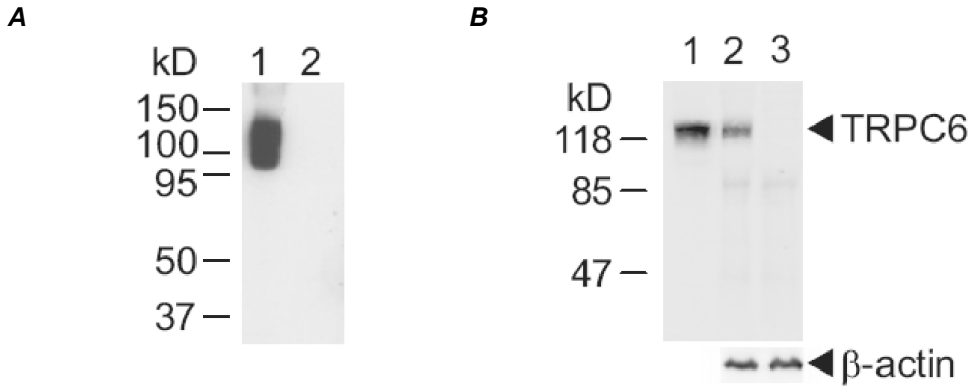

Figure 17: TRPC6 expression in mouse RBCs.

Immunoblotting of the TRPC6 protein in mouse RBCs using anti-TRPC6 antibody 861. ***A,*** *shows the western blot of TRPC6 transfected (lane 1) and shows untransfected COS 7 cells (lane 2).* ***B,*** *Western blot ofmembrane proteins from lung (lane 1), RBCs from wild type mouse (lane 2), and RBCs from TRPC6$^{(-/-)}$ mouse (lane 3). Cited from [73] and with kind permission from Karger).*

3.2.2 TRPC6 contributes to LPA induced Ca^{2+} influx

Ca^{2+} imaging and single cell analysis described in chapter 3.1 were selected to analyze the role of TRPC6 channels in Ca^{2+} influx in RBCs. To confirm that, the single cell analysis was used in mouse RBCs, concentration gradients of LPA were applied to mouse RBCs, and max response values of Ca^{2+} traces under each concentration were analyzed by sigle cell analysis (Figure 18Aa). The EC_{50} of LPA in mouse RBCs was ~3.3 μM, which was similar in human RBCs (~5.0 μM, [232]). To investigate the relation between LPA-induced Ca^{2+} influx and the TRPC6 channel, 5 μM LPA wereapplied to RBCs from mice lacking functional TRPC6 (TRPC6$^{-/-}$) and their wild type littermates (WT, TRPC6$^{+/+}$). In Figure 18Ab, the stimulation of Fluo-4 loaded RBCs with 5 μM LPA induced Ca^{2+} increase in RBCs of wild type mice. In TRPC6$^{(-/-)}$ mouse RBCs, 5 μM LPA also led to Ca^{2+} increase compared with control conditions in Tyrode, but amplitude and max response of LPA-induced Ca^{2+} signal in these cells showed a significant difference compared with RBCs from wild type mice (Figure 18Ab). If I used 5 μM PGE_2, it also resulted in a Ca^{2+} influx

in WT mice, but not in TRPC6 $^{(-/-)}$ mice (Figure 18B). To exclude the species difference, I also applied LPA and PGE_2 in human RBCs. In human RBCs, LPA and PGE_2-induced Ca^{2+} influx also showed significance (Figure 18C). These results suggested that TRPC6 only partly contributed to LPA-induced Ca^{2+} influx. In contrast, in PGE_2-induced Ca^{2+} influx, TRPC6 was the only channel involved in this signal pathway. In summary, these data demonstrated that TRPC6 was involved in LPA-induced Ca^{2+} influx into RBCs, but other signal pathway also existed in this procedure. It was different from PGE_2-induced Ca^{2+} influx, which TRPC6 was the only channel involved in.

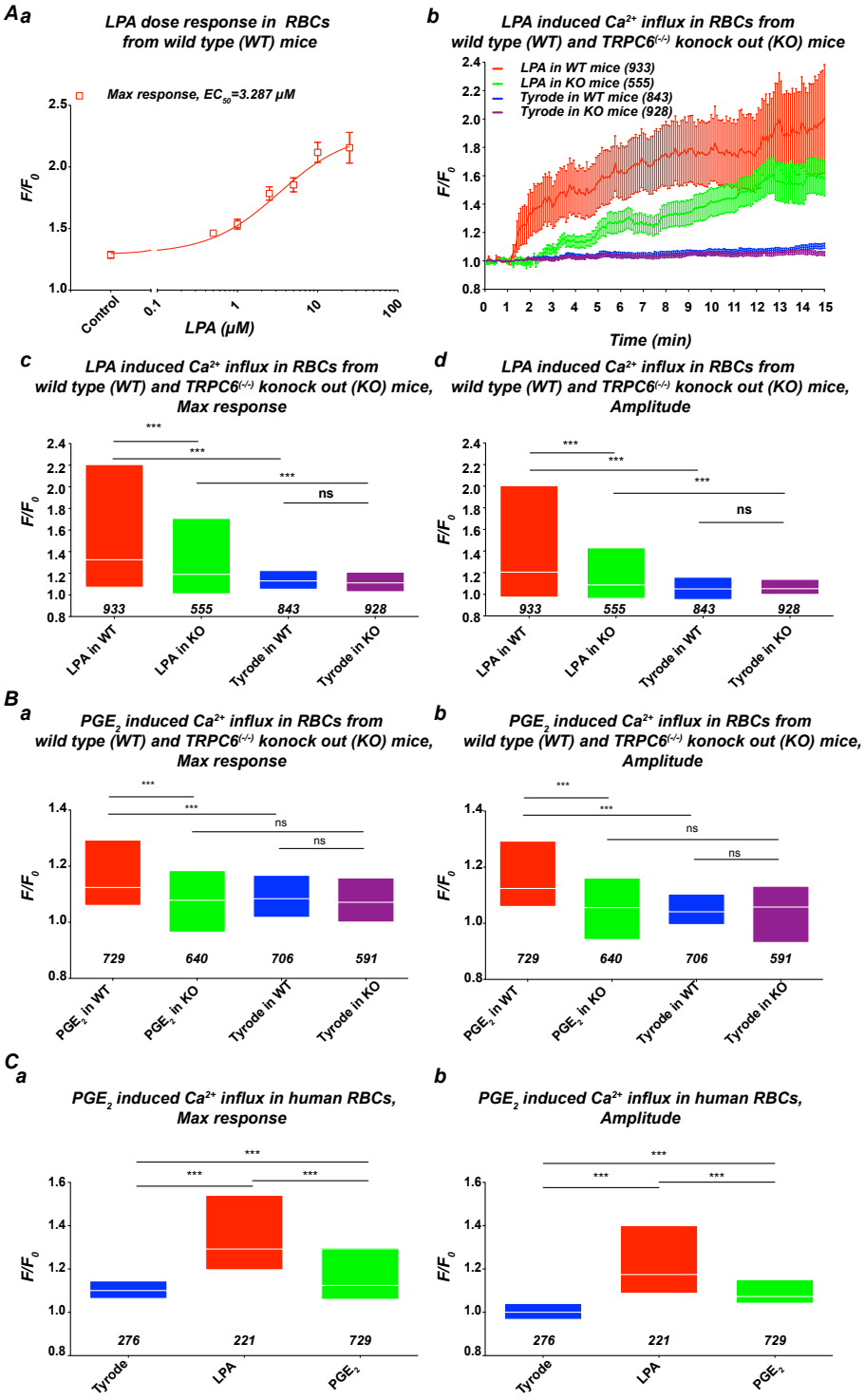

Figure 18: LPA and PGE_2 in wild type and TRPC6$^{(-/-)}$ mice and human RBCs.

***A**, (a) Dose response of LPA induced Ca^{2+} influx in mouse RBCs. Mean normalized increase (b), max response (c) and amplitude (d) of RBCs in TRPC6$^{(-/-)}$ or wild type mice induced by LPA (5 µM) in Fluo-4 fluorescence. **B,** PGE_2 (5 µM) induced Ca^{2+} influx in in TRPC6$^{(-/-)}$ or wild type mice and **C,** in human.*

3.2.3 Expression of LPA Receptor subtypes in RBCs

It was already shown that LPA-induced Ca^{2+} influx was channel mediated and receptor dependent rather than leak promoted [32]. Therefore, I investigated the expression of LPA receptors (LPARs) in RBCs. Because RBCs lack DNA, reverse transcription-polymerase chain reaction (RT-PCR) could not be used to investigate the existence of LPA receptors. Therefore, I used protein-based method like Western blot and immunostaining. LPAR1-5 distribution in human RBCs were shown by Western blot (Figure 19A) and immunostaining (Figure 19B). In Western blot, HeLa cell lysates (Figure 19Aa) and HEK293 cell lysates (Figure 19Ab-Af) were used as a positive control of LPAR1-5 antibody. After the detection of LPARs, the blot membranes were stripped and re-incubated with actin antibody, which was used as a control of loading quantity of protein sample. Western blot and immunostaining results both revealed that the LPAR1 subtype was expressed predominantly (Figure 19Ab and Bb) both in RBCs and HEK293 cells. LPAR2 was also found in Western blot (Figure 19Ac), and immunostaining revealed a“cluster-like” distribution of LPAR2 in RBCs (Figure 19Bc). LPAR3 showed very low presence in Western blot results (Figure 19Ad), but interestingly, ~3% of RBCs showed positive LPAR3 immunostaining (Figure 19Bd). Additionally, even in HEK293 cells, LPAR3 could not be found (Figure 19Bd). Although it was weak, LPAR4 also showed positive results both in immunostaining and Western blot (Figure 19Ae and Be). LPAR5 was neither detectable in Western blot nor in immunostaing (Figure 19Af and Bf).

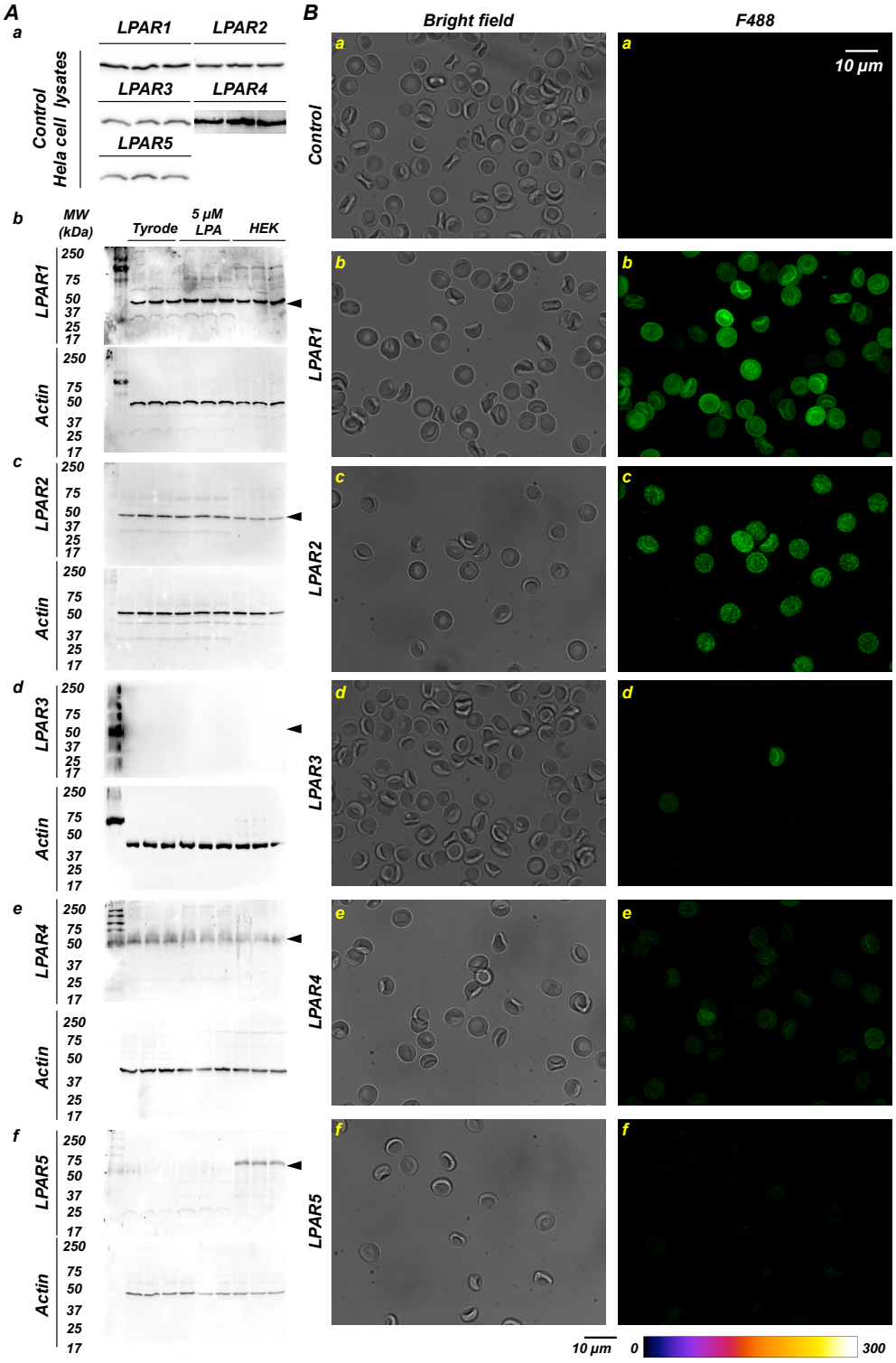

Figure 19: LPA receptors in human RBCs.

A, *Immunoblotting in human RBCs. (a) shows the antibody efficiency in HeLa cell lysates. (b) shows the immunoblotting results to identify the existence of LPA receptor 1, 2, 3, 4 and 5 in human RBCs. Black arrows show the theoretical position of target proteins.* ***B,*** *Immunostaining in human RBCs.*

3.2.4 LPA receptor activation is through G_i protein both in human and mouse RBCs

The effects of LPA at physiological concentrations were in general mediated through five well-described G protein-coupled receptors (LPAR1-LPAR5) and perhaps by additional recently proposed or as yet unidentified receptors [233, 234]. Downstream responses of LPA include elevation of cytosolic free Ca^{2+} concentration ($[Ca^{2+}]_i$), activation of Ras and extracellular signal-regulated kinases (ERK), and phosphatidylinositol 3-kinase (PI_3-K)/Akt signaling [235]. Therefore, I investigated the putative involvement of G protein in LPA induced Ca^{2+} influx in human and mouse RBCs. Human RBCs were stimulated with the broad G protein activator AlF_4^-, and induced extremely high Ca^{2+} influx when compared with LPA and Tyrode control (Figure 21A). These data suggested the possible involvement of G-proteins in the activation of LPA or PGE_2 evoked Ca^{2+} influx.

G proteins are trimeric and comprise a G_α and tightly associated G_β and G_γ subunits. There are 7 classes of G_α subunits, such as $G_s\alpha$ (G stimulatory), $G_i\alpha$ (G inhibitory), $G_o\alpha$ (G other), $G_{q/11}\alpha$, and $G_{12/13}\alpha$, which define different G proteins. They behave differently in the recognition of the effector, but share a similar mechanism of activation. Because I had access to $G_{11}\alpha$ knock out ($G_{11}^{(-/-)}$) mice, I investigated the putative involvement of G_{11} proteins in the signaling pathway leading to Ca^{2+} influx in mouse RBCs. For this, I used LPA to stimulate RBCs from $G_{11}^{(-/-)}$ mice. Figure 20B showed that 5 µM LPA lead to Ca^{2+} influx both in wild type and $G_{11}^{(-/-)}$ mouse RBCs, and there were no significant difference between WT and KO mice, which suggests $G_{11}\alpha$ is not involved in LPA induced Ca^{2+} signal in RBCs.

I further examined the effect of pertussis toxin (PTX), a specific inhibitor of G_i proteins. RBCs were pre-incubated with PTX (1 µg/ml) or its vehicle (Control) at 37°C for 1 h and subsequently treated with LPA (5 µM). The LPA evoked Ca^{2+} rise was abolished in PTX-treated cells when compared to responses

seen in non-treated RBCs (Figure 20C). In human RBCs, 5 µg/ml PTX was sufficient to fully inhibit Ca^{2+} influx induced by 5 µM LPA. These data indicated the involvement of G_i in LPA induced elevation of $[Ca^{2+}]_i$.

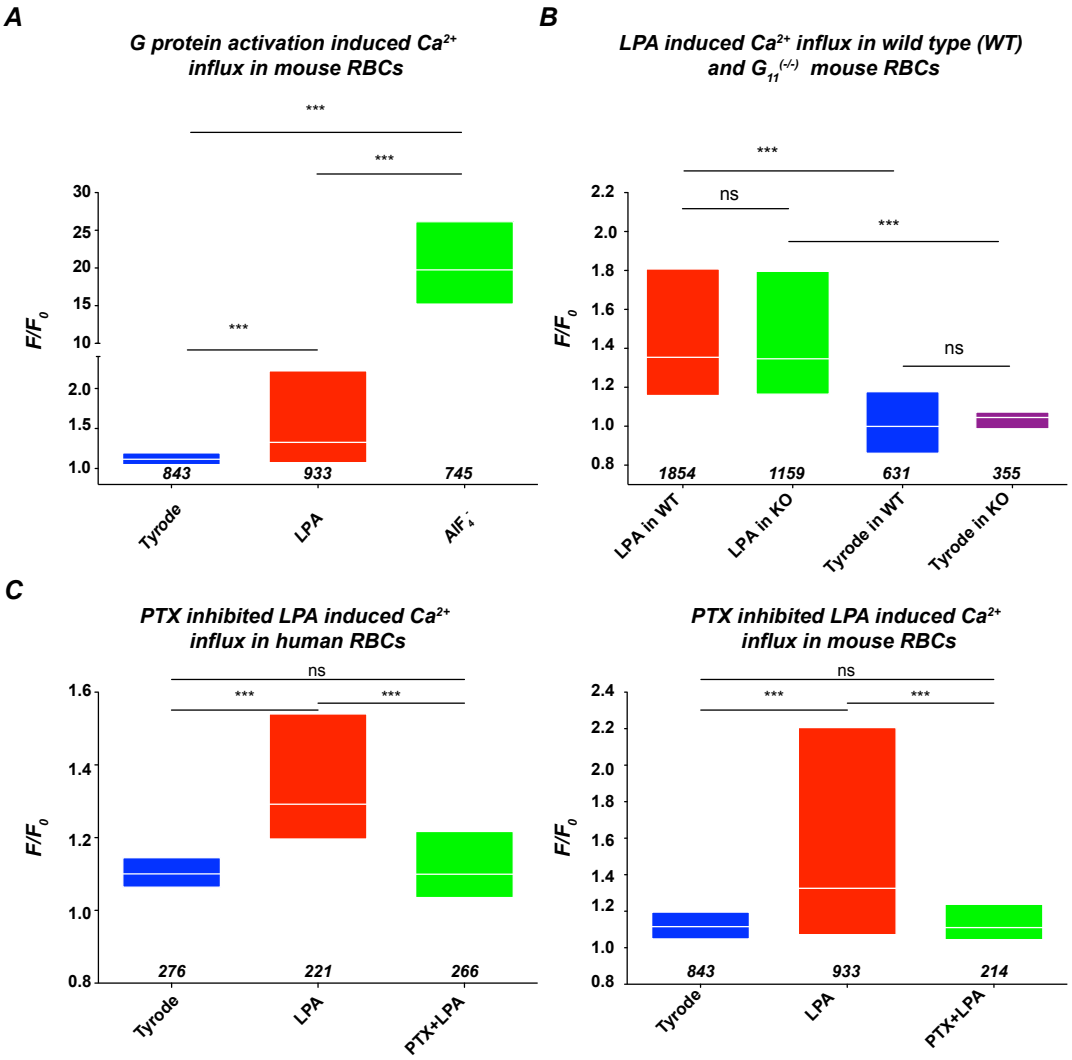

Figure 20: LPA receptors activation through G_i protein both in human and mouse RBCs.

A, *G protein activation induced Ca^{2+} influx.* ***B,*** *$G_{11}\alpha$ is not involved in LPA induced Ca^{2+} influx.* ***C,*** *$G_i\alpha$ is involved in LPA induced Ca^{2+} influx both in human and mouse RBCs.*

3.2.5 PI_3K is involved in the LPA signal pathway in human and mouse RBCs

LPA receptor activation can induce a range of cellular responses, such as cell proliferation, cell migration, cytoskeletal changes and apoptosis; cell to cell contact through serum-response element activation, Ca^{2+} mobilization, and adenylyl cyclase inhibition; and activation of mitogen-activated protein kinase, phospholipase C, Akt, PI_3K/Akt signaling [235] and Rho pathways [233, 234]. Some evidence suggests that LPA signaling might interact with other pathways. For example, LPA mediated signaling was reported to provide inhibitory effects on epidermal growth factor (EGF) induced migration and invasion of pancreatic cancer cells through the $G\alpha_{12/13}$/Rho pathway [236]. Downstream responses of LPA include elevation of cytosolic free Ca^{2+} concentration ($[Ca^{2+}]_i$), activation of Ras and extracellular signal-regulated kinases (ERK), and phosphatidylinositol 3-kinase (PI_3-K)/Akt signaling.

Because I already proved that G_i was involved in LPA-induced Ca^{2+} influx in RBCs, and PI_3K/Akt signaling was reported to be downstream responses of G_i activation in CHO cells [237], ovarian cancer cells [238] and cervical cancer cells [239], it is reasonable to assume that PI_3K is the downstream protein of G_i activation in RBCs. To investigate whether PI_3K might beinvolved in LPA induced Ca^{2+} influx in RBCs, Wortmannin, a widely used inhibitor for PI_3Ks, was tested against PI_3K. Pre-incubation with 5 μM Wortmanninat 37°C for 30 minutes caused a significantly decreased Ca^{2+} influx following LPA stimulation (Figure 21A). 5μM Wortmannin caused complete inhibition of LPA activity in $TRPC6^{(-/-)}$ mice. But in wild type mice, Wortmannin could only partly inhibit LPA induced Ca^{2+} influx (Figure 21B). These data suggests two coexisting signal pathways to induced LPA-evoked Ca^{2+} influx: one is TRPC6 channel dependent, but not PI_3K involved; another one is PI_3K dependent, but does not involve TRPC6 channel.

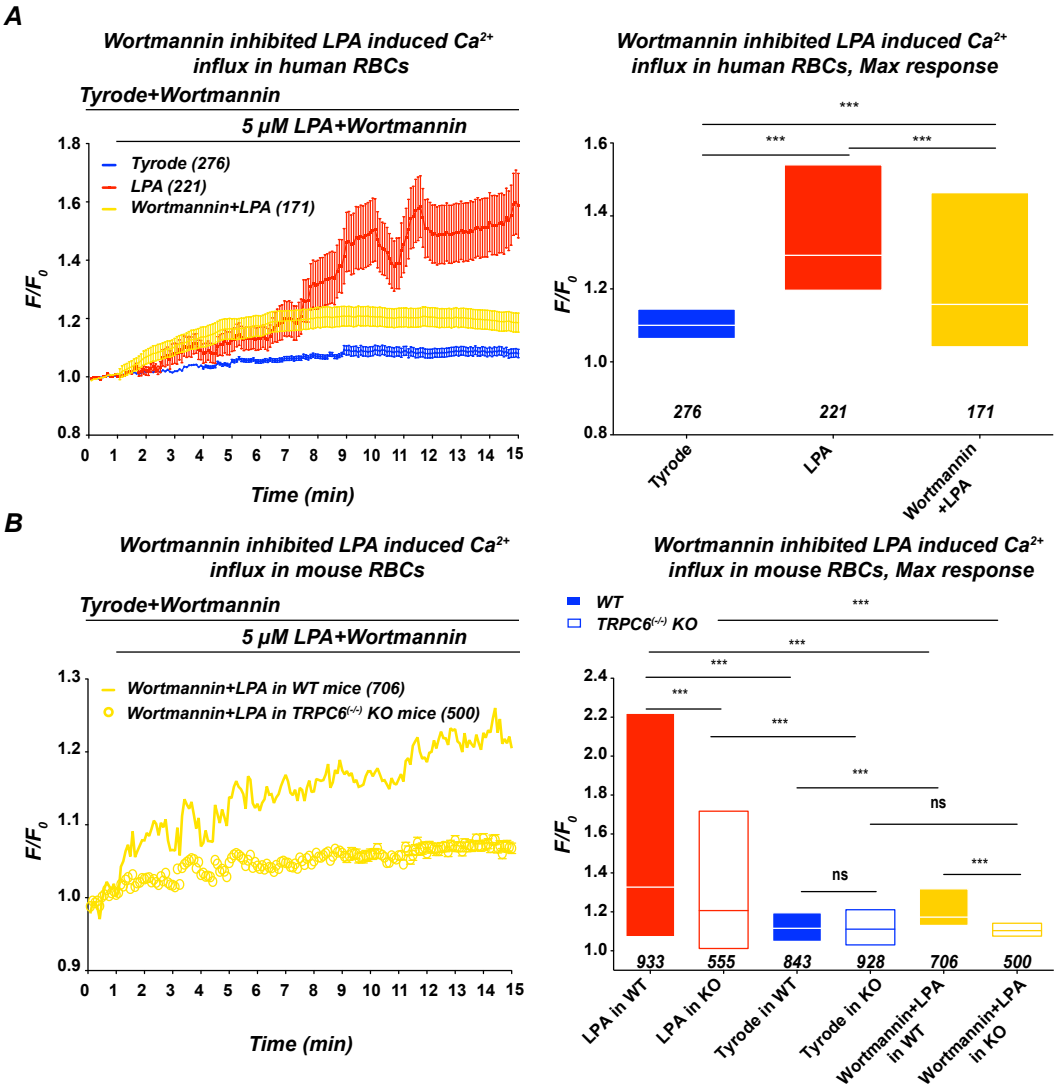

Figure 21: PI_3K is involved in LPA-induced Ca^{2+} influx.

A, *Average and max response of all traces showed that Wortmannin inhibited Ca^{2+} influx induced by LPA in human RBCs.* ***B,*** *Average and max response of all traces showed the inhibition function of Wortmannin in LPA-induced Ca^{2+} influx in mouse RBCs.*

3.2.6 PKCα is involved in the LPA signal pathway in human and mouse RBCs

Protein kinase Cα (PKCα) is known to modulate Ca^{2+} homeostasis in many kinds of cells [240]. Furthermore, it is also abundant in human RBCs [241, 242] and influences both RBCs morphology and ion transport [243]. For these reasons, I considered PKCα as another candidate for regulation of LPA

induced Ca^{2+} influx in RBCs.

To investigate the role of PKCα in LPA induced Ca^{2+} influx in RBCs, I applied the broad PKC inhibitor Gö6983 and the specific PKCα inhibitor Gö6976 in RBCs before LPA stimulation. For this purpose, Fluo-4/AM-loaded human and mouse RBCs were pre-incubated with 1 µM Gö6983 or Gö6976 at room temperature for 15 minutes after which 5 µM LPA was added to the cells. These results suggested that PKCα might be involved in LPA evoked Ca^{2+} influx in WT mice (Figure 22A, B) and human RBCs (Figure 22C, D), but interestingly not in Ca^{2+} rise induced in RBCs from TRPC6-KO mice (Figure 22B). In Figure 22B, one can clearly see that Gö6983 and Gö6976 can greatly, but not fully inhibit LPA induced Ca^{2+} influx in wild type mice, which suggests the PKC activity to be partly involved inLPA signal pathway. However, in $TRPC6^{(-/-)}$ mice, there was no inhibition by Gö6983 and Gö6976 on Ca^{2+} influx, which means a lack of TRPC6 channels leads to a lack of Ca^{2+} signal regulation by PKCα. Taking together, these results support the notion of two coexisting signal pathwaysto induce LPA-evoked Ca^{2+} influx: one does not involve PI_3K but is TRPC6 channel and PKCα dependent; a second one is TRPC6 channel and PKCα independent, but involves PI_3K.

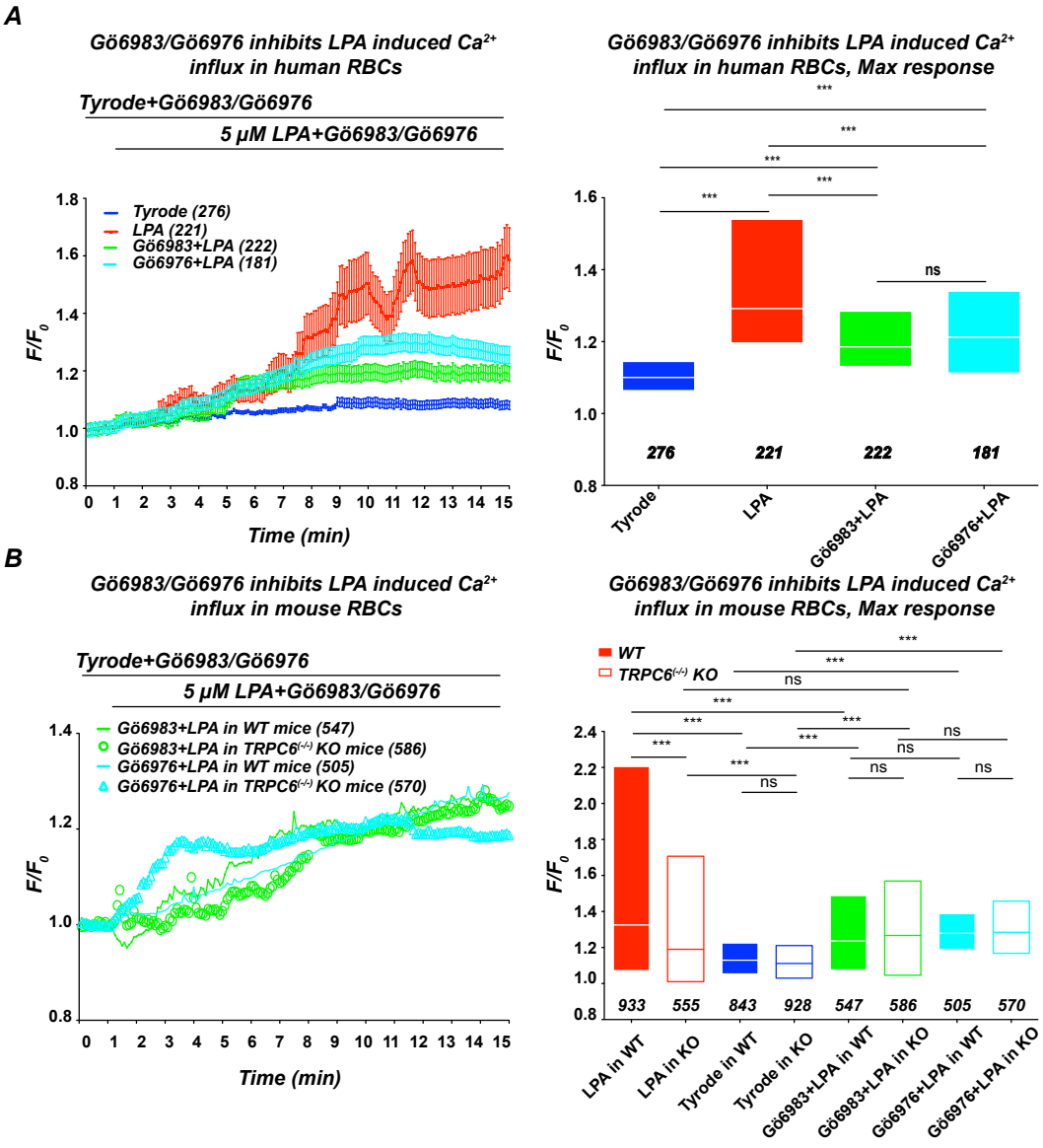

Figure 22:PKCα is involved in LPA induced Ca^{2+} influx.

A, *Average of all traces showing Gö6983 and Gö6976 partly inhibits Ca^{2+} influx induced by LPA in human RBCs (left panel). RBCs were incubated with 1 µM Gö6983 or Gö6976 at room temperature for 15minutes, and then stimulated with 5 µM LPA. Max response of all traces showing Gö6983 partly inhibits Ca^{2+} influx induced by LPA in human RBCs (right panel).* ***B,*** *Average of all traces showing Gö6983 partly inhibits Ca^{2+} influx induced by LPA in mouse RBCs (left panel). Max response of all traces showing Gö6983 partly inhibits Ca^{2+} influx induced by LPA in mouse RBCs (right panel).*

3.2.7 Wortmannin and Gö6976 in combination can fully inhibit LPA-evoked Ca^{2+} influx in human and mouse RBCs

From the results described above, it became apparent that both Gö6976 and Wortmannin could partly but not fully inhibit LPA induced Ca^{2+} influx in wild type mouse and human RBCs. However, in $TRPC6^{(-/-)}$ mice, Wortmannin could only partly inhibit Ca^{2+} influx. Thus, I applied Gö6976 and Wortmannin together in human and mouse RBCs. Under these circumstances, LPA induced Ca^{2+} influx was fully inhibited both in mouse (Figure 23A) and human RBCs (Figure 23B).

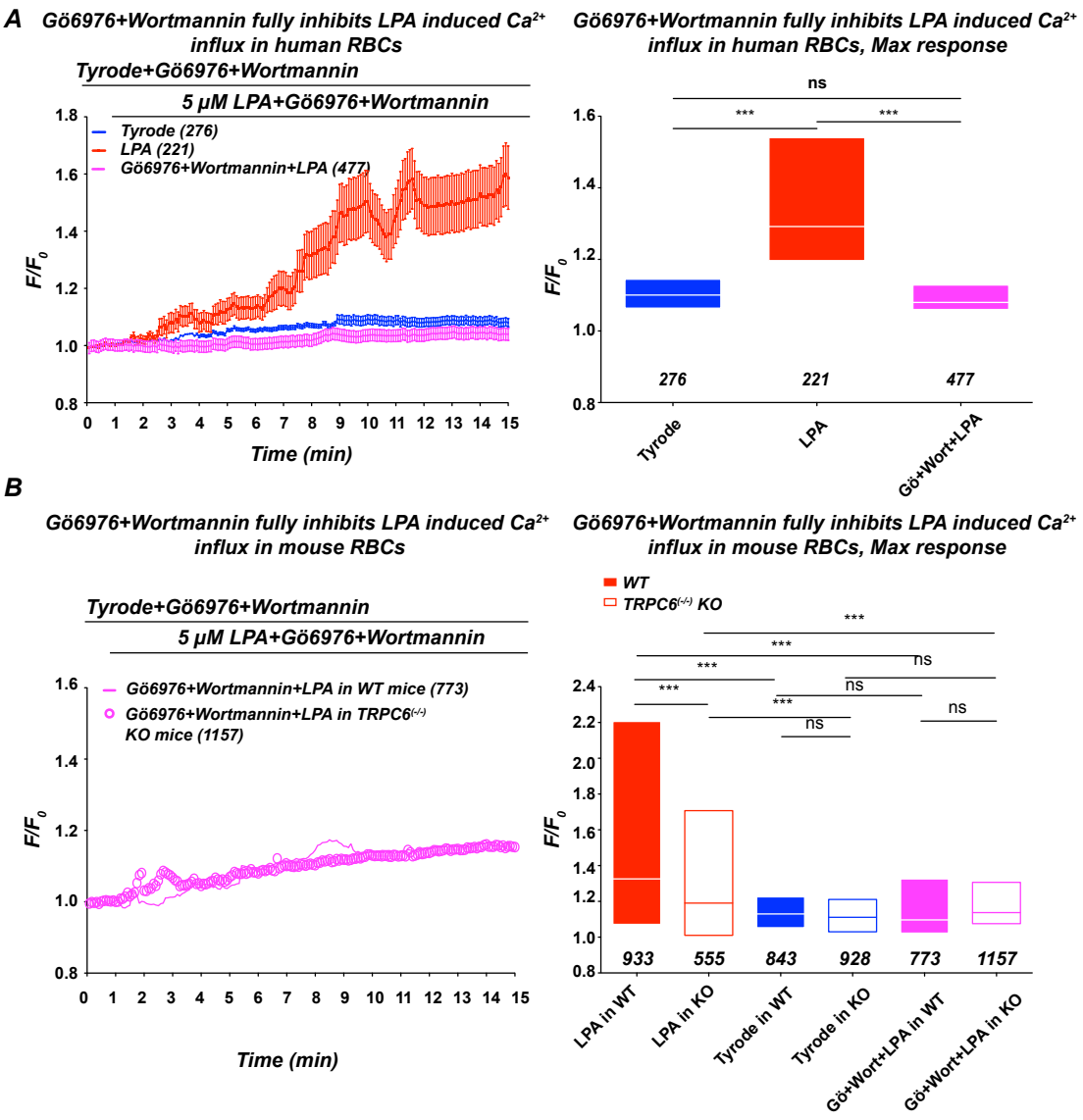

Figure 23: In combination with Wortmannin and Gö6976 could fully inhibit Ca^{2+} influx induced by LPA in human and mouse RBCs.

A, *Wortmannin (5 µM) plus Gö6976 (1 µM) could fully inhibit LPA induced Ca^{2+} influx in human RBCs.* ***B,*** *Wortmannin plus Gö6976 could fully inhibit LPA induced Ca^{2+} influx in wide type mouse RBCs (closed bar) and TRPC6 $^{(-/-)}$ mouse RBCs (open bar).*

3.2.8 MEK is involved in LPA signal pathway in human and mouse RBCs

One downstream target of PI_3K is MEK, and the pathway is PI_3K-PKB-MEK-ERK1/2 [235]. In $[Ca^{2+}]_i$ measurement studies with human and mouse RBCs, PI_3K inhibitor Wortmannin (5μM) greatly reduced the Ca^{2+} signal in response to LPA (5 μM). Thus, the effect of MEK inhibition on LPA-induced Ca^{2+} influx was investigated further.

As shown in Figure 24A, the MEK inhibitor U0126 (10 μM) had inhibitory effect on LPA-induced Ca^{2+} influx in human RBCs. Interestingly, the average of all traces showed an “increase-decrease” feature, which was totally different from the results with LPA only (Figure 8). Max response of all traces in these cells also showed significance between U0126-treated RBCs and U0126-free RBCs.

U0126 shows similar inhibition function also in mouse RBCs (Figure 24B). Similar with the results from human RBCs, U0126 pretreatment could also change the Ca^{2+} trace shape in mouse RBCs. From Figure 24C, after treatment with U0126, all the Ca^{2+} traces began to decrease after reaching its peak value, both in human (Figure 24Ca), wild type (Figure 24Cb), and knock out mice (Figure 24Cc).

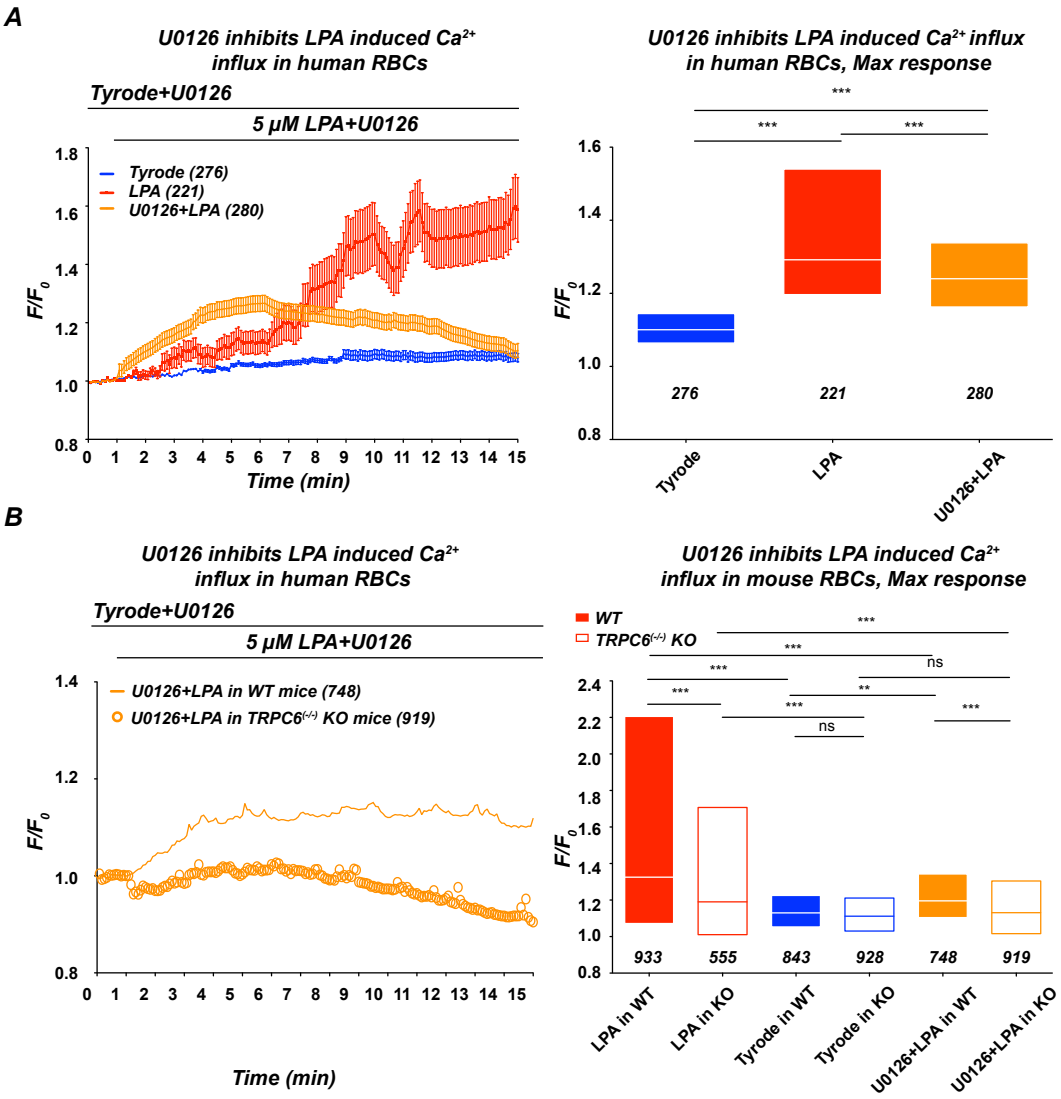

***Figure 24A-B**: MEK is involved in the LPA signal pathway in human and mouse RBCs.*

***A**, The MEK specific inhibitor U0126 can partly inhibit LPA induced Ca^{2+} influx in human RBCs. **B**, U0126 can partly inhibit LPA induced Ca^{2+} influx in wild type mouse RBCs (closed bar) and fully inhibit in TRPC6 $^{(-/-)}$ mouse RBCs (open bar).*

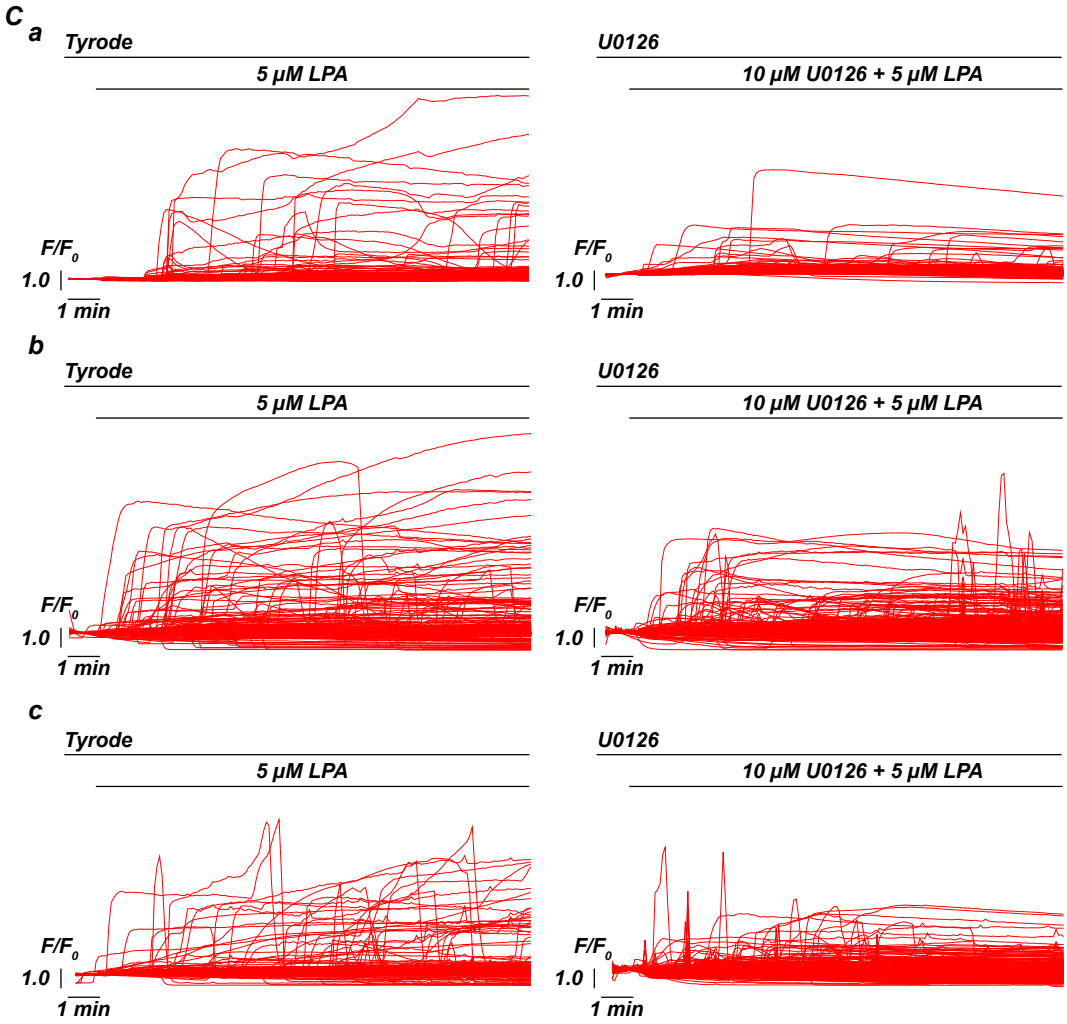

Figure 24C: MEK is involved in the LPA signal pathway in human and mouse RBCs.

***C**, U0126 pretreatment led to Ca^{2+} trace change in human (a), wild type mice (b) and TRPC6 $^{(-/-)}$ mouse RBCs (c).*

3.2.9 Cav2.1 in LPA induced Ca^{2+} influx

Many pharmacologic evidences suggest that voltage-operated Ca^{2+} channels may operate in the mature RBC membrane [45, 244], and some suggested that Cav2.1 Ca^{2+} channel might function in the RBC membrane. Furthermore, PMA also stimulated Ca^{2+} influx in human RBCs, and PMA-induced Ca^{2+} influx could be inhibited by the P-type Ca^{2+} channel blocker ω-agatoxin-TK [32, 49], a toxin from the funnel web spider [245]. Therefore, it is reasonable to investigate whether Cav2.1 channel is involved in LPA-induced Ca^{2+} influx.

Thus, I applied a 20-minutes exposure to 1 μM ω-agatoxin-TK before stimulation with 5 μM LPA. From Figure 25, we could see that agatoxin strongly reduces Ca^{2+} influx induced by LPA both in human and mouse RBCs. Similar to the MEK inhibitor U0126, ω-agatoxin-TK could only greatly but not fully inhibit LPA induced Ca^{2+} signal both in human and wild type mice, but could totally inhibit Ca^{2+} signal in TRPC6$^{(-/-)}$ mice. These data further supported the notion that two signal pathways of LPA coexisted: 1) LPA-Gi-PI_3K-MEK-Cav2.1 and 2) LPA-Gi-PKC-TRPC6 (Figure 36).

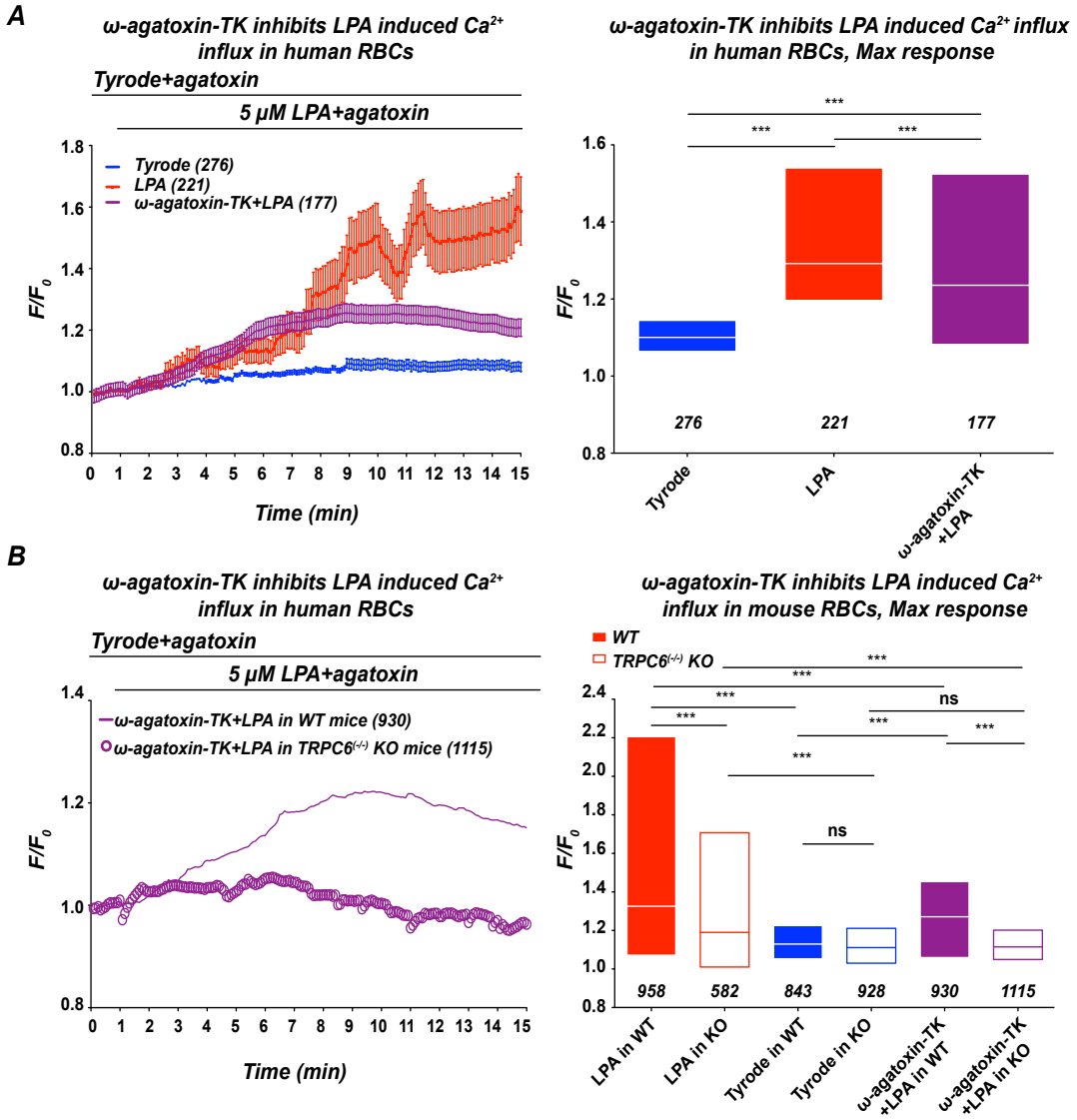

Figure 25: Cav2.1 is involved in LPA induced Ca^{2+} influx.

***A**, specific Cav2.1 channel inhibitor, ω-agatoxin-TK, can partly inhibit LPA induced Ca^{2+} influx in human RBCs. **B**, ω-agatoxin-TK can partly inhibit LPA induced Ca^{2+} influx in wild type mice RBCs (closed bar) and fully inhibit it in TRPC6 $^{(-/-)}$ mice RBCs (open bar).*

3.3 LPAin sickle cell disease

3.3.1 Ca^{2+} in human sickle RBCs

In sickle RBCs, I also investigated the LPA-induced Ca^{2+} signal pathway.

Similar to the experiment of healthy RBCs, sickle RBCs were loaded with 5 µM Fluo-4/AM for 1 hour at 37°C. Then cells were washed in Tyrode and I waited 15 min for the cell to settle down and for dye de-esterification. As shown in Figure 26, Fluo-4-bound Ca^{2+} presented different distributions compared with healthy RBCs. In sickle cells, the Fluo-4 bound Ca^{2+} showed a spots-like and uneven distribution, while in healthy RBCs the distribution was much more homogeneous. The mechanism of this phenomenon was possibly because of the involvement of Ca^{2+}-sensitive Gardos channels and Ca^{2+} pump in sickle cell dehydration [246, 247].

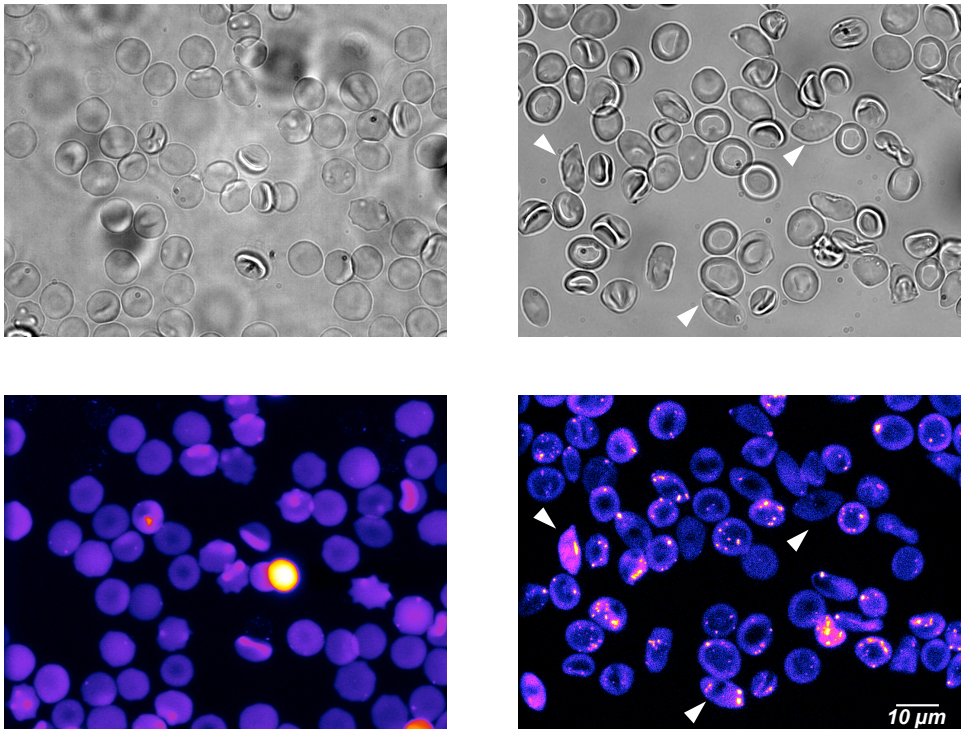

Figure 26: Ca^{2+} distribution in sickle cells before stimulation.

A representative image of Ca^{2+} distribution in human healthy (control) and sickle RBCs after 1 h loading with Fluo-4. The whithe arrowheads depict the typical sickle-shaped RBCs.

3.3.2 LPA receptors in sickle cells

Until now, it is known that the effects of LPA at physiological concentrations are mediated by five LPA receptor isoforms (LPAR1–LPAR5) and perhaps by additional recently proposed or as yet unidentified receptors [248, 249]. LPA is involved in blood clot formation [133], while sickle RBCs usually induce obstruction of capillaries [184], it is reasonable to consider whether LPA receptors are involved in sickle cell disease. Therefore, I investigated the presence of LPA receptor subtype 1-5 in healthy and sickle RBCs by immunostaining and immunoblotting. As shown in Figure 27A, compared with healthy RBCs, LPA receptor subtype 4 (LPAR4) shows an increase in sickle cells. The figures of control cells have been shown in Figure 19, but for easier comparison these figures are repeated in Figure 27. Western blot results further confirmed the markedly increased LPAR4 in sickle cells (Figure 27B). Furthermore, cell-to-cell differences in LPA receptor compositions both occur in healthy and sickle cells (Figure 27A).

Because LPAR4 was highly expressed in sickle cells, I investigated the LPA induced Ca^{2+} influx in sickle RBCs (Figure 27C). Compared with healthy RBCs (control), LPA induced much stronger Ca^{2+} influx in sickle RBCs, both in average traces (a) and max response value (b). And both healthy and sickle cells did not show Ca^{2+} influx in LPA-free Tyrode.

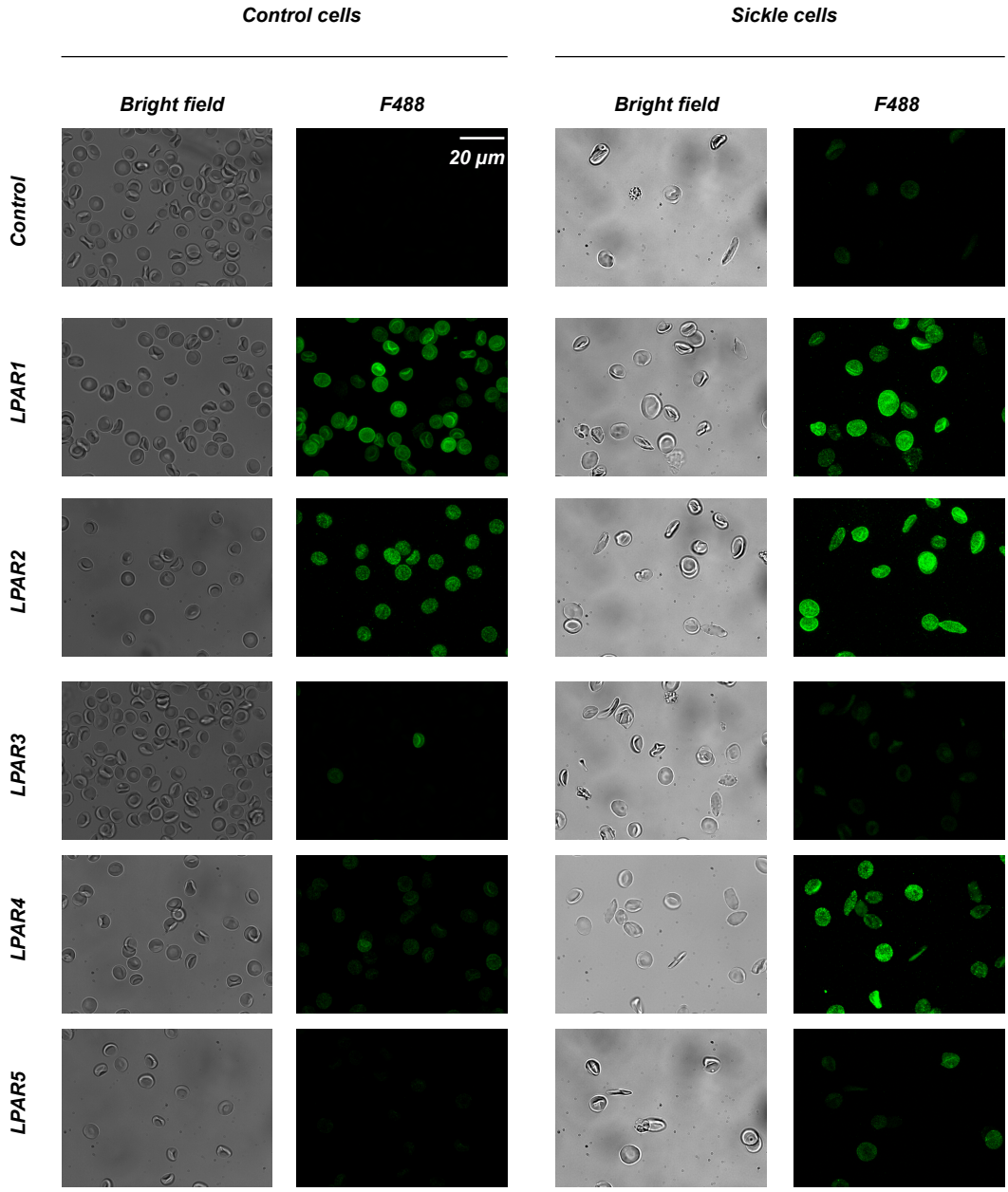

Figure 27A: LPA receptor distributions and LPA induced Ca^{2+} influx in sickle cells.

***A**, Immnostaining of healthy RBCs (control) and sickle cells using antibodies against LPA receptor subtype 1-5.*

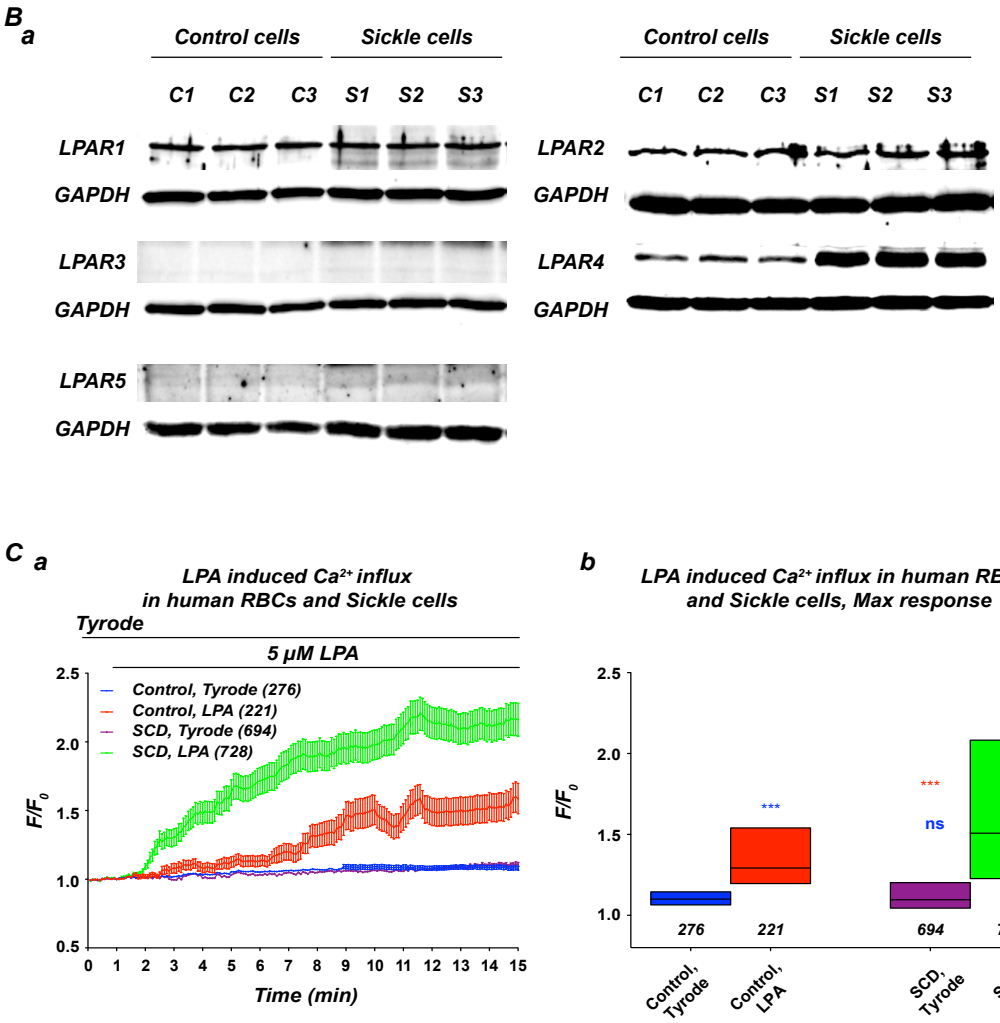

Figure 27B-C: LPA receptor distributions and LPA induced Ca^{2+} influx in sickle cells.

***B**, Western blots of SDS-PAGEs of total cellular protein prepared from healthy RBCs (control) and sickle cells probed with the same antibodies in **A**. Each group contains 3 individual blood samples. GAPDH was used as protein amount control. Note the markedly increased LPA receptor subtype 4 (LPAR4) in sickle cells. **C,** LPA induced Ca^{2+} influx in healthy RBCs and sickle cells.*

3.3.3 PTX inhibits LPA-induced Ca^{2+} influx in healthy RBCs and sickle cells

I further examined the effect of PTX on sickle cells. RBCs from healthy donor and sickle cell disease patient were incubated with PTX (5 μg/ml) or its

vehicle (Control) in 37°C for 1h and subsequently treated with LPA (5 µM). The Ca^{2+} rise by LPA was fully abolished by PTX both in healthy RBCs and sickle cells (Figure 28). This result strongly suggests that the LPA-induced Ca^{2+} influx in sickle cells is also through G_i protein, which is the same as for healthy RBCs.

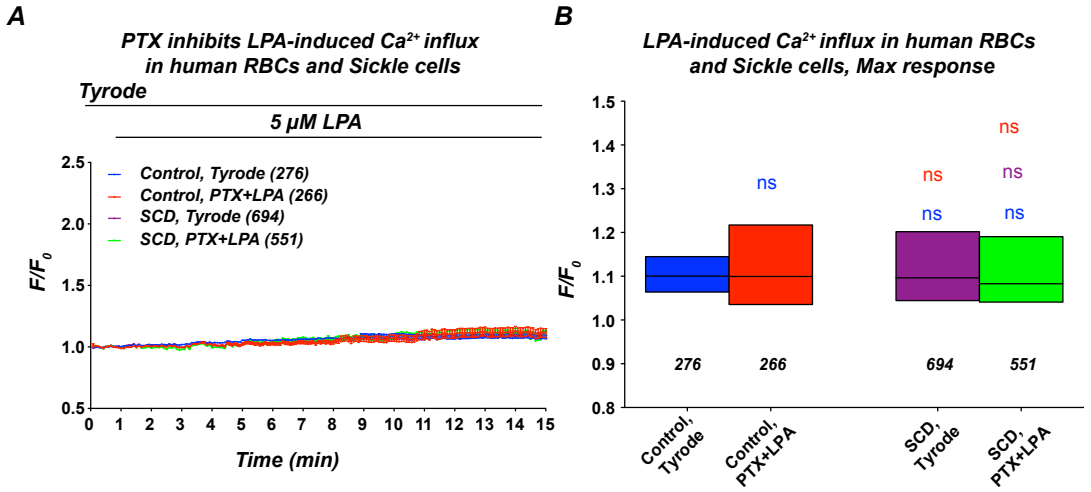

Figure 28: PTX inhibited LPA-induced Ca^{2+} influx in human healthy RBCs and sickle RBCs.

***A**, Comparison of average Ca^{2+} increase induced by LPA in PTX pretreated healthy RBCs (Control) and sickle RBCs (SCD). All measurements were performed with freshly prepared RBCs from 3 healthy donor or patients with sickle cell disease. **B**, Statistical analysis of the max response.*

3.3.4 PI_3K-MAPK-Cav2.1 branch of LPA-induced signal pathway in healthy RBCs and sickle cells

As described in section 3.2, there is evidence that two signal pathways of LPA coexisted in healthy human RBCs: one is LPA-G_i-PI_3K-MEK-Cav2.1 and another one is LPA-G_i-PKC-TRPC6 (Figure 36). I also found that LPAR4 receptors are highly expressed in human sickle RBCs (Figure 27), and G_i protein is also involved in LPA signal pathway in sickle cells, the same as in healthy RBCs (Figure 28). Therefore, I investigated the existence of these two sigal pathways in sickle cells.

The first branch of the signal pathway is PI_3K-MEK-Cav2.1. Wortmannin, the PI_3K inhibitor, was applied on healthy human RBCs and sickle cells. From the average trace (Figure 29Aa) and the max response value (Figure 29Ab), I can conclude that Wortmannin only partly inhibits LPA-induced Ca^{2+} influx in healthy RBCs and sickle cells. The MEK inhibitor, U0126, also show limited inhibition function in sickle cells (Figure 29B). To further investigate the MEK function in sickle cells, I used ELISA to check the activity of phospho-Mitogen-activated protein kinases (p-MAPK), which is the catalytic product of MEK. In Figure 29Bc, one can see that LPA increases the p-MAPK activity in healthy RBCs and sickle RBCs. Furthermore, the p-MAPK activity of sickle cells in the basal condition, which means in LPA-free Tyrode, is higher than in healthy RBCs (blue bar v.s. purple bar). The sickle cells are more sensitive to LPA compared with healthy RBCs (red bar v.s. green bar). Concerning the Cav2.1, I firstly performed western blots to confirm the existence of Cav2.1 in human and mouse RBCs (Figure 29Da). Then the Cav2.1 inhibitor ω-agatoxin-TK was applied and showed a partial inhibition of the Ca^{2+} influx in both healthy and sickle RBCs (Figure 29Db and Dc). In summary, these data strongly suggest that one of the LPA induced signal pathways in sickle cells is also LPA-G_i-PI_3K-MEK-Cav2.1 mediated, the same as in healthy RBCs.

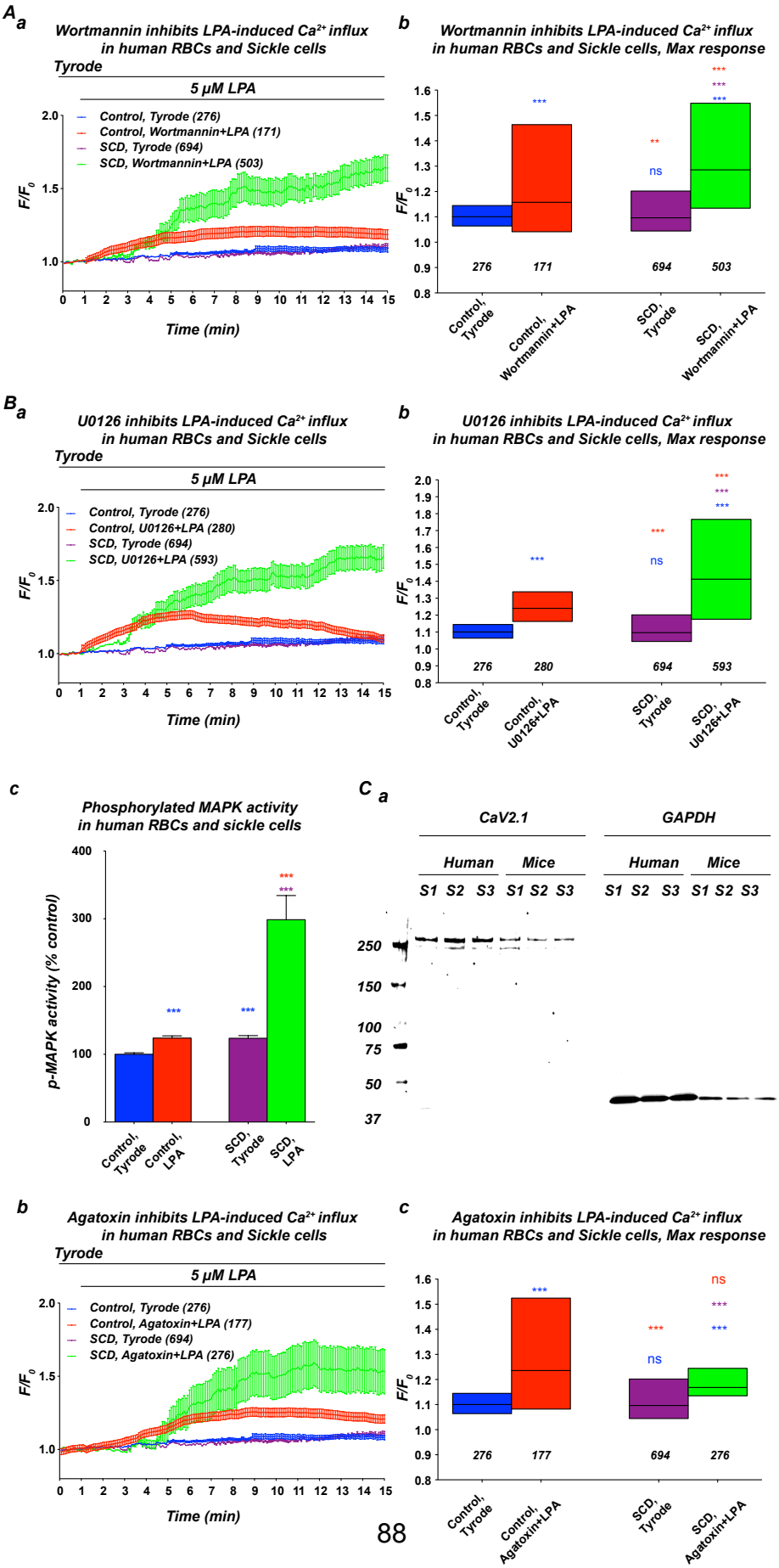
A a
Wortmannin inhibits LPA-induced Ca2+ influx
in human RBCs and Sickle cells
Tyrode
5 µM LPA
Control, Tyrode (276)
Control, Wortmannin+LPA (171)
SCD, Tyrode (694)
SCD, Wortmannin+LPA (503)
F/F0
Time (min)
b
Wortmannin inhibits LPA-induced Ca2+ influx
in human RBCs and Sickle cells, Max response
276
171
694
503
ns
Control, Tyrode
Control, Wortmannin+LPA
SCD, Tyrode
SCD, Wortmannin+LPA
B a
U0126 inhibits LPA-induced Ca2+ influx
in human RBCs and Sickle cells
Tyrode
5 µM LPA
Control, Tyrode (276)
Control, U0126+LPA (280)
SCD, Tyrode (694)
SCD, U0126+LPA (593)
F/F0
Time (min)
b
U0126 inhibits LPA-induced Ca2+ influx
in human RBCs and Sickle cells, Max response
276
280
694
593
ns
Control, Tyrode
Control, U0126+LPA
SCD, Tyrode
SCD, U0126+LPA
c
Phosphorylated MAPK activity
in human RBCs and sickle cells
p-MAPK activity (% control)
Control, Tyrode
Control, LPA
SCD, Tyrode
SCD, LPA
C a
CaV2.1
GAPDH
Human
Mice
S1 S2 S3 S1 S2 S3
250
150
100
75
50
37
b
Agatoxin inhibits LPA-induced Ca2+ influx
in human RBCs and Sickle cells
Tyrode
5 µM LPA
Control, Tyrode (276)
Control, Agatoxin+LPA (177)
SCD, Tyrode (694)
SCD, Agatoxin+LPA (276)
F/F0
Time (min)
c
Agatoxin inhibits LPA-induced Ca2+ influx
in human RBCs and Sickle cells, Max response
276
177
694
276
ns
Control, Tyrode
Control, Agatoxin+LPA
SCD, Tyrode
SCD, Agatoxin+LPA

Figure 29: PI_3K branch in LPA-induced Ca^{2+} influx in normal RBCs and sickle cells.

***A**, PI_3K is involved in LPA-induced Ca^{2+} influx in RBCs from healthy human donorsand patients of sickle cell disease (SCD). 1 μM Wortmannin, the specific PI_3K inhibitor, partly inhibits LPA-induced Ca^{2+} influx, both in the average trace (a) and max response (b). **B**, MAPK is involved in LPA-induced Ca^{2+} influx in human healthy and sickle RBCs. 10 μM U0126, the specific MEK inhibitor, partly inhibits LPA-induced Ca^{2+} influx, both in average trace (a) and maxresponse (b). The activity of phospho-MAPK, the product of MEK catalysis, was investigated by ELISA (c). **C**, Cav2.1 is involved in LPA-induced Ca^{2+} influx in healthy human RBCs and sickle cells. (a), western blots of total cellular protein prepared from human RBCs (control) and mouse RBCs probed with antibodies against Cav2.1. 1 μM ω-agatoxin-TK, the specific Cav2.1 inhibitor, partly inhibits LPA-induced Ca^{2+} influx, both in the average trace (b) and max response (c).*

3.3.5 Gö6976 inhibits LPA-induced Ca^{2+} influx in healthy RBCs and sickle cells

In chapter 3.3.4, we already discussed the PI_3K-MEK-Cav2.1 branch of the LPA induced signal cascade. I also investigated the PKC-TRPC6 branch. Gö6976, the specific PKCα inhibitor, was applied on human healthy and sickle RBCs. As shown in Figure 30, Gö6976 only showed partial inhibition function both in healthy and sickle RBCs. For TRPC6 in human sickle RBCs, because lack of specific inhibitor of TRPC6, the possibility of TRPC6 knockout model in sickle cell disease mouse was considered and discussed.

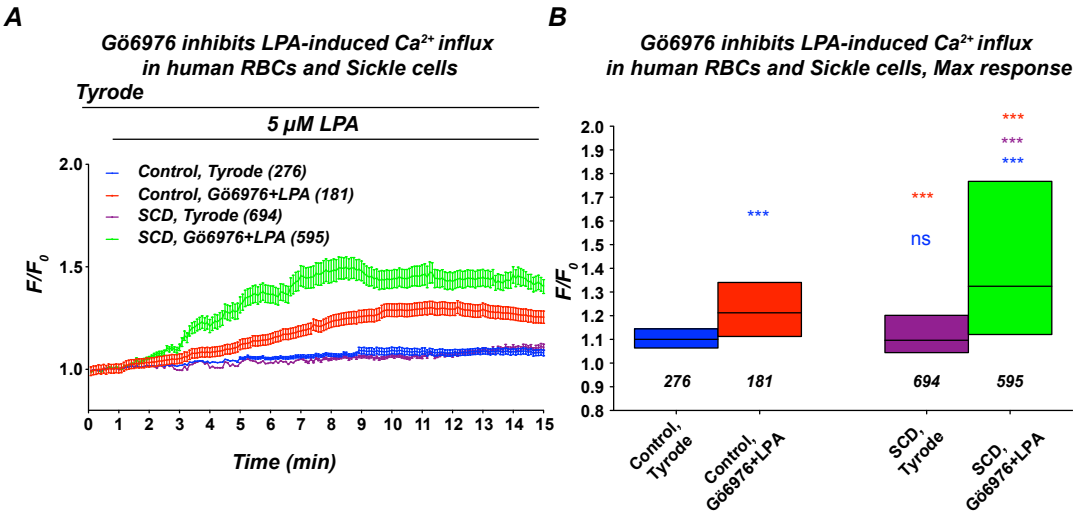

Figure 30: Gö6976 inhibits LPA-induced Ca^{2+} influx in healthy RBCs and sickle cells.

***A**, Comparison of average Ca^{2+} increase induced by LPA in Gö6976 pretreated healthy RBCs (Control) and sickle RBCs (SCD). All measurements were performed with freshly prepared RBCs from 3 healthy donor or patients with sickle cell disease. **B**, Statistical analysis of the max response.*

3.3.6 Gö6976 in combination with Wortmannin fully inhibit LPA-induced Ca^{2+} influx in healthy RBCs and sickle cells

From the results described above, both Gö6976 and Wortmannin can partly but not fully inhibit LPA induced Ca^{2+} influx into human healthy RBCs and sickle RBCs. Thus, I applied Gö6976 and Wortmannin together in healthy and sickle RBCs. Under this condition, LPA induced Ca^{2+} influx was fully inhibited by Wortmannin together with Gö6976 both in healthy and sickle RBCs (Figure 31).

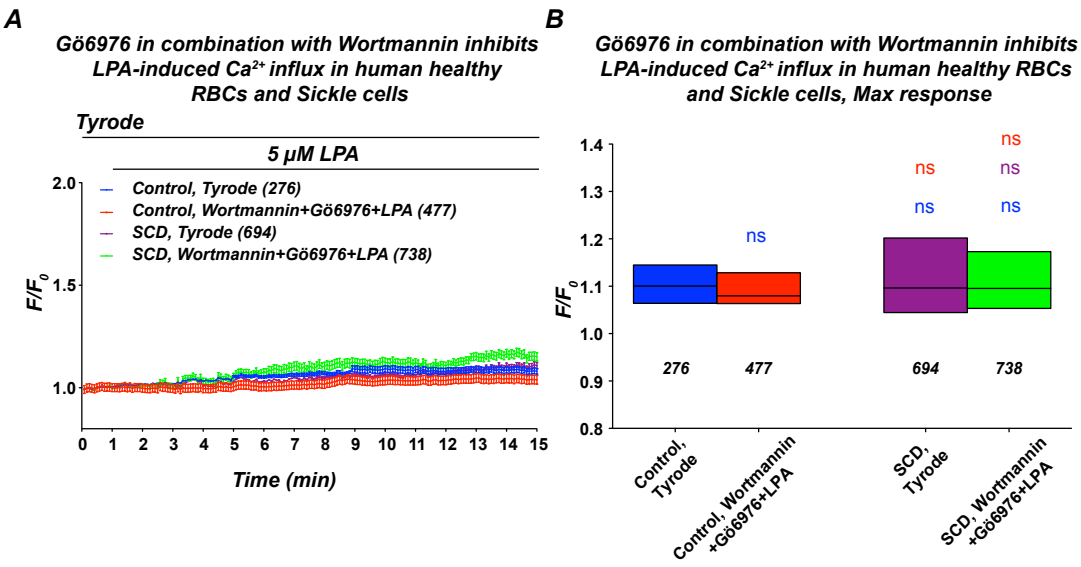

Figure 31: Gö6976 in combination with Wortmannin fully inhibited LPA-induced Ca^{2+} influx in normal RBCs and sickle cells.

***A**, Comparison of average Ca^{2+} signal induced by LPA in Gö6976 in combination with Wortmannin pretreated healthy RBCs (Control) and sickle RBCs (SCD). All measurements were performed with freshly prepared RBCs from 3 healthy donor or patients with sickle cell disease. **B**, Statistical analysis of the max response.*

4. Discussion

In this work, I show that although RBCs have a high morphological homogeneity, they are functionally heterogeneous (Figure 9). Despite extensive past investigations of RBCs (they are among the most studied cells in natural history), this heterogeneity was widely ignored because bulk or suspension experiments could not reveal such properties. Nevertheless, other single-cell experiments, namely the patch-clamp technique, may lead to similar conclusions due to discrepancies between different laboratories. For example, Kaestner *et al.* [250] reported contradictions with Christophersen and Bennekou [45] in the open probability and conductance of the non-selective voltage-activated cation channel in healthy human RBCs. In malaria parasite infected RBCs, Sanjay A. Desai *et al.* reported that the malaria-infected RBCs exhibited voltage-dependent, non-saturating currents that were 150-fold larger, predominantly carried by anions and abruptly abolished by channel blockers compared with healthy RBCs [251], but Stéphane Egée *et al.* believed that the host membrane of malaria-infected RBCs possessed spontaneously active anion channel activity, with identical conductances, pharmacology and selectivity to the linear conductance channel measured in stimulated uninfected RBCs [252]. Stephan M. Huber *et al.* also supported that the malaria-infected RBCs showed identical conductances and hemolysis properties compared with non-infected RBCs [253]. However, the inherent complexity of the technique combined with relatively small cell numbers rendered conclusions difficult. In addition, we provided novel approaches to quantitatively analyze RBC responses to processes such as hormonal stimulation on the level of individual cells (Figure 10) that are not accessible by any other technique.

4.1 Single cell analysis discussion

4.1.1 Fluorescence indicator in RBCs

Although the Ca^{2+} is important for the RBCs (see introduction), little is known for the regulation of the Ca^{2+} concentration in RBCs. Usually, the basal intracellular Ca^{2+} concentrations of cells under physiological condition was measured by fluorescent indicators, such as Fura-2, Indo-1, Fluo-3 and Fluo-4. Fluo-4 is a single-excitation and single-emission, in other words a non-ratiometric indicator, which can only be used for qualitative but not quantitative investigations. Compared with Fura-2 (dual excitation) and Indo-1 (dual emission), Fluo-4 fluorescence recording is much easier to be influenced by systematic errors occurring in experiment, which led to Fura-2 and Indo-1 as the better choices. However, Kaestner and co-workers [128] found that Fura-2 and Indo-1 for intracellular Ca^{2+} measurement in RBCs was not reasonable because hemoglobin influenced its excitation and emission properties. In brief, both Fura-2 and Indo-1 display massively altered spectral properties in the presence of hemoglobin that greatly influence fluorescence recordings of the Ca^{2+} concentration and changes, because the interactions between hemoglobin and the indicators seems to be wavelength and Ca^{2+} dependent (Figure 32). Another problem is the requirement for UV-excitation of Indo-1 and Fura-2. This excitation induces strong transient auto-fluorescence (Figure 32B). For Fluo-4, hemoglobin only has a low absorption at 480 nm and 520 nm, and irradiation at 480 nm did not result in changes of the auto fluorescence even for high intensities and longer time. Taken all together, Fluo-4 seems still to be the best candidate for recordings of Ca^{2+} changes in RBCs and is currently without alternatives.

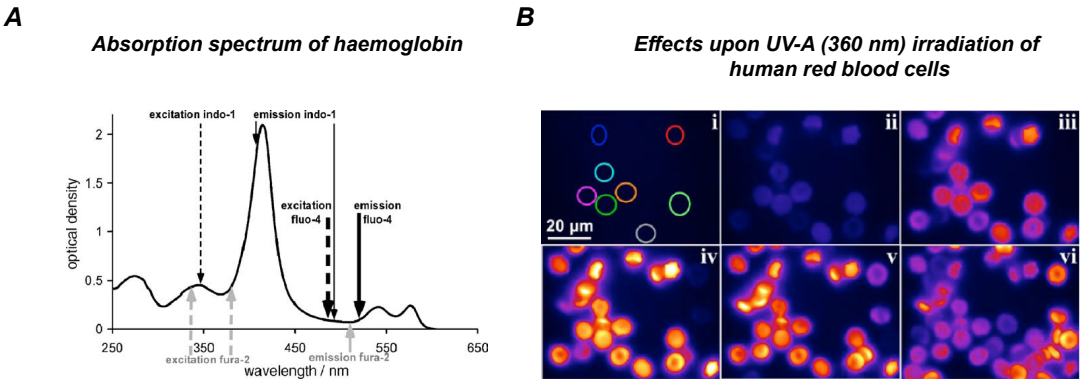

Figure 32: Absorption spectrum of hemoglobin and autofluoresence excited by UV irradiation.

A, *The arrows point to the typical excitation wavelength and emission maxima of the Ca^{2+} fluorophors Fura-2, Indo-1 and Fluo-4 (Cited from [128] with kind permission from Elsevier).* ***B*** *shows fluorescence images of RBCs population before, during and after irradiation with UV-A (360 nm). The fluorescence images i, ii, iii, iv, v and vi correspond to exposure times of 0, 5, 10, 15, 20 and 30 min, respectively. The light power out of the objective was approximately 35 µW. Warm colors correspond to a high fluorescence intensity and cold colors to a weak fluorescence. There is virtually no fluorescence before the irradiation (image i). The RBCs population is a representative example, and the result was verified with RBCs of three different donors. (Cited from [128] with kind permission from Elsevier)*

4.1.2 Ca^{2+} concentrations and changes are not homogenous amongst individual RBCs

It was already known that LPA induces Ca^{2+} influx into human RBCs. There are evidences that it is Ca^{2+} channel mediated rather than a nonspecific Ca^{2+} leak [215, 254-256]. For example, the Ca^{2+} influx can be inhibited by Ca^{2+} channel blockers [32]; the influx induced by LPA is in a gradient dependent way, higher LPA concentrations promotes higher rates of Ca^{2+} entry; and other substances, such as phosphatidic acid and sphingosine-1-phosphate(Sph-1-P), have no effect on RBCs Ca^{2+} uptake even at high concentrations [32].

So far, the physiological function of Ca^{2+} influx itself in RBCs is not very well understood and links between Ca^{2+} and RBCs-related diseases still need to be investigated. Treatment of RBCs with the ionophore A23187 led to intracellular Ca^{2+} increase, and consecutively to Gardos channel activation, which results in K^+ efflux (followed by Cl^-) and the consequent reduction of the RBC volume. It has been reported that the threshold of the Gardos channel activation is around 40 nM of free Ca^{2+} in normal cells [257]. The increase of intracellular Ca^{2+} also induces activation of many other proteins, such as scramblase [258, 259] and PKCα [242]. The consequence is thought to be PS exposure on the outer leaflet of the cell membrane. The exposure of PS is also a key signal for eryptosis, RBCs programmed cell death [260-264]. It is also necessary for the recognition and engulfment by macrophages [262, 264-268].

The accurate value of intracellular Ca^{2+} concentration is still uncertain, but it appears to be reasonable to consider the physiological intracellular Ca^{2+} level in human RBCs to be about 100 nM [105, 269]. From my own observation, I can see that even the basal Ca^{2+} concentration is different from one RBC to another. Ca^{2+} concentration in some cells is 10 times higher than other ones before stimulation, and this phenomenon is more common in mouse RBCs. To deal with this problem, I use the F/F_0 value to record the Ca^{2+} change during the experiment procedure, instead of absolute fluorescence values. Another point to discuss in our experiment, with or without Tyrode flow, is around 1% of RBCs show Ca^{2+} influx even without further stimulation (Figure 9). This phenomenon was also found in FACS analysis. These observations suggest that some channels can be activated after washing and dye loading. In other words, maybe washing will influence the Ca^{2+} measurements, although it is necessary for the operation and therefore there is no alternative and we have to live with this potential artifact.

Another question is why different RBCs show different Ca^{2+} influx properties after LPA stimulation. One possibility is because of different ages of individual cells. As we know, human RBCs are produced through a process named

erythropoiesis, developing from committed stem cells of mature RBCs in about 7 days. After matured, the lifespan of the cells in the circulation is about 100 – 120 days. At the end of their lifespan, they become senescent, and are removed from circulation. Matured RBCs lack organelles and the nucleus, while immature RBCs called reticulocytes have mesh-like ribosome RNAs. In other words, in its lifespan, the structure of RBCs, such as the nucleus, membrane proteins, and cytoskeleton change greatly. However, until now, there is no perfect method to separate RBCs according cell age. The most widely used method is Percoll gradient centrifugation, but this approval still has some problems, such as specific receptor activation (NMDA receptor) induced cell shrinkage and subsequently density increase, which greatly influence cell distribution in Percoll gradient solution. The old cells are considered to contain an increased Ca^{2+} [129, 270], but this is still controversial [271]. So one explanation for the differences of Ca^{2+} influx is: each individual cell has different receptor numbers, different Ca^{2+} channel numbers and different membrane stabilities.

Furthermore, RBCs do not show an immediate response after stimulation but a delayed reaction, which suggests there are processes happen before Ca^{2+} influx. In other words, this delay suggests that Ca^{2+} is not the first messenger after stimulation, maybe other ions or substances, such as Na^{+} and ATP, join the signaling cascade before Ca^{2+}. Only when this substance reached some kinds of threshold, maybe ATP concentration, then the Ca^{2+} channels open, Ca^{2+} influx is observed. This hypothesis could explain the time delay of Ca^{2+} influx after stimulation.

4.1.3 Analysis protocols

We already knew Ca^{2+} concentrations and changes were not homogenous amongst individual RBCs (chapter 3.1.2). To solve this problem, Live-cell video imaging, which allows for the analysis of individual cells, appeared to be the most appropriate method to determine intracellular Ca^{2+} changes when

compared to other techniques (Figure 9). Considering the complexity of single-cell responses (Figure 9D), I firstly tested whether a simple averaging of all cells might be an adequate approach. To evaluate the best method of analysis, I compared Ca^{2+} signals under control conditions and in the presence of 2.5 and 10 µM LPA (Figure 33A,B). Figure 33C shows the averaged traces of the cellular responses. The traces appear shallow, small and independent of the LPA concentration. However, this finding might be a misinterpretation because the onsets of the responses of each single cell differed largely (Figure 33A, B). Therefore, we synchronized the responses to their onset before averaging. As demonstrated in Figure 33D, the RBCs generated steep Ca^{2+} increases with an amplitude that was dependent on the LPA concentration. Thus, postexperimental synchronization might be adequate to analyse LPA-induced Ca^{2+} response in RBCs. It is noteworthy to mention that a full characterization of the RBC responses to external stimulation might be associated with a long-lasting delay period. Therefore, the recording time (limited here to 15 min) should be extended to obtain a maximum of responding cells. However, an extension of these experiments is limited because RBCs with high intracellular Ca^{2+} levels tend to have a fragile plasma membrane with an increased risk of membrane breakdown.

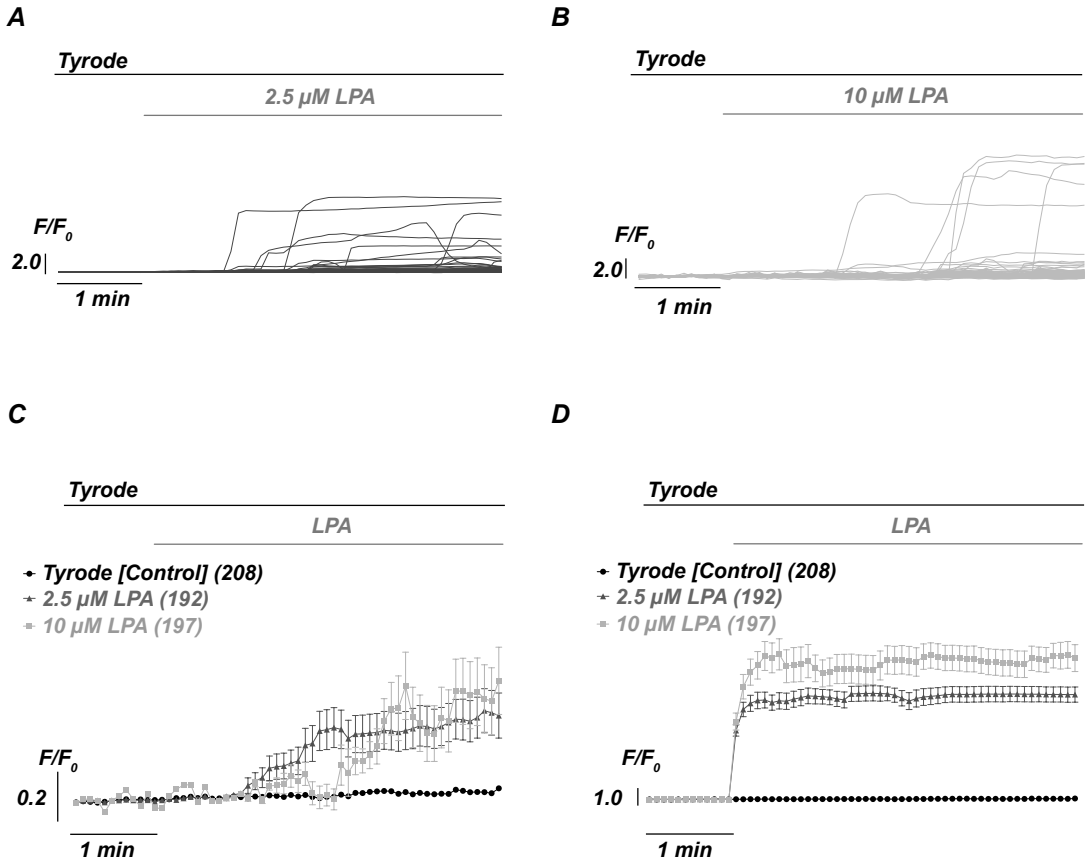

Figure 33: Protocols and handling of LPA-induced Ca^{2+} influx.

***A**, Fluorescence signals of single RBCs treated with 2.5 µM LPA. **B**, Fluorescent signals of single RBCs treated with 10 µM LPA. **C**, Comparison of average Ca^{2+} signals induced by different concentrations of LPA [same data as in (**A**) and (**B**)]. **D,** Average of the Ca^{2+} signals after their synchronization to the onset of the response.*

Therefore, we also considered achieving cellular synchronization using a three-step protocol (Figure 34). However, this approach required blocking the plasma membrane Ca^{2+}-pump with sodium orthovanadate, which complicates the interpretation and comparison with other protocols. Such a multi-step protocol might be appropriate if the pure LPA mediated the influx capacity but not the physiological response of the cells is in question. Furthermore, kinetic information on the Ca^{2+} signals would be lost in such a multi-step protocol. Consequently, we focused on the stimulation protocol shown in Figure 33, and examined a large number of parameters from individual responses, as depicted in Figure 11. Each single cell fluorescence trace was fitted with a Hill

equation as outlined in the Materials and Methods section, which allowed us to extract numerous types of quantitative information, such as the cellular reaction time (time between LPA application and the onset of the Ca^{2+} signal), the time for halfmaximal stimulation ("X_{half}"), the steepness of the upstroke (Hill slope or "S_H") and the amplitude of the cellular response ("amplitude").

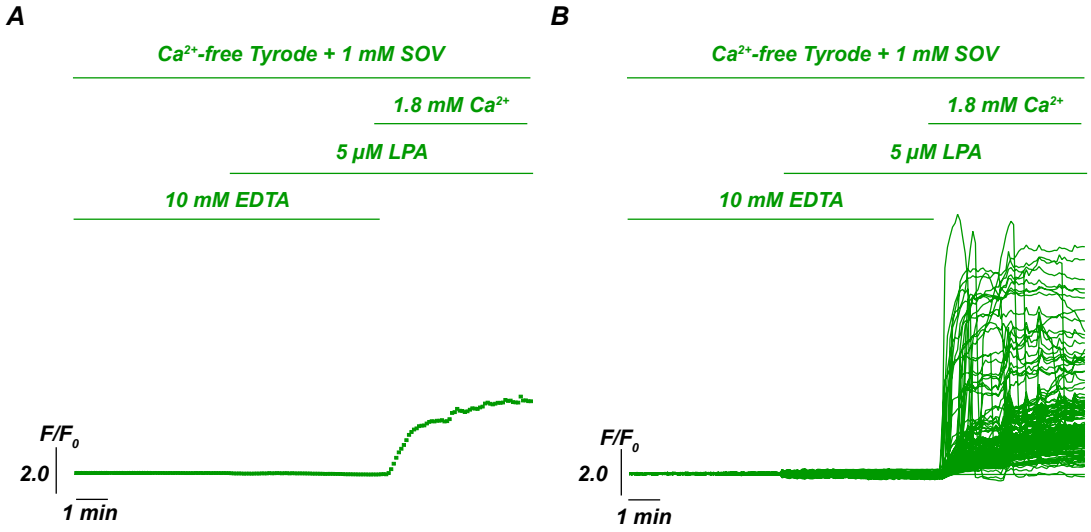

Figure 34: 3-steps protocol and handling of LPA-induced Ca^{2+} influx.

A, *depicts the attempt to "synchronize" the cells by applying a three steps protocol starting with the application of a Ca^{2+}free solution and inhibition of the Ca^{2+}pump with sodium orthovanadate (SOV). Then, the RBCs were stimulated with LPA for 5 min, and Ca^{2+}(1.8 mM) was added, leading to a synchronized cell response.* ***B,*** *Single-cell traces show [same data as in (**A**)] that the cells still respond variably to the Ca^{2+} readdition.*

Such parameters were analysed statistically as depicted in Figure 11B for an experimental series in which we tested the effects of varying LPA concentrations. We found significant differences in all parameters, indicating that the LPA concentration significantly impacted all the parameters. It is noteworthy that the distribution of the analysed parameters for responding cells (see histograms and their insets in Figure 11B) was characterized by a broad scattering rather than a specific distribution. Therefore, we investigated the putative reasons underlying the scattered distribution of the cellular responses (chapter 3.1.5).

4.1.4 Fe^{2+} and folate deficiency leads to abnormal Ca^{2+} influx in RBCs during repetitive bleeding induced reticulocytosis

As described in chapter 2.3.3, I used repetitive bleeding method to induce reticulocytosis. During the period of repetitive retro-orbital puncture, drinking water must be supplemented with iron (3 mg Fe^{2+}/100 ml) and folate (20 µg/100 ml). I found that RBCs from Fe^{2+}-deficiency mice show abnormal Ca^{2+} influx under control conditions (in Tyrode without any stimulation). From average valuesdepicted in Figure 35A, RBCs from different days after bleeding in Fe^{2+} deficiency mice show a different spontaneous activity (in Tyrode). From 4^{th} day to 7^{th} day after the initial bleeding procedure, RBCs show a steadily increasing Ca^{2+} influx in Tyrode.

I additionally analyzed the parameter **"**Max response" of the Ca^{2+} influx induced by LPA into RBCs at different days after bleeding in Fe^{2+} deficient mice (Figure 35B). The black stars denote significance compared with control conditions ("LPA" compared with "Ctrl (LPA)", and "Tyrode" compared with "Ctrl (Tyrode)", respectively). Red stars refer to significance of "LPA" compared with "Tyrode" at the same day. In Figure 35B, an abnormal Ca^{2+} influx can be recognised even in Tyrode. From 4^{th} day to 7^{th} day, the abnormal Ca^{2+} influx increases and after the 7^{th} day, the abnormal Ca^{2+} influx begins to decrease. After the ~28^{th} day, it returns to the normal level (Figure 35B). The mechanism of this abnormal "Ca^{2+} influx" is not clear, but maybe it is an artifact related to hemoglobin synthesis. Hemoglobin synthesis requires Fe^{2+}, and one of its absorption wavelength peak is ~540 nm. And Fluo-4 emission wavelength is ~520 nm, so the concentration of hemoglobin may influence the fluorescence intensity of Fluo-4. Nevertheless, this finding showed the extreme importance of Fe^{2+} and folate supplement in repetitive bleeding through retro-orbital puncture and the following Ca^{2+} influx investigation.

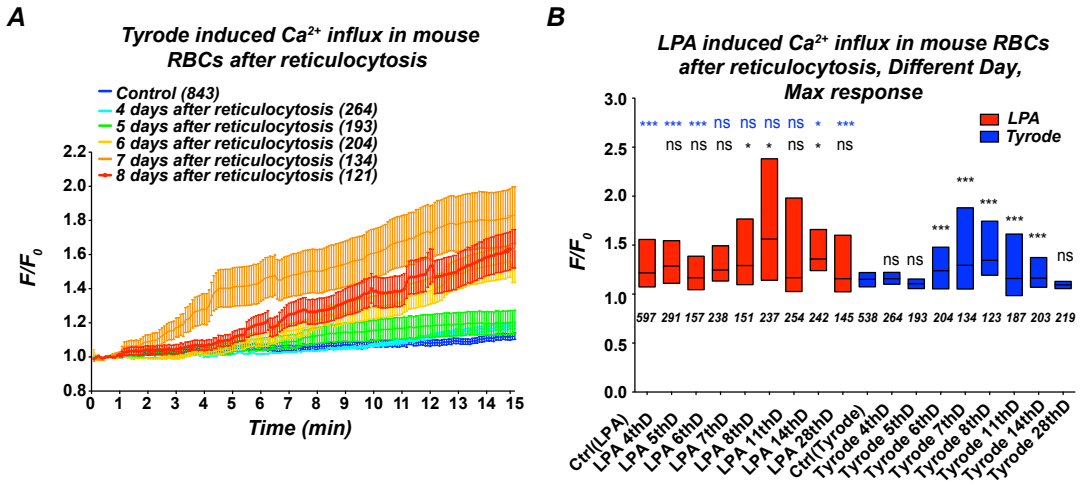

Figure 35: Fe^{2+} and folate deficiency leads to abnormal Ca^{2+} increase

A, *The lack of Fe^{2+} and folate supplement in the food after bleeding will lead to abnormal Ca^{2+} influx, even in Tyrode.* ***B,*** *Max response of Ca^{2+} influx induced by LPA from RBCs at different days after bleeding in Fe^{2+}deficiened mice. Black stars indicate significance compared with control conditions ("LPA" compared with "Ctrl (LPA)" and "Tyrode" compared with "Ctrl (Tyrode)", respectively). Red stars refer to significance of "LPA" compared with "Tyrode" at the same day.*

4.1.5 The influence of cell age on LPA-induced Ca^{2+}-influx

Cellular properties change with cell age, which also applies to RBCs [272]. An established method to differentiate RBCs by age is a separation using Stractan or Percoll density gradients. This approach is based on the assumption that RBCs gain density with age. However, recent findings indicated that the densification with age reversed in cells approaching the age of clearance [273] and that those methods may activate receptors or channels in the RBCs´ plasma membranes [274] and unpublished results of the Bogdanova lab. This change might lead to a dehydration of young cells and their movement to the fraction of dense cells. Although such effects may only apply to a subpopulation of the separated fractions, I used a more reliable and reproducible approach to compare LPA-induced Ca^{2+} signals of very young RBCs (reticulocytes) and RBCs on the verge of clearance (i.e., very old).

Because this approach was not applicable to RBCs of human donors, we used the RBCs of BALB/c mice.

I identified reticulocytes following the Ca^{2+}-imaging experiments by new methylene blue staining. Because the normal fraction of reticulocytes in the blood is very low (approximately 1%), we increased their number by reticulocytosis [214]. As depicted in the right panel of Figure 14, the substantial increase in the number of reticulocytes was apparent following this intervention. We then challenged different cell populations with 5 µM LPA (Figure 15) and found that in comparison to the fraction of RBCs (purple box in Figure 15Ad), the reticulocytes (green box in Figure 15Ad) did not show any response to the LPA stimulation.

To identify very old RBCs at the verge of clearance, I drew blood from mice subjected to reticulocytosis and stained RBCs with the plasma membrane stain PKH26 [229] (Figure 16, upper panels). At least 67.9% of the cells that were re-injected into the same mouse were stained with PKH26. The fluorescence of the cells was analyzed again after 7 and 43 days (Figure 16A, lower panels). After 7 days in circulation, 5.7% of the cells were PKH26-stained; after 43 days, this portion was reduced to less than 1%, indicating that the rest of the PKH26 positive RBCs were cleared in the mouse body. Because the average lifetime of RBCs in BALB/c mice has been determined to be 46 days [230], we waited for 43 days until we isolated PKH26-stained RBCs by fluorescence activated cell sorting (region R2 in Figure 16A). Those cells were regarded as old cells close to clearance. Ca^{2+} signals were compared to non-stained RBCs representing cells of all ages. Figure 16B-D summarizes the results obtained with these two cell populations. PKH26-negative cells responded only with a very small but significant increase when stimulated with 5 µM LPA (green box in Figure 16B). In contrast, the PKH26-positive cells that were manually selected from the original blood sample (purple box in Figure 16B) and the PKH26-positive cells enriched by FACS (red box in Figure 16B) both displayed a substantially augmented Ca^{2+}

response. Nevertheless, neither visually identified PKH+ cells (VIS) nor FACS sorted cells showed LPA responses that were uniform. Instead, both populations of responders still displayed a substantial heterogeneity, as observed in the response histograms in Figure 16C and in the representative traces in Figure 16D.

In summary, the age of RBCs appeared to be an important factor responsible for the heterogeneity of LPA-induced responses. However, my data also indicate that the age of RBCs is not the only characteristic responsible for the observed variability.

In conclusion, I found Ca^{2+} influx induced by LPA and PGE_2 in human RBCs is surprisingly dynamic and heterogeneous. This could not be extracted from FACS analysis, because FACS can only show a Ca^{2+} concentration of a single cell at a single time point, not in time series. Only parts of RBCs react to LPA stimulation, and even in responding cells, each individual cell shows different Ca^{2+} influx properties. The cell age of RBCs is involved in but not the only reason of this phenomenon. These unexpected findings need to be taken into account in further studies that require approaches for single-cell analysis. The identified heterogeneity in the RBC response described in our study is important because it not only impacts our basic understanding of RBCs signaling but also our understanding of their contribution to numerous diseases. Taken together with the emerging knowledge of an active role of RBCs in blood clotting, understanding the dynamics of RBC Ca^{2+} signaling might offer new targets for modulating thrombotic activity. Nevertheless, In this work we proposed a way to analyze the Ca^{2+} influx data, which is more precise and can get more information of Ca^{2+} change than simple average analysis. It is helpful for better understanding of Ca^{2+} influx and Ca^{2+} function in human RBCs.

4.1.6 Ca^{2+} balance in RBCs

Ca^{2+} is a universal signalling molecule involved in regulating cell cycle and fate, metabolism and structural integrity, motility and volume. In healthy human RBCs, basal free Ca^{2+} concentration in RBCs under physiological conditions is estimated to be in the range of 30 to 60 nM [105]. The RBCs membrane had extremely low basal permeability to Ca^{2+} and maintained intracellular free Ca^{2+} concentration [105]. The main Ca^{2+} extrusion pathway is through the plasma membrane Ca^{2+} pump (PMCA) [105] while the Ca^{2+} influx pathway mediated by several kinds of cation channels, such as voltage-activated non-selective cation channels [48, 275-277], Cav2.1 channels [49], TRPC6 channels [278], and NMDA channels [37]. Like in other cells, Ca^{2+} plays important role in RBCs biological activities. In the beginning of RBCs lifespan, Ca^{2+}-dependent signal induced RBCs to differentiate from precursor cells [279, 280]. In mature RBCs, Ca^{2+} activates numerous Ca^{2+}-dependent proteins, such as calmodulin [281], PKCα [282] and PI_3K [283], to take part in physiological and pathophysiological processes. To activate these proteins, phosphorylation is the most important and most polular modulations of protein activity in RBCs, especially in PKCs [284]. With the activation of these Ca^{2+} sensors, cytoskeletal flexibility was changed, followed by the regulation of RBCs volume [27, 285]. Ca^{2+} uptake could also activate scramblase, a protein responsible for bidirectional transmembrane movement of phospholipids [286], leading to the break-down of the originally asymmetrical distribution of phospholipids between the inner and outer membrane leaflet and PS exposure [287]. Some metabolic enzymes including pyruvate kinase were also under regulation of Ca^{2+} in RBCs [288, 289]. Furthermore, the haemoglobin oxygen saturation [290] and RBC's redox state [291, 292] also related to the intracellular Ca^{2+}. In old RBCs, Ca^{2+} concentration is belived to exceed those in reticulocytes and young RBCs [293] and involved in cell clearance. In brief, Intracellular Ca^{2+} levels in the human RBCs not only join in biophysical properties regulation such as membrane composition, volume and rheological properties, but also in physiological properties such as metabolic activity, redox state and cell

clearance. Furthermore, besides the physiological function, Ca^{2+} is also associated with a number of pathological states including clotting formation [232, 294], sickle cell disease [295-297], thalassemia [298, 299] and phosphofructokinase deficiency [300].

Therefore, the role of Ca^{2+} in RBCs physiology and pathophysiology need to be appreciated and valued. Recently, as a complement of cell population measurements, single cell based methods became more and more important and was applied to many experiments [301]. This is because of the recent finding that heterogeneous distribution of Ca^{2+} in RBCs cytosol are related to the abnormally high Ca^{2+} levels [302], which are extremely important in patients with haematological disorders, such as sickle cell disease. However, the Ca^{2+} binding properties and related proteins within the cells need further attention and investigation. Considering the broad variety of Ca^{2+} involved procedure, the following processes could probably be used to indirectly investigate the function of abnormally increased intracellular free Ca^{2+} levels in RBCs: (1) cell volume and morphology changes, such as microcytosis, echinocytosis, stomatocytosis, high MCHC and increase in cell density; (2) congenital haemolytic anaemia associated with stomatocytosis, reticulocytosis, and shortened RBC survival; (3) decrease in the intracellular K^+ levels, pseudohyperkalemia; (4) loss of RBC deformability, changes in osmotic resistance, an increase when dehydration has occurred but cytoskeletal stability is still maintained, or a decrease when cytoskeleton is partially disassembled; (5) appearance of calpain-induced band 3 cleavage fragments; (6) oxidative stress or unusually high NO production (nitrosated Hb, met-Hb); (7) ATP depletion due to hyperactivation of PMCA; (8) increase in inter-RBC aggregability; and (9) increase in PS exposure.

4.2 Signal pathway induced by LPA in RBCs

4.2.1 Scheme showing the involving signal transduction pathway

We demonstrated that LPA can induce Ca^{2+} influx in human RBCs, and both Cav2.1 and TRPC6 channels are involved in this procedure. On one hand, these events were confirmed in a TRPC6 $^{(-/-)}$ mouse model, where Ca^{2+} influx induced by LPA was significantly decreased. However, TRPC6 knock out could only partly decrease LPA induced Ca^{2+} influx, while in combination with inhibition of the Cav2.1 channel could fully inhibit it. Inhibition of PKCα in human RBCs has a similar effect as TRPC6 knock out in mouse RBCs. On the other hand, blocking Cav2.1 can also partly inhibit LPA induced Ca^{2+} influx in human RBCs and wild type mouse RBCs, but can fully inhibit it in TRPC6 knock out mouse. Taken all together, we proposed the schematic diagram for LPA-induced Ca^{2+} influx in RBCs (Figure 36A). Furthermore, these two co-existed signal pathways induce two kinds of different Ca^{2+} influx. Figure 36B-D showed the idealized stereotypical responses. The one through Cav2.1 activation is smooth increase (Figure 36B) and the other one, which is through PKCα and TRPC6, is faster and more instant (Figure 36C). These two signal pathways coexisted in most of RBCs, thus a typical Ca^{2+} trace seems like the trace shown in (Figure 36D).

However, there are still some questions need to be answered. For example, it is well known that the activation of PKCα requires Ca^{2+}, but where the Ca^{2+} for PKCα activation is from in LPA induced signal pathway (Figure 36)? One explanation is constitutive activation of PKCα by the Ca^{2+} in the cell. Another possibility is the Ca^{2+} entry through the Cav2.1 channel. If this is true, blocking Cav2.1 should fully inhibit LPA induced Ca^{2+} influx, which is not the case in our experiment (Figure 25), but this could be explained by LPA induced unspecific activation of other channels. Nevertheless, this question needs to be further investigated.

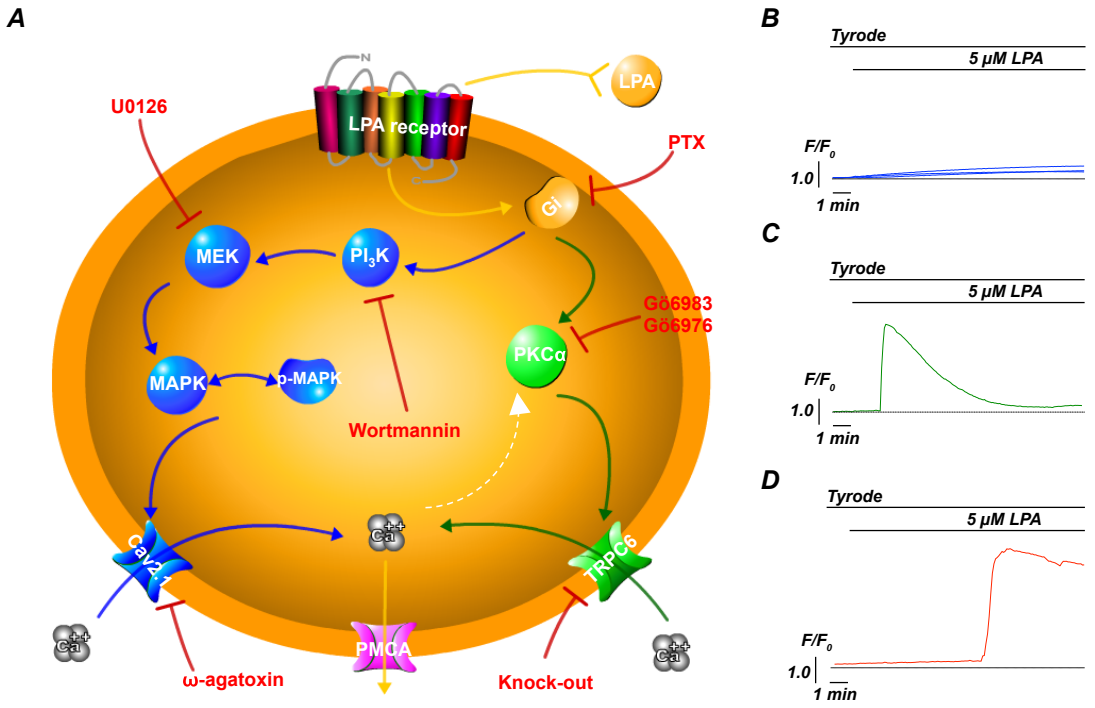

Figure 36: Schematic showing the involving signal transduction pathway.

***A**, I proposed two coexisted signal pathways in LPA induced Ca^{2+} influx in RBCs: 1) LPA--G_i--PI_3K--MEK--Cav2.1 and 2) LPA--G_i--PKC--TRPC6. **B-D,** Putative single cell behavior. **B**, Ca^{2+} influx through the LPA--G_i--PI_3K--MEK--Cav2.1 branch and **C**, Ca^{2+} influx through LPA--G_i--PKC--TRPC6 branch. Usually, these two signal pathways coexisted in most of RBCs, thus a typical Ca^{2+} trace is shown in **D**.*

4.2.2 Ca^{2+} free pretreatment induced Ca^{2+} influx

Physiological saline buffer and PBS, which are Ca^{2+} free, are the most widely used buffer in RBCs research [32, 278, 303]. Usually, the experiments were operated in the way as follow: RBCs were put into saline or PBS, stimulated with desired substance and then Ca^{2+} was added to observe Ca^{2+} influx [32]. In other words, RBCs were in Ca^{2+} free condition before the desired substance application.

Therefore, the influence of Ca^{2+} free pretreatment on Ca^{2+} influx was investigated. RBCs were put into Ca^{2+} free Tyrode containing EDTA for 15

minutes, and then transferred into normal Tyrode. As shown in Figure 37, even though in the absence of LPA or any other stimulation, cells show a clear Ca^{2+} influx (green line). In the existence of LPA, the Ca^{2+} influx (cyan line) was greatly enhanced compared with control condition (red line). The max response value of single cells also shows the same trend (right panel). Taken together, these results suggest that preincubation of RBCs in Ca^{2+} free condition enhances the following Ca^{2+} influx when RBCs were put into Ca^{2+} containing condition, therefore the usage of PBS or saline in Ca^{2+} research in RBCs should be reconsidered.

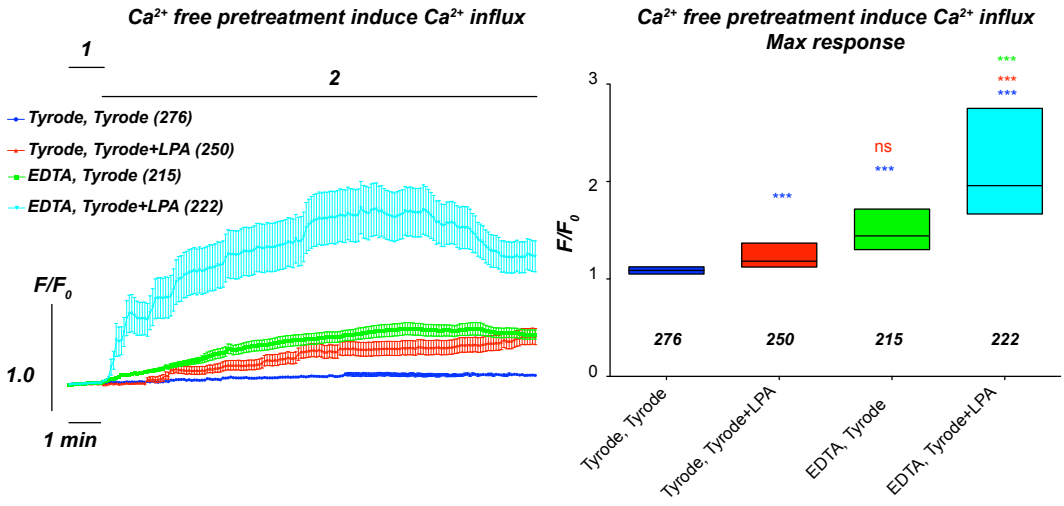

Figure 37: Ca^{2+} free pretreatment induced Ca^{2+} influx in human RBCs.

Pretreatment with EDTA (green line, stage 1) and then with Tyrode (stage 2) directly induced Ca^{2+} influx in human RBCs. It also enhanced the LPA-induced Ca^{2+} influx (cyan line) compared with normal condition (red line). The statistics of max response also shows the same trend (right panel).

4.2.3 ω-agatoxin-TK could not fully inhibit PMA/LPA induced Ca^{2+} influx

In 2000, Yang and co-workers showed that LPA stimulates a rapid, dose-dependent Ca^{2+} influx in RBCs. They found an inhibition by ω-agatoxin-TK, a Ca^{2+} channel blocker specific for Cav2.1, using flow cytometry [32]. However, through video imaging, we found that LPA induced Ca^{2+} influx in RBCs can

only partly be inhibited by ω-agatoxin-TK (Figure 25). Furthermore, Andrews and co-workers also proposed that PMA shows a similar function as LPA and can also be inhibited by ω-agatoxin-TK [49]. Therefore, I also investigated the PMA function in RBCs according to the same protocol as this group.

Andrews and co-workers treated RBCs with 1 μM ω-agatoxin-TK or PBS (control) for 10 minutes, and then stimulated cells with 3 μM PMA [49]. 3 minutes after PMA stimulation, cells were analyzed by flow cytometry. The result shows that ω-agatoxin-TK pretreatment can fully inhibit PMA induced Ca^{2+} influx. However, in video-imaging experiments, I found that 1 μM ω-agatoxin-TK can only partly inhibit 3 μM PMA induced Ca^{2+} influx, even though we use exactly the same protocol (Figure 38A). Analysis of the amplitude from each cell also showed the same trend, after 3 minutes as well as after 14 minutes PMA stimulation (Figure 38B, left panel). Furthermore, the distribution of the amplitude also changed with time (Figure 38B, right panel).

Taken together, I proposed that LPA or PMA induced Ca^{2+} influx could not be fully inhibited by ω-agatoxin-TK. One explanation of the conflict between our data and others might be the loss (lysis) of cells with high Ca^{2+} concentration in FACS. As it is known, in FACS, a high shear stress is applied to RBCs, which may lead to a significant cell break. Furthermore, RBCs with high Ca^{2+} is more fragile than normal RBCs, which means high Ca^{2+} cells lyse much easier than normal cells under the shear stress. Therefore, it is reasonable to hypothesize that FACS could not fully reveal the Ca^{2+} change in RBCs. Nevertheless, it is widely accepted that LPA or PMA induces Ca^{2+} influx in RBCs and Cav2.1 is involved in this process, but whether other signal pathway exists in this procedure need to be further investigated.

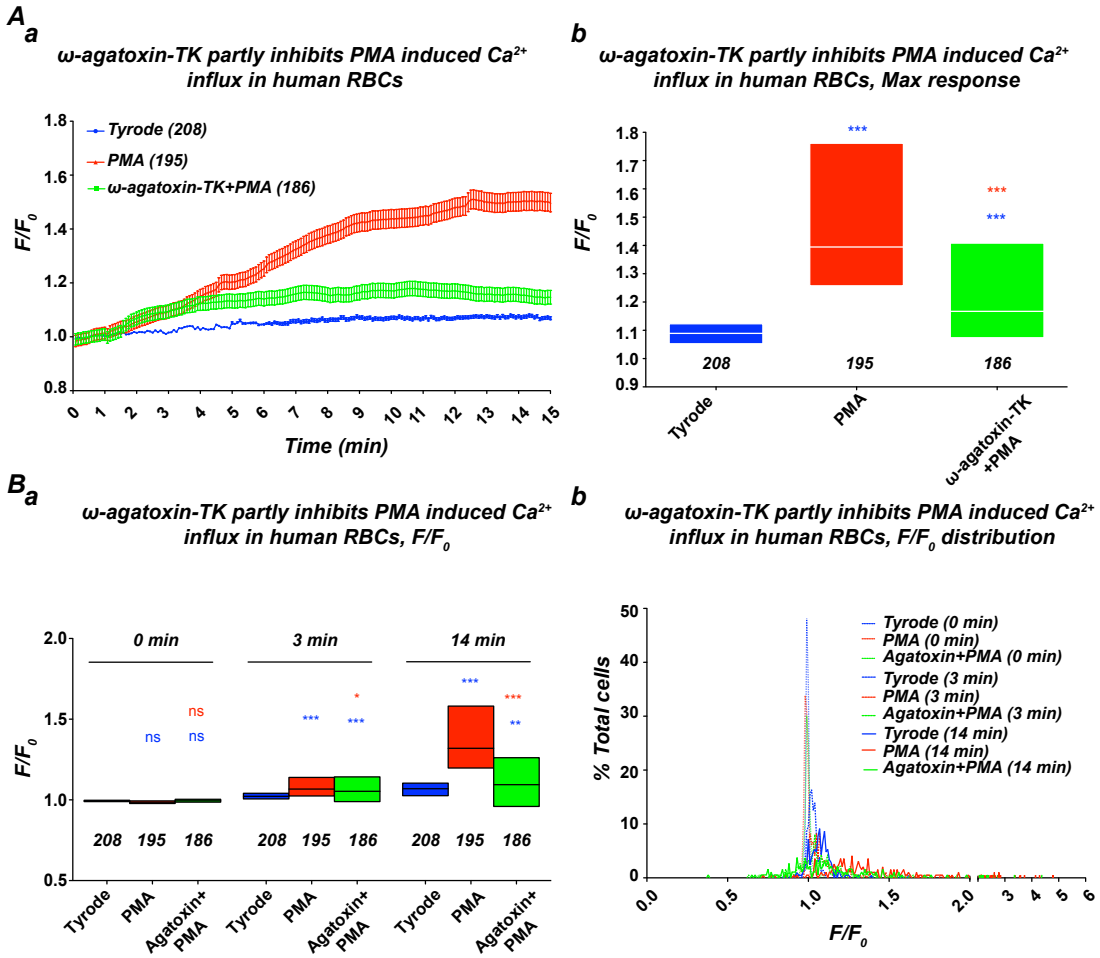

Figure 38: 1 µM ω-agatoxin-TK can partly but not fully inhibit 3 µM PMA induced Ca^{2+} influx in human RBCs.

A, *In our video imaging experiments, ω-agatoxin-TK only shows a partly inhibition of the PMA-induced Ca^{2+} influx both in (a) averaged traces and (b) statistical analysis of the max response, with the same condition as Andrewsand co-workers described [49]. In brief, RBCs pretreated with 1 µM ω-agatoxin-TK for 10 minutes and then 3 µM PMA was added, and the cells were incubated for an additional 3 minutes before analysis.* ***B,*** *Ca^{2+} content analysis 3 minutes and 14 minutes after PMA stimulation. At both time points, the average value (left panel) and the distribution (right panel) of F/F_0 from individual cells show that agatoxin can only partly inhibit PMA induced Ca^{2+} influx. Colored stars represent the significance between the bar below the stars compared and the bar with the same color of stars.*

4.3 Ca^{2+} homeostasis and LPA in sickle cell disease

In this thesis I additionally focused on the altered Ca^{2+} homeostasis of sickle RBCs. The altered Ca^{2+} homeostasis is extremely important for the understanding of sickle cell disease. In 1973, Eaton [295] and Palek [304] independently discovered that the total Ca^{2+} content of sickle cells was highly increased. These findings revealed the possible link between deoxy- HbS polymerization and sickle cell dehydration and Ca^{2+}-sensitive IK1 channels were believed to be involved in this link. Furthermore, the elevated Ca^{2+} content of sickle cells was found to be unevenly distributed (chapter 3.3.1) with more total Ca^{2+} contained within progressively denser cells [246, 295, 305]. However, many questions of the role of Ca^{2+} in sickle cell disease need to be resolved.

The first question was by which mechanism Ca^{2+} entered the RBCs. The relationship between deoxy-HbS polymerization and increased membrane permeability had been found by Tosteson *et.al* [306-308], but he only documented the increased permeability of Na^+ and K^+. The Ca^{2+} permeability increase in SCD was firstly found by Eaton *et al.* in 1973 [295] and was further investigated from heterozygote and homozygotes sickle cell anaemia subjects by many other groups [246, 304, 305, 309]. And more recently, Bookchin *et al.* additionally investigated the Ca^{2+} permeability increase in in different density subpopulations of sickle cells [310]. The Mg^{2+} permeability in sickle cells was also investigated by Ortiz *et al*. in 1990 [311]. In summary, these results showed that in sickle cells the Ca^{2+} permeability of the RBCs membrane increased from 50 µmol/(lcells·h) (normal value) to up to ~300 µmol/(lcells·h) at physiological $[Ca^{2+}]_o$ levels [296]. These results clearly showed that the Ca^{2+} permeability greatly increased in sickle cells, but how the Ca^{2+} was retained within the RBCs membrane remained unclear.

In this thesis I found that LPA receptor subtype 4 (LPAR4) was overexpressed in human sickle RBCs (chapter 3.3.2), which might be one explanation of

stronger LPA-induced Ca^{2+} influx in sickle RBCs compared with the one in healthy RBCs. Despite the overexpression of LPAR4, LPA induced the same signal pathway both in sickle and healthy RBCs (chapter 3.3.3-3.3.6). Interestingly, the orphan G protein-coupled receptor p2y9/GPR23, was recently identified to be LPA4 [312, 313]. P2Y receptors are a family of purinergic G protein-coupled receptors and could be activated by nucleotides such as ATP [314]. Therefore, the overexpression of LPAR4 in sickle RBCs might be related to ATP metabolism. Meanwhile, a recent study [315] suggests that the cytoskeleton underneath the RBCs plasma membrane, which consists by a cytoskeletal protein named spectrin, might act as a steric barrier restricting membrane undulations toward the intracellular cytoskeleton networkand this procedure is ATP dependent. Other studies also showed the inhibitory function of ATP on spectrin-membrane interaction both in RBCs ghost [316] and intact RBCs [317]. In brief, the topology of RBCs membrane is the integrity of the underlying spectrin cytoskeleton dependent and ATP-dependent. Thus, the LPAR4 overexpression might contribute to the cytoskeleton change and sickle shape formation in sickle RBCs. Taken together, the finding of LPAR4 overexpression in sickle RBCs appears important for better understanding of RBC physiology and pathophysiology.

4.4 Summary and perspective

In conclusion, I found Ca^{2+} signaling in RBCs is surprisingly dynamic and diverse. RBC age is just one of the determinants for the diversity. Therefore, a single-cell analysis method was developed to analyze heterogeneity in the RBC response. Using this method, two coexisted signal pathways of LPA-induced Ca^{2+} influx were found in healthy human RBCs: one is LPA-G_i-PI_3K-MEK-Cav2.1 and another one is LPA-G_i-PKC-TRPC6. In sickle human RBCs, LPAR4 was found to present an increased expression, but LPA-induced Ca^{2+} influx followed the same signal pathway as in healthy human RBCs.

For the future I believe that the diversity of Ca^{2+} signalling in RBCs need to be taken into account in further studies, and the single-cell analysis enables us to extract Ca^{2+} signalling information and is flexible to be used on different research purposes, such as LPA-induced Ca^{2+} signaling in sickle RBCs. The identified heterogeneity in the RBC response described in our study is important because it not only impacts our basic understanding of RBCs signalling but also our understanding of their contribution to numerous RBCs diseases. Our findings about LPA in sickle human RBCs also provided a better understanding of sickle cell disease. Taken together with the emerging knowledge of an active role of RBCs in blood clotting, understanding the dynamics of RBC Ca^{2+} signaling might offer new targets for modulating thrombotic activity and better understanding of RBCs diseases.

5. References

1. Hochmuth RM, Waugh RE (1987) Erythrocyte membrane elasticity and viscosity. Annual review of physiology 49:209-219.
2. Mills JP, Qie L, Dao M, Lim CT, Suresh S (2004) Nonlinear elastic and viscoelastic deformation of the human red blood cell with optical tweezers. Mechanics & chemistry of biosystems : MCB 1 (3):169-180.
3. Chien S (1987) Red cell deformability and its relevance to blood flow. Annual review of physiology 49:177-192.
4. Mohandas N, Evans E (1994) Mechanical properties of the red cell membrane in relation to molecular structure and genetic defects. Annu Rev Biophys Biomol Struct 23:787-818.
5. Rybicki AC, Heath R, Lubin B, Schwartz RS (1988) Human erythrocyte protein 4.1 is a phosphatidylserine binding protein. J Clin Invest 81 (1):255-260.
6. An X, Guo X, Sum H, Morrow J, Gratzer W, Mohandas N (2004) Phosphatidylserine binding sites in erythroid spectrin: location and implications for membrane stability. Biochemistry 43 (2):310-315.
7. Engelmann B, Duhm J (1989) Distinction of two components of passive Ca^{2+} transport into human erythrocytes by Ca^{2+} entry blockers. Biochim Biophys Acta 981 (1):36-42.
8. Dodge JT, Mitchell C, Hanahan DJ (1963) The preparation and chemical characteristics of hemoglobin-free ghosts of human erythrocytes. Arch Biochem Biophys 100:119-130.
9. Verkleij AJ, Zwaal RF, Roelofsen B, Comfurius P, Kastelijn D, van Deenen LL (1973) The asymmetric distribution of phospholipids in the human red cell membrane. A combined study using phospholipases and freeze-etch electron microscopy. Biochim Biophys Acta 323 (2):178-193.
10. Zwaal RF, Schroit AJ (1997) Pathophysiologic implications of membrane phospholipid asymmetry in blood cells. Blood 89 (4):1121-1132.
11. Nelson GJ (1973) The lipid composition of the blood of marine mammals. 3. The fatty acid composition of plasma and erythrocytes of Atlantic bottlenose dolphin, Tursiopstruncatus. Comp Biochem Physiol B 46 (2):257-268.
12. Broekhuyse RM (1974) Improved lipid extraction of erythrocytes. Clin Chim Acta 51 (3):341-343.
13. Broekhuyse RM (1969) Quantitative two-dimensional thin-layer chromatography of blood phospholipids. Clin Chim Acta 23 (3):457-461.
14. Woon LA, Holland JW, Kable EP, Roufogalis BD (1999) Ca^{2+} sensitivity of phospholipid scrambling in human red cell ghosts. Cell Calcium 25 (4):313-320.
15. Daleke DL (2008) Regulation of phospholipid asymmetry in the erythrocyte membrane. Curr Opin Hematol 15 (3):191-195.

16. Sims PJ, Wiedmer T (2001) Unraveling the mysteries of phospholipid scrambling. Thromb Haemost 86 (1):266-275.
17. Salzer U, Prohaska R (2001) Stomatin, flotillin-1, and flotillin-2 are major integral proteins of erythrocyte lipid rafts. Blood 97 (4):1141-1143.
18. Murphy SC, Samuel BU, Harrison T, Speicher KD, Speicher DW, Reid ME, Prohaska R, Low PS, Tanner MJ, Mohandas N, Haldar K (2004) Erythrocyte detergent-resistant membrane proteins: their characterization and selective uptake during malarial infection. Blood 103 (5):1920-1928.
19. Hugel B, Martinez MC, Kunzelmann C, Freyssinet JM (2005) Membrane microparticles: two sides of the coin. Physiology (Bethesda) 20:22-27.
20. Wood BL, Gibson DF, Tait JF (1996) Increased erythrocyte phosphatidylserine exposure in sickle cell disease: flow-cytometric measurement and clinical associations. Blood 88 (5):1873-1880.
21. Yasin Z, Witting S, Palascak MB, Joiner CH, Rucknagel DL, Franco RS (2003) Phosphatidylserine externalization in sickle red blood cells: associations with cell age, density, and hemoglobin F. Blood 102 (1):365-370.
22. Kuypers FA, Yuan J, Lewis RA, Snyder LM, Kiefer CR, Bunyaratvej A, Fucharoen S, Ma L, Styles L, de Jong K, Schrier SL (1998) Membrane phospholipid asymmetry in human thalassemia. Blood 91 (8):3044-3051.
23. Setty BN, Kulkarni S, Stuart MJ (2002) Role of erythrocyte phosphatidylserine in sickle red cell-endothelial adhesion. Blood 99 (5):1564-1571.
24. An X, Debnath G, Guo X, Liu S, Lux SE, Baines A, Gratzer W, Mohandas N (2005) Identification and functional characterization of protein 4.1R and actin-binding sites in erythrocyte beta spectrin: regulation of the interactions by phosphatidylinositol-4,5-bisphosphate. Biochemistry 44 (31):10681-10688.
25. Manno S, Takakuwa Y, Mohandas N (2002) Identification of a functional role for lipid asymmetry in biological membranes: Phosphatidylserine-skeletal protein interactions modulate membrane stability. Proc Natl Acad Sci U S A 99 (4):1943-1948.
26. An X, Zhang X, Debnath G, Baines AJ, Mohandas N (2006) Phosphatidylinositol-4,5-biphosphate (PIP2) differentially regulates the interaction of human erythrocyte protein 4.1 (4.1R) with membrane proteins. Biochemistry 45 (18):5725-5732.
27. Mohandas N, Gallagher PG (2008) Red cell membrane: past, present, and future. Blood 112 (10):3939-3948.
28. Yawata Y (2003) Cell membrane: the red blood cell as a model. WILEY-VCH Verlag.
29. Reid ME, Mohandas N (2004) Red blood cell blood group antigens: structure and function. Semin Hematol 41 (2):93-117.
30. Anstee DJ (1995) Blood group antigens defined by the amino acid sequences of red cell surface proteins. Transfus Med 5 (1):1-13.

31. Cartron JP, Colin Y (2001) Structural and functional diversity of blood group antigens. Transfus Clin Biol 8 (3):163-199.
32. Yang L, Andrews DA, Low PS (2000) Lysophosphatidic acid opens a Ca(++) channel in human erythrocytes. Blood 95 (7):2420-2425.
33. Makhro A, Wang J, Vogel J, Boldyrev AA, Gassmann M, Kaestner L, Bogdanova A Functional NMDA receptors in rat erythrocytes. American journal of physiology 298 (6):C1315-1325.
34. Telen MJ (1995) Erythrocyte blood group antigens: not so simple after all. Blood 85 (2):299-306.
35. Cohen CM, Gascard P (1992) Regulation and post-translational modification of erythrocyte membrane and membrane-skeletal proteins. Semin Hematol 29 (4):244-292.
36. Bernhardt I, Weiss, E., (2003) Passive membrane permeability for ions and the membrane potential. Red cell membrane transport in health and disease (eds. Bernhardt, I., Elorry, J.C.):pp. 83-109.
37. Makhro A, Wang J, Vogel J, Boldyrev AA, Gassmann M, Kaestner L, Bogdanova A (2010) Functional NMDA receptors in rat erythrocytes. Am J Physiol Cell Physiol 298 (6):C1315-1325.
38. Bennekou P (1993) The voltage-gated non-selective cation channel from human red cells is sensitive to acetylcholine. Biochim Biophys Acta 1147 (1):165-167.
39. Bennekou P, Barksmann TL, Christophersen P, Kristensen BI (2006) The human red cell voltage-dependent cation channel. Part III: Distribution homogeneity and pH dependence. Blood Cells Mol Dis 36 (1):10-14.
40. Bennekou P, Barksmann TL, Jensen LR, Kristensen BI, Christophersen P (2004) Voltage activation and hysteresis of the non-selective voltage-dependent channel in the intact human red cell. Bioelectrochemistry 62 (2):181-185.
41. Alabi AA, Bahamonde MI, Jung HJ, Kim JI, Swartz KJ (2007) Portability of paddle motif function and pharmacology in voltage sensors. Nature 450 (7168):370-375.
42. Long SB, Tao X, Campbell EB, MacKinnon R (2007) Atomic structure of a voltage-dependent K+ channel in a lipid membrane-like environment. Nature 450 (7168):376-382.
43. Donlon JA RA (1969) The cation permeability of erythrocytes in low ionic strength media of various tinicities. J Membr Biol 1:37-52.
44. Halperin JA, Brugnara C, Tosteson MT, Van Ha T, Tosteson DC (1989) Voltage-activated cation transport in human erythrocytes. Am J Physiol 257 (5 Pt 1):C986-996.
45. Christophersen P, Bennekou P (1991) Evidence for a voltage-gated, non-selective cation channel in the human red cell membrane. Biochim Biophys Acta 1065 (1):103-106.
46. Bennekou P, Barksmann TL, Kristensen BI, Jensen LR, Christophersen P (2004) Pharmacology of the human red cell voltage-dependent cation channel. Part II: inactivation and blocking. Blood Cells Mol Dis 33 (3):356-361.

47. Barksmann TL, Kristensen BI, Christophersen P, Bennekou P (2004) Pharmacology of the human red cell voltage-dependent cation channel; Part I. Activation by clotrimazole and analogues. Blood Cells Mol Dis 32 (3):384-388.
48. Kaestner L, Christophersen P, Bernhardt I, Bennekou P (2000) The non-selective voltage-activated cation channel in the human red blood cell membrane: reconciliation between two conflicting reports and further characterisation. Bioelectrochemistry 52 (2):117-125.
49. Andrews DA, Yang L, Low PS (2002) Phorbol ester stimulates a protein kinase C-mediated agatoxin-TK-sensitive calcium permeability pathway in human red blood cells. Blood 100 (9):3392-3399.
50. Li Q, Jungmann V, Kiyatkin A, Low PS (1996) Prostaglandin E2 stimulates a Ca^{2+}-dependent K^+ channel in human erythrocytes and alters cell volume and filterability. J Biol Chem 271 (31):18651-18656.
51. Kaestner L, Tabellion W, Lipp P, Bernhardt I (2004) Prostaglandin E2 activates channel-mediated calcium entry in human erythrocytes: an indication for a blood clot formation supporting process. Thromb Haemost 92 (6):1269-1272.
52. Huber SM, Gamper N, Lang F (2001) Chloride conductance and volume-regulatory nonselective cation conductance in human red blood cell ghosts. Pflugers Arch 441 (4):551-558.
53. Duranton C, Huber SM, Lang F (2002) Oxidation induces a Cl(-)-dependent cation conductance in human red blood cells. J Physiol 539 (Pt 3):847-855.
54. Lang KS, Myssina S, Tanneur V, Wieder T, Huber SM, Lang F, Duranton C (2003) Inhibition of erythrocyte cation channels and apoptosis by ethylisopropylamiloride. Naunyn Schmiedebergs Arch Pharmacol 367 (4):391-396.
55. Myssina S, Huber SM, Birka C, Lang PA, Lang KS, Friedrich B, Risler T, Wieder T, Lang F (2003) Inhibition of erythrocyte cation channels by erythropoietin. J Am Soc Nephrol 14 (11):2750-2757.
56. Gardos G (1958) The function of calcium in the potassium permeability of human erythrocytes. Biochim Biophys Acta 30 (3):653-654.
57. Neylon CB, Lang RJ, Fu Y, Bobik A, Reinhart PH (1999) Molecular cloning and characterization of the intermediate-conductance Ca(2+)-activated K(+) channel in vascular smooth muscle: relationship between K(Ca) channel diversity and smooth muscle cell function. Circ Res 85 (9):e33-43.
58. Ishii TM, Silvia C, Hirschberg B, Bond CT, Adelman JP, Maylie J (1997) A human intermediate conductance calcium-activated potassium channel. Proc Natl Acad Sci U S A 94 (21):11651-11656.
59. Klein H, Garneau L, Banderali U, Simoes M, Parent L, Sauve R (2007) Structural determinants of the closed KCa3.1 channel pore in relation to channel gating: results from a substituted cysteine accessibility analysis. J Gen Physiol 129 (4):299-315.
60. Gardos G (1959) The role of calcium in the potassium permeability of human erythrocytes. Acta physiologica Hungarica 15 (2):121-125.

61. Grygorczyk R, Schwarz W (1983) Properties of the CA^{2+}-activated K^+ conductance of human red cells as revealed by the patch-clamp technique. Cell Calcium 4 (5-6):499-510.
62. Grygorczyk R, Schwarz W, Passow H (1984) Ca^{2+}-activated K^+ channels in human red cells. Comparison of single-channel currents with ion fluxes. Biophys J 45 (4):693-698.
63. Jensen BS, Strobaek D, Christophersen P, Jorgensen TD, Hansen C, Silahtaroglu A, Olesen SP, Ahring PK (1998) Characterization of the cloned human intermediate-conductance Ca^{2+}-activated K^+ channel. Am J Physiol 275 (3 Pt 1):C848-856.
64. Hunter MI, Thirkell D (1971) Variation in fatty acid composition of Sarcina flava membrane lipid with the age of the bacterial culture. J Gen Microbiol 65 (1):115-118.
65. Hunter MJ (1977) Human erythrocyte anion permeabilities measured under conditions of net charge transfer. J Physiol 268 (1):35-49.
66. Lassen UV, Lew VL, Pape L, Simonsen LO (1977) Transient increase in the K permeability of intact human and Amphiuma red cells induced by external Ca at alkaline pH [proceedings]. J Physiol 266 (1):72P-73P.
67. Jacobs MH, Stewart DR (1947) Osmotic properties of the erythrocyte; ionic and osmotic equilibria with a complex external solution. J Cell Physiol 30 (1):79-103.
68. Lew VL, Bookchin RM (1986) Volume, pH, and ion-content regulation in human red cells: analysis of transient behavior with an integrated model. J Membr Biol 92 (1):57-74.
69. Freeman CJ, Bookchin RM, Ortiz OE, Lew VL (1987) K-permeabilized human red cells lose an alkaline, hypertonic fluid containing excess K over diffusible anions. J Membr Biol 96 (3):235-241.
70. Lew VL, Bookchin RM (1991) Osmotic effects of protein polymerization: analysis of volume changes in sickle cell anemia red cells following deoxy-hemoglobin S polymerization. J Membr Biol 122 (1):55-67.
71. Teresa Tiffert, Robert M. Bookchin, Lew VL (2003) Calcium Homeostasis in Normal and Abnormal Human Red Cells. Red Cell Membrane Transport in Health and Disease:373-405.
72. Garcia-Sancho J, Lew VL (1988) Properties of the residual calcium pools in human red cells exposed to transient calcium loads. J Physiol 407:541-556.
73. Foller M, Kasinathan RS, Koka S, Lang C, Shumilina E, Birnbaumer L, Lang F, Huber SM (2008) TRPC6 contributes to the Ca(2+) leak of human erythrocytes. Cell Physiol Biochem 21 (1-3):183-192.
74. Hofmann T, Obukhov AG, Schaefer M, Harteneck C, Gudermann T, Schultz G (1999) Direct activation of human TRPC6 and TRPC3 channels by diacylglycerol. Nature 397 (6716):259-263.
75. Abramowitz J, Birnbaumer L (2009) Physiology and pathophysiology of canonical transient receptor potential channels. Faseb J 23 (2):297-328.
76. Dingledine R, Borges K, Bowie D, Traynelis SF (1999) The glutamate receptor ion channels. Pharmacological reviews 51 (1):7-61.

77. Liu Y, Zhang J (2000) Recent development in NMDA receptors. Chinese medical journal 113 (10):948-956.
78. Cull-Candy S, Brickley S, Farrant M (2001) NMDA receptor subunits: diversity, development and disease. Current opinion in neurobiology 11 (3):327-335.
79. Paoletti P, Neyton J (2007) NMDA receptor subunits: function and pharmacology. Current opinion in pharmacology 7 (1):39-47.
80. Chen H, Fitzgerald R, Brown AT, Qureshi I, Breckenridge J, Kazi R, Wang Y, Wu Y, Zhang X, Mukunyadzi P, Eidt J, Moursi MM (2005) Identification of a homocysteine receptor in the peripheral endothelium and its role in proliferation. J Vasc Surg 41 (5):853-860.
81. Tsai JC, Wang H, Perrella MA, Yoshizumi M, Sibinga NE, Tan LC, Haber E, Chang TH, Schlegel R, Lee ME (1996) Induction of cyclin A gene expression by homocysteine in vascular smooth muscle cells. The Journal of clinical investigation 97 (1):146-153.
82. Nasstrom J, Boo E, Stahlberg M, Berge OG (1993) Tissue distribution of two NMDA receptor antagonists, [3H]CGS 19755 and [3H]MK-801, after intrathecal injection in mice. Pharmacology, biochemistry, and behavior 44 (1):9-15.
83. Bogdanova A MA, Goede J (2009) NMDA receptors in mammalien erythrocytes. Clin Biochem 42:1858-1859.
84. Benga G, Popescu O, Pop VI (1985) Water exchange through erythrocyte membranes: p-chloromercuribenzene sulfonate inhibition of water diffusion in ghosts studied by a nuclear magnetic resonance technique. Bioscience reports 5 (3):223-228.
85. Agre P (2006) The aquaporin water channels. Proc Am Thorac Soc 3 (1):5-13.
86. Cucuianu M (2006) The discovery by Gh. Benga of the first water channel protein in 1985 in Cluj-Napoca, Romania, A few years before P. Agre (2003 Nobel Prize in Chemistry). Romanian journal of internal medicine = Revue roumaine de medecine interne 44 (3):323-334.
87. Bennett V, Baines AJ (2001) Spectrin and ankyrin-based pathways: metazoan inventions for integrating cells into tissues. Physiological reviews 81 (3):1353-1392.
88. Goodman SR, Krebs KE, Whitfield CF, Riederer BM, Zagon IS (1988) Spectrin and related molecules. CRC critical reviews in biochemistry 23 (2):171-234.
89. Luna EJ, Hitt AL (1992) Cytoskeleton--plasma membrane interactions. Science 258 (5084):955-964.
90. Mohandas N, Evans E (1994) Mechanical properties of the red cell membrane in relation to molecular structure and genetic defects. Annu Rev Biophys Biomol Struct 23:787-818.
91. Walensky LD MN, Lux SE. In: HandinRI, Lux SE, Stossel TP (2003) Blood, Principles and Practice of Hematology (2nd edition). PA: Lippincott Williams & Wilkins;:1726-1744.
92. Speicher DW, Marchesi VT (1984) Erythrocyte spectrin is comprised of many homologous triple helical segments. Nature 311 (5982):177-180.

93. Djinovic-Carugo K, Gautel M, Ylanne J, Young P (2002) The spectrin repeat: a structural platform for cytoskeletal protein assemblies. FEBS Lett 513 (1):119-123.
94. An X, Guo X, Zhang X, Baines AJ, Debnath G, Moyo D, Salomao M, Bhasin N, Johnson C, Discher D, Gratzer WB, Mohandas N (2006) Conformational stabilities of the structural repeats of erythroid spectrin and their functional implications. J Biol Chem 281 (15):10527-10532.
95. DeSilva TM, Peng KC, Speicher KD, Speicher DW (1992) Analysis of human red cell spectrin tetramer (head-to-head) assembly using complementary univalent peptides. Biochemistry 31 (44):10872-10878.
96. Speicher DW, DeSilva TM, Speicher KD, Ursitti JA, Hembach P, Weglarz L (1993) Location of the human red cell spectrin tetramer binding site and detection of a related "closed" hairpin loop dimer using proteolytic footprinting. J Biol Chem 268 (6):4227-4235.
97. Lecomte MC, Nicolas G, Dhermy D, Pinder JC, Gratzer WB (1999) Properties of normal and mutant polypeptide fragments from the dimer self-association sites of human red cell spectrin. Eur Biophys J 28 (3):208-215.
98. Karinch AM, Zimmer WE, Goodman SR (1990) The identification and sequence of the actin-binding domain of human red blood cell beta-spectrin. J Biol Chem 265 (20):11833-11840.
99. Ohanian V, Wolfe LC, John KM, Pinder JC, Lux SE, Gratzer WB (1984) Analysis of the ternary interaction of the red cell membrane skeletal proteins spectrin, actin, and 4.1. Biochemistry 23 (19):4416-4420.
100. Kuhlman PA, Hughes CA, Bennett V, Fowler VM (1996) A new function for adducin. Calcium/calmodulin-regulated capping of the barbed ends of actin filaments. J Biol Chem 271 (14):7986-7991.
101. Siegel DL, Branton D (1985) Partial purification and characterization of an actin-bundling protein, band 4.9, from human erythrocytes. J Cell Biol 100 (3):775-785.
102. An X, Salomao M, Guo X, Gratzer W, Mohandas N (2007) Tropomyosin modulates erythrocyte membrane stability. Blood 109 (3):1284-1288.
103. Porro F, Costessi L, Marro ML, Baralle FE, Muro AF (2004) The erythrocyte skeletons of beta-adducin deficient mice have altered levels of tropomyosin, tropomodulin and EcapZ. FEBS letters 576 (1-2):36-40.
104. Pasini EM, Kirkegaard M, Mortensen P, Lutz HU, Thomas AW, Mann M (2006) In-depth analysis of the membrane and cytosolic proteome of red blood cells. Blood 108 (3):791-801.
105. Tiffert T, Lew VL (1997) Apparent Ca^{2+} dissociation constant of Ca^{2+} chelators incorporated non-disruptively into intact human red cells. J Physiol 505 (Pt 2):403-410.
106. Ferreira HG, Lew VL (1976) Use of ionophore A23187 to measure cytoplasmic Ca buffering and activation of the Ca pump by internal Ca. Nature 259 (5538):47-49.
107. Schatzmann HJ (1966) ATP-dependent Ca++-extrusion from human red cells. Experientia 22 (6):364-365.

108. Schatzmann HJ, Vincenzi FF (1969) Calcium movements across the membrane of human red cells. J Physiol 201 (2):369-395.
109. Carafoli E (1992) The Ca^{2+} pump of the plasma membrane. J Biol Chem 267 (4):2115-2118.
110. Larsen FL, Katz S, Roufogalis BD (1981) Calmodulin regulation of Ca^{2+} transport in human erythrocytes. Biochem J 200 (2):185-191.
111. Romero PJ, Romero EA (1999) Effect of cell ageing on Ca^{2+} influx into human red cells. Cell Calcium 26 (3-4):131-137.
112. Bookchin RM, Ortiz OE, Somlyo AV, Somlyo AP, Sepulveda MI, Hockaday A, Lew VL (1985) Calcium-accumulating inside-out vesicles in sickle cell anemia red cells. Trans Assoc Am Physicians 98:10-20.
113. Glaser T, Schwarz-Benmeir N, Barnoy S, Barak S, Eshhar Z, Kosower NS (1994) Calpain ($Ca^{(2+)}$-dependent thiol protease) in erythrocytes of young and old individuals. Proc Natl Acad Sci U S A 91 (17):7879-7883.
114. Davis JQ, Bennett V (1985) Human erythrocyte clathrin and clathrin-uncoating protein. J Biol Chem 260 (27):14850-14856.
115. Gonzalez Flecha FL, Castello PR, Caride AJ, Gagliardino JJ, Rossi JP (1993) The erythrocyte calcium pump is inhibited by non-enzymic glycation: studies in situ and with the purified enzyme. Biochem J 293 (Pt 2):369-375.
116. Leclerc L, Vasseur C, Bursaux E, Marden M, Poyart C (1988) Inhibition of membrane erythrocyte (Ca^{2+} + Mg^{2+})-ATPase by hemin. Biochim Biophys Acta 946 (1):49-56.
117. Leclerc L, Marden M, Poyart C (1991) Inhibition of the erythrocyte (Ca^{2+} + Mg^{2+})-ATPase by nonheme iron. Biochim Biophys Acta 1062 (1):35-38.
118. Bessis M Living blood cells and their ultrastructure. Springer-Verlag, Berlin, Heidelberg, New York, 1973, pp. 85-261.
119. Kemp P, Ellory JC, Munn EA (1975) Changes in the phospholipid composition of sheep reticulocytes on maturation. Biochemical Society transactions 3 (5):749-751.
120. Lutz HU, Stammler P, Fasler S, Ingold M, Fehr J (1992) Density separation of human red blood cells on self forming Percoll gradients: correlation with cell age. Biochim Biophys Acta 1116 (1):1-10.
121. Canham PB (1969) Difference in geometry of young and old human erythrocytes explained by a filtering mechanism. Circulation research 25 (1):39-45.
122. Tiffert T, Daw N, Etzion Z, Bookchin RM, Lew VL (2007) Age decline in the activity of the Ca^{2+}-sensitive K^+ channel of human red blood cells. The Journal of general physiology 129 (5):429-436.
123. McLellan AC, Thornalley PJ (1989) Glyoxalase activity in human red blood cells fractioned by age. Mechanisms of ageing and development 48 (1):63-71.
124. Burton GW, Cheng SC, Webb A, Ingold KU (1986) Vitamin E in young and old human red blood cells. Biochimica et biophysica acta 860 (1):84-90.

125. Magnani M, Cucchiarini L, Stocchi V, Dacha M, Fornaini G (1982) Adult and fetal galactokinases in human red blood cells. Mechanisms of ageing and development 18 (3):215-223.
126. Shimizu Y, Suzuki M (1991) The relationship between red cell aging and enzyme activities in experimental animals. Comp Biochem Physiol B 99 (2):313-316.
127. Romero PJ, Romero EA (1997) Differences in Ca^{2+} pumping activity between sub-populations of human red cells. Cell Calcium 21 (5):353-358.
128. Kaestner L, Tabellion W, Weiss E, Bernhardt I, Lipp P (2006) Calcium imaging of individual erythrocytes: problems and approaches. Cell calcium 39 (1):13-19.
129. Romero PJ, Romero EA, Winkler MD (1997) Ionic calcium content of light dense human red cells separated by Percoll density gradients. Biochim Biophys Acta 1323 (1):23-28.
130. Kirkpatrick FH, Muhs AG, Kostuk RK, Gabel CW (1979) Dense (aged) circulating red cells contain normal concentrations of adenosine triphosphate (ATP). Blood 54 (4):946-950.
131. Moolenaar WH (1995) Lysophosphatidic acid signalling. Current opinion in cell biology 7 (2):203-210.
132. Goetzl EJ, An S (1998) Diversity of cellular receptors and functions for the lysophospholipid growth factors lysophosphatidic acid and sphingosine 1-phosphate. Faseb J 12 (15):1589-1598.
133. Tokumura A, Fukuzawa K, Isobe J, Tsukatani H (1981) Lysophosphatidic acid-induced aggregation of human and feline platelets: structure-activity relationship. Biochemical and biophysical research communications 99 (2):391-398.
134. Alexander JS, Patton WF, Christman BW, Cuiper LL, Haselton FR (1998) Platelet-derived lysophosphatidic acid decreases endothelial permeability in vitro. The American journal of physiology 274 (1 Pt 2):H115-122.
135. Yakubu MA, Liliom K, Tigyi GJ, Leffler CW (1997) Role of lysophosphatidic acid in endothelin-1- and hematoma-induced alteration of cerebral microcirculation. The American journal of physiology 273 (2 Pt 2):R703-709.
136. Tokumura A, Iimori M, Nishioka Y, Kitahara M, Sakashita M, Tanaka S (1994) Lysophosphatidic acids induce proliferation of cultured vascular smooth muscle cells from rat aorta. The American journal of physiology 267 (1 Pt 1):C204-210.
137. Jalink K, van Corven EJ, Moolenaar WH (1990) Lysophosphatidic acid, but not phosphatidic acid, is a potent Ca2(+)-mobilizing stimulus for fibroblasts. Evidence for an extracellular site of action. J Biol Chem 265 (21):12232-12239.
138. Zhang Q, Checovich WJ, Peters DM, Albrecht RM, Mosher DF (1994) Modulation of cell surface fibronectin assembly sites by lysophosphatidic acid. The Journal of cell biology 127 (5):1447-1459.

139. Chettibi S, Lawrence AJ, Stevenson RD, Young JD (1994) Effect of lysophosphatidic acid on motility, polarisation and metabolic burst of human neutrophils. FEMS Immunol Med Microbiol 8 (3):271-281.
140. Rosskopf D, Daelman W, Busch S, Schurks M, Hartung K, Kribben A, Michel MC, Siffert W (1998) Growth factor-like action of lysophosphatidic acid on human B lymphoblasts. The American journal of physiology 274 (6 Pt 1):C1573-1582.
141. Zhou D, Luini W, Bernasconi S, Diomede L, Salmona M, Mantovani A, Sozzani S (1995) Phosphatidic acid and lysophosphatidic acid induce haptotactic migration of human monocytes. The Journal of biological chemistry 270 (43):25549-25556.
142. Cayouette S, Boulay G (2007) Intracellular trafficking of TRP channels. Cell Calcium 42 (2):225-232.
143. Perraud AL, Takanishi CL, Shen B, Kang S, Smith MK, Schmitz C, Knowles HM, Ferraris D, Li W, Zhang J, Stoddard BL, Scharenberg AM (2005) Accumulation of free ADP-ribose from mitochondria mediates oxidative stress-induced gating of TRPM2 cation channels. J Biol Chem 280 (7):6138-6148.
144. Cosens DJ, Manning A (1969) Abnormal electroretinogram from a Drosophila mutant. Nature 224 (5216):285-287.
145. Montell C, Rubin GM (1989) Molecular characterization of the Drosophila trp locus: a putative integral membrane protein required for phototransduction. Neuron 2 (4):1313-1323.
146. Hardie RC (2001) Phototransduction in Drosophila melanogaster. J Exp Biol 204 (Pt 20):3403-3409.
147. Raghu P, Usher K, Jonas S, Chyb S, Polyanovsky A, Hardie RC (2000) Constitutive activity of the light-sensitive channels TRP and TRPL in the Drosophila diacylglycerol kinase mutant, rdgA. Neuron 26 (1):169-179.
148. Wes PD, Chevesich J, Jeromin A, Rosenberg C, Stetten G, Montell C (1995) TRPC1, a human homolog of a Drosophila store-operated channel. Proceedings of the National Academy of Sciences of the United States of America 92 (21):9652-9656.
149. Pedersen SF, Owsianik G, Nilius B (2005) TRP channels: an overview. Cell Calcium 38 (3-4):233-252.
150. Bracci R, Perrone S, Buonocore G (2001) Red blood cell involvement in fetal/neonatal hypoxia. Biology of the neonate 79 (3-4):210-212.
151. Strubing C, Krapivinsky G, Krapivinsky L, Clapham DE (2003) Formation of novel TRPC channels by complex subunit interactions in embryonic brain. The Journal of biological chemistry 278 (40):39014-39019.
152. Clapham DE (2003) TRP channels as cellular sensors. Nature 426 (6966):517-524.
153. Venkatachalam K, van Rossum DB, Patterson RL, Ma HT, Gill DL (2002) The cellular and molecular basis of store-operated calcium entry. Nat Cell Biol 4 (11):E263-272.
154. Roos J, DiGregorio PJ, Yeromin AV, Ohlsen K, Lioudyno M, Zhang S, Safrina O, Kozak JA, Wagner SL, Cahalan MD, Velicelebi G,

Stauderman KA (2005) STIM1, an essential and conserved component of store-operated Ca^{2+} channel function. J Cell Biol 169 (3):435-445.
155. Trost C, Bergs C, Himmerkus N, Flockerzi V (2001) The transient receptor potential, TRP4, cation channel is a novel member of the family of calmodulin binding proteins. Biochem J 355 (Pt 3):663-670.
156. Kiselyov K, Xu X, Mozhayeva G, Kuo T, Pessah I, Mignery G, Zhu X, Birnbaumer L, Muallem S (1998) Functional interaction between InsP3 receptors and store-operated Htrp3 channels. Nature 396 (6710):478-482.
157. Montell C (2005) The TRP superfamily of cation channels. Sci STKE 2005 (272):re3.
158. Hofmann T, Schaefer M, Schultz G, Gudermann T (2000) Transient receptor potential channels as molecular substrates of receptor-mediated cation entry. J Mol Med (Berl) 78 (1):14-25.
159. Inoue R, Okada T, Onoue H, Hara Y, Shimizu S, Naitoh S, Ito Y, Mori Y (2001) The transient receptor potential protein homologue TRP6 is the essential component of vascular alpha(1)-adrenoceptor-activated Ca(2+)-permeable cation channel. Circ Res 88 (3):325-332.
160. Jung S, Strotmann R, Schultz G, Plant TD (2002) TRPC6 is a candidate channel involved in receptor-stimulated cation currents in A7r5 smooth muscle cells. Am J Physiol Cell Physiol 282 (2):C347-359.
161. Antoniotti S, Lovisolo D, Fiorio Pla A, Munaron L (2002) Expression and functional role of bTRPC1 channels in native endothelial cells. FEBS Lett 510 (3):189-195.
162. Basora N, Boulay G, Bilodeau L, Rousseau E, Payet MD (2003) 20-hydroxyeicosatetraenoic acid (20-HETE) activates mouse TRPC6 channels expressed in HEK293 cells. J Biol Chem 278 (34):31709-31716.
163. Shi J, Mori E, Mori Y, Mori M, Li J, Ito Y, Inoue R (2004) Multiple regulation by calcium of murine homologues of transient receptor potential proteins TRPC6 and TRPC7 expressed in HEK293 cells. J Physiol 561 (Pt 2):415-432.
164. Hisatsune C, Kuroda Y, Nakamura K, Inoue T, Nakamura T, Michikawa T, Mizutani A, Mikoshiba K (2004) Regulation of TRPC6 channel activity by tyrosine phosphorylation. J Biol Chem 279 (18):18887-18894.
165. Lussier MP, Cayouette S, Lepage PK, Bernier CL, Francoeur N, St-Hilaire M, Pinard M, Boulay G (2005) MxA, a member of the dynamin superfamily, interacts with the ankyrin-like repeat domain of TRPC. J Biol Chem 280 (19):19393-19400.
166. Oguz Baskurt BN, Herbert J. Meiselman (2011) *Red Blood Cell Aggregation*. (2011).
167. Andrews DA, Low PS (1999) Role of red blood cells in thrombosis. Current opinion in hematology 6 (2):76-82.
168. Duke WW (1983) The relation of blood platelets to hemorrhagic disease. By W.W. Duke. JAMA : the journal of the American Medical Association 250 (9):1201-1209.

169. Duke WW (1983) The relation of blood platelets to hemorrhagic disease. By W.W. Duke. Jama 250 (9):1201-1209.
170. Blajchman MA, Bordin JO, Bardossy L, Heddle NM (1994) The contribution of the haematocrit to thrombocytopenic bleeding in experimental animals. British journal of haematology 86 (2):347-350.
171. Hellem AJ, Borchgrevink, C.F., Ames, S.B (1961) The role of red cells in haemostasis: the relation between haematocrit, bleeding time and platelet adhesiveness. Br J Haematol. Br J Haematol 7:42-50.
172. Fox JE (1994) Shedding of adhesion receptors from the surface of activated platelets. Blood Coagul Fibrinolysis 5 (2):291-304.
173. Rampling MW (1990) "rouleaux formation -its causes, estimation and consequences". Doga Turkish Journal of Medical Sciences 14:447{453.
174. O.Baskurt BN, and H. H.J. Meiselman (2012) Red blood cell aggregation. CRC Press taylor and Francis Group.
175. Pribush A, Zilberman-Kravits D, Meyerstein N (2007) The mechanism of the dextran-induced red blood cell aggregation. European biophysics journal : EBJ 36 (2):85-94.
176. D.E. Brooks (1988) Mechanism of red cell aggregation. blood cells, rheology and aging, (Springer-Verlag).
177. Mills PSaP (1985) Effect of dextran polymer on glycocalyx structure and cell electrophoretic mobility. Colloid and Polymer Science 263:no. 6, 494-500.
178. D.E. Brooks RGG, and J. Jansen (1980) Erythrocyte mechanics and blood flow, ch. Mechanism of Erythrocyte Aggregation.pp. 119-140, New York:A.R. Liss;, .
179. Chien S (1975) Biophysical behavior of red cells in suspensions. The Red Blood Cell.
180. Lominadze D, Dean WL (2002) Involvement of fibrinogen specific binding in erythrocyte aggregation. FEBS letters 517 (1-3):41-44.
181. Neu B, Meiselman HJ (2002) Depletion-mediated red blood cell aggregation in polymer solutions. Biophysical journal 83 (5):2482-2490.
182. Baumler H, Donath E, Krabi A, Knippel W, Budde A, Kiesewetter H (1996) Electrophoresis of human red blood cells and platelets. Evidence for depletion of dextran. Biorheology 33 (4-5):333-351.
183. Herrick JB (1910) Peculiar elongated and sickleshaped red blood corpuscules in a case of severe anemia. Arch. Int. Med 6:517–521.
184. Glassberg J (2011) Evidence-based management of sickle cell disease in the emergency department. Emerg Med Pract 13 (8):1-20; quiz 20.
185. Anie KA, Green J (2012) Psychological therapies for sickle cell disease and pain. Cochrane Database Syst Rev 2:CD001916.
186. Pearson HA (1977) Sickle cell anemia and severe infections due to encapsulated bacteria. The Journal of infectious diseases 136 Suppl:S25-30.
187. Wong WY, Powars DR, Chan L, Hiti A, Johnson C, Overturf G (1992) Polysaccharide encapsulated bacterial infection in sickle cell anemia: a thirty year epidemiologic experience. Am J Hematol 39 (3):176-182.

188. Kaul DK, Liu XD, Choong S, Belcher JD, Vercellotti GM, Hebbel RP (2004) Anti-inflammatory therapy ameliorates leukocyte adhesion and microvascular flow abnormalities in transgenic sickle mice. Am J Physiol Heart Circ Physiol 287 (1):H293-301.
189. Belcher JD, Mahaseth H, Welch TE, Otterbein LE, Hebbel RP, Vercellotti GM (2006) Heme oxygenase-1 is a modulator of inflammation and vaso-occlusion in transgenic sickle mice. J Clin Invest 116 (3):808-816.
190. Ingram VM (1958) Abnormal human haemoglobins. I. The comparison of normal human and sickle-cell haemoglobins by fingerprinting. Biochim Biophys Acta 28 (3):539-545.
191. Ingram VM (1989) Abnormal human haemoglobins. I. The comparison of normal human and sickle-cell haemoglobins by "fingerprinting". 1958. Biochim Biophys Acta 1000:151-157.
192. Ingram VM (1959) Abnormal human haemoglobins. III. The chemical difference between normal and sickle cell haemoglobins. Biochim Biophys Acta 36:402-411.
193. Ferrone FA (2004) Polymerization and sickle cell disease: a molecular view. Microcirculation 11 (2):115-128.
194. Frenette PS, Atweh GF (2007) Sickle cell disease: old discoveries, new concepts, and future promise. J Clin Invest 117 (4):850-858.
195. Wautier MP, Heron E, Picot J, Colin Y, Hermine O, Wautier JL (2011) Red blood cell phosphatidylserine exposure is responsible for increased erythrocyte adhesion to endothelium in central retinal vein occlusion. J Thromb Haemost 9 (5):1049-1055.
196. Hebbel RP, Yamada O, Moldow CF, Jacob HS, White JG, Eaton JW (1980) Abnormal adherence of sickle erythrocytes to cultured vascular endothelium: possible mechanism for microvascular occlusion in sickle cell disease. J Clin Invest 65 (1):154-160.
197. Hoover R, Rubin R, Wise G, Warren R (1979) Adhesion of normal and sickle erythrocytes to endothelial monolayer cultures. Blood 54 (4):872-876.
198. Joneckis CC, Ackley RL, Orringer EP, Wayner EA, Parise LV (1993) Integrin alpha 4 beta 1 and glycoprotein IV (CD36) are expressed on circulating reticulocytes in sickle cell anemia. Blood 82 (12):3548-3555.
199. Swerlick RA, Eckman JR, Kumar A, Jeitler M, Wick TM (1993) Alpha 4 beta 1-integrin expression on sickle reticulocytes: vascular cell adhesion molecule-1-dependent binding to endothelium. Blood 82 (6):1891-1899.
200. Kaul DK, Tsai HM, Liu XD, Nakada MT, Nagel RL, Coller BS (2000) Monoclonal antibodies to alphaVbeta3 (7E3 and LM609) inhibit sickle red blood cell-endothelium interactions induced by platelet-activating factor. Blood 95 (2):368-374.
201. Spring FA, Parsons SF, Ortlepp S, Olsson ML, Sessions R, Brady RL, Anstee DJ (2001) Intercellular adhesion molecule-4 binds alpha(4)beta(1) and alpha(V)-family integrins through novel integrin-binding mechanisms. Blood 98 (2):458-466.

202. Gee BE, Platt OS (1995) Sickle reticulocytes adhere to VCAM-1. Blood 85 (1):268-274.
203. Natarajan M, Udden MM, McIntire LV (1996) Adhesion of sickle red blood cells and damage to interleukin-1 beta stimulated endothelial cells under flow in vitro. Blood 87 (11):4845-4852.
204. Embury SH, Matsui NM, Ramanujam S, Mayadas TN, Noguchi CT, Diwan BA, Mohandas N, Cheung AT (2004) The contribution of endothelial cell P-selectin to the microvascular flow of mouse sickle erythrocytes in vivo. Blood 104 (10):3378-3385.
205. Hillery CA, Scott JP, Du MC (1999) The carboxy-terminal cell-binding domain of thrombospondin is essential for sickle red blood cell adhesion. Blood 94 (1):302-309.
206. Wautier JL, Pintigny D, Wautier MP, Paton RC, Galacteros F, Passa P, Caen JP (1983) Fibrinogen, a modulator of erythrocyte adhesion to vascular endothelium. J Lab Clin Med 101 (6):911-920.
207. Kasschau MR, Barabino GA, Bridges KR, Golan DE (1996) Adhesion of sickle neutrophils and erythrocytes to fibronectin. Blood 87 (2):771-780.
208. Thevenin BJ, Crandall I, Ballas SK, Sherman IW, Shohet SB (1997) Band 3 peptides block the adherence of sickle cells to endothelial cells in vitro. Blood 90 (10):4172-4179.
209. Hillery CA, Du MC, Montgomery RR, Scott JP (1996) Increased adhesion of erythrocytes to components of the extracellular matrix: isolation and characterization of a red blood cell lipid that binds thrombospondin and laminin. Blood 87 (11):4879-4886.
210. Nguyen DB, Wagner-Britz L, Maia S, Steffen P, Wagner C, Kaestner L, Bernhardt I (2011) Regulation of phosphatidylserine exposure in red blood cells. Cell Physiol Biochem 28 (5):847-856.
211. Gee KR, Brown KA, Chen WN, Bishop-Stewart J, Gray D, Johnson I (2000) Chemical and physiological characterization of fluo-4 Ca(2+)-indicator dyes. Cell Calcium 27 (2):97-106.
212. Haugland RP (2002) *Handbook of fluorescent probes and research chemicals*. (2002).
213. Janet Hoff L, RLATG (2000, November) Methods of Blood Collection in the Mouse. Lab Animal 29:10.
214. Joiner CH, Franco RS, Jiang M, Franco MS, Barker JE, Lux SE (1995) Increased cation permeability in mutant mouse red blood cells with defective membrane skeletons. Blood 86 (11):4307-4314.
215. Eichholtz T, Jalink K, Fahrenfort I, Moolenaar WH (1993) The bioactive phospholipid lysophosphatidic acid is released from activated platelets. Biochem J 291 (Pt 3):677-680.
216. Gaits F, Fourcade O, Le Balle F, Gueguen G, Gaige B, Gassama-Diagne A, Fauvel J, Salles JP, Mauco G, Simon MF, Chap H (1997) Lysophosphatidic acid as a phospholipid mediator: pathways of synthesis. FEBS Lett 410 (1):54-58.
217. Pertoft H, Laurent TC, Laas T, Kagedal L (1978) Density gradients prepared from colloidal silica particles coated by polyvinylpyrrolidone (Percoll). Anal Biochem 88 (1):271-282.

218. Inaba M, Maede, Y (1988) Correlation between protein 4.1a/4.1b ratio and erythrocyte life span. Biochimica et biophysica acta 944:256-264.
219. Siren AL, Fratelli M, Brines M, Goemans C, Casagrande S, Lewczuk P, Keenan S, Gleiter C, Pasquali C, Capobianco A, Mennini T, Heumann R, Cerami A, Ehrenreich H, Ghezzi P (2001) Erythropoietin prevents neuronal apoptosis after cerebral ischemia and metabolic stress. Proc Natl Acad Sci U S A 98 (7):4044-4049.
220. Haroon ZA, Amin K, Jiang X, Arcasoy MO (2003) A novel role for erythropoietin during fibrin-induced wound-healing response. Am J Pathol 163 (3):993-1000.
221. Ashby DR, Gale DP, Busbridge M, Murphy KG, Duncan ND, Cairns TD, Taube DH, Bloom SR, Tam FW, Chapman R, Maxwell PH, Choi P (2010) Erythropoietin administration in humans causes a marked and prolonged reduction in circulating hepcidin. Haematologica 95 (3):505-508.
222. Masaratana P, Latunde-Dada GO, Patel N, Simpson RJ, Vaulont S, McKie AT (2012) Iron metabolism in hepcidin1 knockout mice in response to phenylhydrazine-induced hemolysis. Blood Cells Mol Dis 49 (2):85-91.
223. Hara H, Ogawa M (1976) Erthropoietic precursors in mice with phenylhydrazine-induced anemia. Am J Hematol 1 (4):453-458.
224. Vemula S, Shi J, Mali RS, Ma P, Liu Y, Hanneman P, Koehler KR, Hashino E, Wei L, Kapur R (2012) ROCK1 functions as a critical regulator of stress erythropoiesis and survival by regulating p53. Blood.
225. Tong Q, Hirschler-Laszkiewicz I, Zhang W, Conrad K, Neagley DW, Barber DL, Cheung JY, Miller BA (2008) TRPC3 is the erythropoietin-regulated calcium channel in human erythroid cells. J Biol Chem 283 (16):10385-10395.
226. Barreda DR, Neumann NF, Belosevic M (2000) Flow cytometric analysis of PKH26-labeled goldfish kidney-derived macrophages. Dev Comp Immunol 24 (4):395-406.
227. Ashley DM, Bol SJ, Waugh C, Kannourakis G (1993) A novel approach to the measurement of different in vitro leukaemic cell growth parameters: the use of PKH GL fluorescent probes. Leuk Res 17 (10):873-882.
228. Askenasy N, Farkas DL (2002) Optical imaging of PKH-labeled hematopoietic cells in recipient bone marrow in vivo. Stem Cells 20 (6):501-513.
229. Kenney NJ, Smith GH, Lawrence E, Barrett JC, Salomon DS (2001) Identification of Stem Cell Units in the Terminal End Bud and Duct of the Mouse Mammary Gland. J Biomed Biotechnol 1 (3):133-143.
230. Horky J, Vacha J, Znojil V (1978) Comparison of life span of erythrocytes in some inbred strains of mouse using 14C-labelled glycine. Physiologia Bohemoslovaca 27 (3):209-217.
231. Roedding AS, Li PP, Warsh JJ (2006) Characterization of the transient receptor potential channels mediating lysophosphatidic acid-stimulated calcium mobilization in B lymphoblasts. Life Sci 80 (2):89-97.

232. Kaestner L, Steffen P, Nguyen DB, Wang J, Wagner-Britz L, Jung A, Wagner C, Bernhardt I (2012) Lysophosphatidic acid induced red blood cell aggregation in vitro. Bioelectrochemistry 87:89-95.
233. Fukushima N, Ishii I, Contos JJ, Weiner JA, Chun J (2001) Lysophospholipid receptors. Annu Rev Pharmacol Toxicol 41:507-534.
234. Ishii I, Fukushima N, Ye X, Chun J (2004) Lysophospholipid receptors: signaling and biology. Annu Rev Biochem 73:321-354.
235. Choi JW, Herr DR, Noguchi K, Yung YC, Lee CW, Mutoh T, Lin ME, Teo ST, Park KE, Mosley AN, Chun J LPA receptors: subtypes and biological actions. Annual review of pharmacology and toxicology 50:157-186.
236. Komachi M, Tomura H, Malchinkhuu E, Tobo M, Mogi C, Yamada T, Kimura T, Kuwabara A, Ohta H, Im DS, Kurose H, Takeyoshi I, Sato K, Okajima F (2009) LPA1 receptors mediate stimulation, whereas LPA2 receptors mediate inhibition, of migration of pancreatic cancer cells in response to lysophosphatidic acid and malignant ascites. Carcinogenesis 30 (3):457-465.
237. Takeda H, Matozaki T, Takada T, Noguchi T, Yamao T, Tsuda M, Ochi F, Fukunaga K, Inagaki K, Kasuga M (1999) PI 3-kinase gamma and protein kinase C-zeta mediate RAS-independent activation of MAP kinase by a Gi protein-coupled receptor. Embo J 18 (2):386-395.
238. Chou CH, Wei LH, Kuo ML, Huang YJ, Lai KP, Chen CA, Hsieh CY (2005) Up-regulation of interleukin-6 in human ovarian cancer cell via a Gi/PI3K-Akt/NF-kappaB pathway by lysophosphatidic acid, an ovarian cancer-activating factor. Carcinogenesis 26 (1):45-52.
239. Chen RJ, Chen SU, Chou CH, Lin MC (2012) Lysophosphatidic acid receptor 2/3-mediated IL-8-dependent angiogenesis in cervical cancer cells. Int J Cancer 131 (4):789-802.
240. Shimamura K, Kusaka M, Sperelakis N (1994) Protein kinase C stimulates Ca^{2+} current in pregnant rat myometrial cells. Can J Physiol Pharmacol 72 (11):1304-1307.
241. Kanzaki M, Zhang YQ, Mashima H, Li L, Shibata H, Kojima I (1999) Translocation of a calcium-permeable cation channel induced by insulin-like growth factor-I. Nat Cell Biol 1 (3):165-170.
242. Govekar RB, Zingde SM (2001) Protein kinase C isoforms in human erythrocytes. Ann Hematol 80 (9):531-534.
243. Danilov YN, Fennell R, Ling E, Cohen CM (1990) Selective modulation of band 4.1 binding to erythrocyte membranes by protein kinase C. J Biol Chem 265 (5):2556-2562.
244. Soldati L, Spaventa R, Vezzoli G, Zerbi S, Adamo D, Caumo A, Rivera R, Bianchi G (1997) Characterization of voltage-dependent calcium influx in human erythrocytes by fura-2. Biochem Biophys Res Commun 236 (3):549-554.
245. Llinas R, Sugimori M, Lin JW, Cherksey B (1989) Blocking and isolation of a calcium channel from neurons in mammals and cephalopods utilizing a toxin fraction (FTX) from funnel-web spider poison. Proc Natl Acad Sci U S A 86 (5):1689-1693.

246. Bookchin RM, Lew VL (1981) Effect of a 'sickling pulse' on calcium and potassium transport in sickle cell trait red cells. J Physiol 312:265-280.
247. Lew VL, Ortiz OE, Bookchin RM (1997) Stochastic nature and red cell population distribution of the sickling-induced Ca^{2+} permeability. J Clin Invest 99 (11):2727-2735.
248. Fukushima N, Ishii I, Contos JJ, Weiner JA, Chun J (2001) Lysophospholipid receptors. Annu Rev Pharmacol Toxicol 41:507-534.
249. Ishii I, Fukushima N, Ye X, Chun J (2004) Lysophospholipid receptors: signaling and biology. Annu Rev Biochem 73:321-354.
250. Kaestner L, Bollensdorff C, Bernhardt I (1999) Non-selective voltage-activated cation channel in the human red blood cell membrane. Biochim Biophys Acta 1417 (1):9-15.
251. Desai SA, Bezrukov SM, Zimmerberg J (2000) A voltage-dependent channel involved in nutrient uptake by red blood cells infected with the malaria parasite. Nature 406 (6799):1001-1005.
252. Egee S, Lapaix F, Decherf G, Staines HM, Ellory JC, Doerig C, Thomas SL (2002) A stretch-activated anion channel is up-regulated by the malaria parasite Plasmodium falciparum. J Physiol 542 (Pt 3):795-801.
253. Huber SM, Uhlemann AC, Gamper NL, Duranton C, Kremsner PG, Lang F (2002) Plasmodium falciparum activates endogenous Cl(-) channels of human erythrocytes by membrane oxidation. Embo J 21 (1-2):22-30.
254. Shahrestanifar M, Fan X, Manning DR (1999) Lysophosphatidic acid activates NF-kappaB in fibroblasts. A requirement for multiple inputs. The Journal of biological chemistry 274 (6):3828-3833.
255. Dixon RJ, Young K, Brunskill NJ (1999) Lysophosphatidic acid-induced calcium mobilization and proliferation in kidney proximal tubular cells. The American journal of physiology 276 (2 Pt 2):F191-198.
256. Meerschaert K, De Corte V, De Ville Y, Vandekerckhove J, Gettemans J (1998) Gelsolin and functionally similar actin-binding proteins are regulated by lysophosphatidic acid. The EMBO journal 17 (20):5923-5932.
257. Tiffert T, Spivak JL, Lew VL (1988) Magnitude of calcium influx required to induce dehydration of normal human red cells. Biochim Biophys Acta 943 (2):157-165.
258. Stout JG, Zhou Q, Wiedmer T, Sims PJ (1998) Change in conformation of plasma membrane phospholipid scramblase induced by occupancy of its Ca^{2+} binding site. Biochemistry 37 (42):14860-14866.
259. Basse F, Stout JG, Sims PJ, Wiedmer T (1996) Isolation of an erythrocyte membrane protein that mediates Ca^{2+}-dependent transbilayer movement of phospholipid. The Journal of biological chemistry 271 (29):17205-17210.
260. Uchida K, Emoto K, Daleke DL, Inoue K, Umeda M (1998) Induction of apoptosis by phosphatidylserine. J Biochem 123 (6):1073-1078.
261. Schlegel RA, Williamson P (2001) Phosphatidylserine, a death knell. Cell Death Differ 8 (6):551-563.

262. Ravichandran KS, Lorenz U (2007) Engulfment of apoptotic cells: signals for a good meal. Nature reviews 7 (12):964-974.
263. Kuypers FA, de Jong K (2004) The role of phosphatidylserine in recognition and removal of erythrocytes. Cell Mol Biol (Noisy-le-grand) 50 (2):147-158.
264. Verhoven B, Schlegel RA, Williamson P (1995) Mechanisms of phosphatidylserine exposure, a phagocyte recognition signal, on apoptotic T lymphocytes. The Journal of experimental medicine 182 (5):1597-1601.
265. Fadok VA, Bratton DL, Frasch SC, Warner ML, Henson PM (1998) The role of phosphatidylserine in recognition of apoptotic cells by phagocytes. Cell Death Differ 5 (7):551-562.
266. Wu Y, Tibrewal N, Birge RB (2006) Phosphatidylserine recognition by phagocytes: a view to a kill. Trends Cell Biol 16 (4):189-197.
267. Schlegel RA, Callahan MK, Williamson P (2000) The central role of phosphatidylserine in the phagocytosis of apoptotic thymocytes. Ann N Y Acad Sci 926:217-225.
268. Krieser RJ, White K (2002) Engulfment mechanism of apoptotic cells. Current opinion in cell biology 14 (6):734-738.
269. Tiffert T, Etzion Z, Bookchin RM, Lew VL (1993) Effects of deoxygenation on active and passive Ca^{2+} transport and cytoplasmic Ca^{2+} buffering in normal human red cells. The Journal of physiology 464:529-544.
270. Romero PJ, Romero EA (1999) The role of calcium metabolism in human red blood cell ageing: a proposal. Blood Cells Mol Dis 25 (1):9-19.
271. Szabo I, Kappelmayer J, Alekseev SI, Ziskin MC (2006) Millimeter wave induced reversible externalization of phosphatidylserine molecules in cells exposed in vitro. Bioelectromagnetics 27 (3):233-244.
272. Minetti G, Ciana A, Profumo A, Zappa M, Vercellati C, Zanella A, Arduini A, Brovelli A (2001) Cell age-related monovalent cations content and density changes in stored human erythrocytes. Biochim Biophys Acta 1527 (3):149-155.
273. Lew VL, Daw N, Etzion Z, Tiffert T, Muoma A, Vanagas L, Bookchin RM (2007) Effects of age-dependent membrane transport changes on the homeostasis of senescent human red blood cells. Blood 110 (4):1334-1342.
274. Dyrda A, Cytlak U, Ciuraszkiewicz A, Lipinska A, Cueff A, Bouyer G, Egee S, Bennekou P, Lew VL, Thomas SL (2010) Local membrane deformations activate Ca^{2+}-dependent K+ and anionic currents in intact human red blood cells. PloS one 5 (2):e9447.
275. Bennekou P (1993) The voltage-gated non-selective cation channel from human red cells is sensitive to acetylcholine. Biochim Biophys Acta 1147 (1):165-167.
276. Christophersen P, Bennekou P (1991) Evidence for a voltage-gated, non-selective cation channel in the human red cell membrane. Biochim Biophys Acta 1065 (1):103-106.

277. Kaestner L, Bollensdorff C, Bernhardt I (1999) Non-selective voltage-activated cation channel in the human red blood cell membrane. Biochim Biophys Acta 1417 (1):9-15.
278. Foller M, Kasinathan RS, Koka S, Lang C, Shumilina E, Birnbaumer L, Lang F, Huber SM (2008) TRPC6 contributes to the Ca(2+) leak of human erythrocytes. Cell Physiol Biochem 21 (1-3):183-192.
279. Miller BA, Cheung JY (1994) Mechanisms of erythropoietin signal transduction: involvement of calcium channels. Proc Soc Exp Biol Med 206 (3):263-267.
280. Schaefer A, Magocsi M, Marquardt H (1997) Signalling mechanisms in erythropoiesis: the enigmatic role of calcium. Cell Signal 9 (7):483-495.
281. Hoeflich KP, Ikura M (2002) Calmodulin in action: diversity in target recognition and activation mechanisms. Cell 108 (6):739-742.
282. Lisa Wagner-Britz JW, Lars Kaestner, Ingolf Bernhardt (2013) Protein Kinase Cα and P-Type Ca^{2+}-Channel CaV2.1 in Red Blood Cells Calcium Signaling. J. Cell. Physiol. Biochem Accepted.
283. Cho W, Stahelin RV (2005) Membrane-protein interactions in cell signaling and membrane trafficking. Annu Rev Biophys Biomol Struct 34:119-151.
284. Govekar RB, Zingde SM (2001) Protein kinase C isoforms in human erythrocytes. Ann Hematol 80 (9):531-534.
285. Bruce LJ, Beckmann R, Ribeiro ML, Peters LL, Chasis JA, Delaunay J, Mohandas N, Anstee DJ, Tanner MJ (2003) A band 3-based macrocomplex of integral and peripheral proteins in the RBC membrane. Blood 101 (10):4180-4188.
286. Basse F, Stout JG, Sims PJ, Wiedmer T (1996) Isolation of an erythrocyte membrane protein that mediates Ca^{2+}-dependent transbilayer movement of phospholipid. J Biol Chem 271 (29):17205-17210.
287. Verkleij AJ, Zwaal RF, Roelofsen B, Comfurius P, Kastelijn D, van Deenen LL (1973) The asymmetric distribution of phospholipids in the human red cell membrane. A combined study using phospholipases and freeze-etch electron microscopy. Biochim Biophys Acta 323 (2):178-193.
288. Beitner R (1993) Control of glycolytic enzymes through binding to cell structures and by glucose-1,6-bisphosphate under different conditions. The role of Ca^{2+} and calmodulin. Int J Biochem 25 (3):297-305.
289. Nakashima K, Fujii S, Kaku K, Kaneko T (1982) Calcium-calmodulin dependent phosphorylation of erythrocyte pyruvate kinase. Biochem Biophys Res Commun 104 (1):285-289.
290. Tiffert T, Etzion Z, Bookchin RM, Lew VL (1993) Effects of deoxygenation on active and passive Ca^{2+} transport and cytoplasmic Ca^{2+} buffering in normal human red cells. J Physiol 464:529-544.
291. Alderton WK, Cooper CE, Knowles RG (2001) Nitric oxide synthases: structure, function and inhibition. Biochem J 357 (Pt 3):593-615.
292. Spratt DE, Newman E, Mosher J, Ghosh DK, Salerno JC, Guillemette JG (2006) Binding and activation of nitric oxide synthase isozymes by calmodulin EF hand pairs. Febs J 273 (8):1759-1771.

293. Bosman GJ, Willekens FL, Werre JM (2005) Erythrocyte aging: a more than superficial resemblance to apoptosis? Cell Physiol Biochem 16 (1-3):1-8.
294. Steffen P, Jung A, Nguyen DB, Muller T, Bernhardt I, Kaestner L, Wagner C (2011) Stimulation of human red blood cells leads to Ca^{2+}-mediated intercellular adhesion. Cell Calcium 50 (1):54-61.
295. Eaton JW, Skelton TD, Swofford HS, Kolpin CE, Jacob HS (1973) Elevated erythrocyte calcium in sickle cell disease. Nature 246 (5428):105-106.
296. Etzion Z, Tiffert T, Bookchin RM, Lew VL (1993) Effects of deoxygenation on active and passive Ca^{2+} transport and on the cytoplasmic Ca^{2+} levels of sickle cell anemia red cells. J Clin Invest 92 (5):2489-2498.
297. Joiner CH, Jiang M, Franco RS (1995) Deoxygenation-induced cation fluxes in sickle cells. IV. Modulation by external calcium. Am J Physiol 269 (2 Pt 1):C403-409.
298. Bookchin RM, Ortiz OE, Shalev O, Tsurel S, Rachmilewitz EA, Hockaday A, Lew VL (1988) Calcium transport and ultrastructure of red cells in beta-thalassemia intermedia. Blood 72 (5):1602-1607.
299. Lew VL, Hockaday A, Sepulveda MI, Somlyo AP, Somlyo AV, Ortiz OE, Bookchin RM (1985) Compartmentalization of sickle-cell calcium in endocytic inside-out vesicles. Nature 315 (6020):586-589.
300. Sabina RL, Waldenstrom A, Ronquist G (2006) The contribution of Ca^{2+} calmodulin activation of human erythrocyte AMP deaminase (isoform E) to the erythrocyte metabolic dysregulation of familial phosphofructokinase deficiency. Haematologica 91 (5):652-655.
301. Minetti G, Egee S, Morsdorf D, Steffen P, Makhro A, Achilli C, Ciana A, Wang J, Bouyer G, Bernhardt I, Wagner C, Thomas S, Bogdanova A, Kaestner L (2013) Red cell investigations: art and artefacts. Blood Rev 27 (2):91-101.
302. Jue Wang, Lisa Wagner-Britz, Anna Bogdanova, Sandra Ruppenthal, Kathrina Wiesen, Elisabeth Kaiser, Qinghai Tian, Elmar Krause, Ingolf Bernhardt, Peter Lipp, Stephan E. Philipp, Kaestner L (2013) Morphologically Homogeneous Red Blood Cells Present a Heterogeneous Response to Hormonal Stimulation. PLoS One 8(6): e67697. doi:10.1371/journal.pone.0067697.
303. Chung SM, Bae ON, Lim KM, Noh JY, Lee MY, Jung YS, Chung JH (2007) Lysophosphatidic acid induces thrombogenic activity through phosphatidylserine exposure and procoagulant microvesicle generation in human erythrocytes. Arterioscler Thromb Vasc Biol 27 (2):414-421.
304. Palek J, Thomae M, Ozog D (1977) Red cell calcium content and transmembrane calcium movements in sickle cell anemia. J Lab Clin Med 89 (6):1365-1374.
305. Bookchin RM, Raventos C, Lew VL (1981) Abnormal vesiculation and calcium transport by 'one-step' inside-out vesicles from sickle cell anemia red cells. Comparisons with transport by intact cells. Prog Clin Biol Res 55:163-182.

306. Tosteson DC, Shea E, Darling RC (1952) Potassium and sodium of red blood cells in sickle cell anemia. J Clin Invest 31 (4):406-411.
307. Tosteson DC (1955) The effects of sickling on ion transport. II. The effect of sickling on sodium and cesium transport. J Gen Physiol 39 (1):55-67.
308. Tosteson DC, Carlsen E, Dunham ET (1955) The effects of sickling on ion transport. I. Effect of sickling on potassium transport. J Gen Physiol 39 (1):31-53.
309. Palek J (1977) Red cell membrane injury in sickle cell anaemia. Br J Haematol 35 (1):1-9.
310. Bookchin RM, Ortiz OE, Lew VL (1991) Evidence for a direct reticulocyte origin of dense red cells in sickle cell anemia. J Clin Invest 87 (1):113-124.
311. Ortiz OE, Lew VL, Bookchin RM (1990) Deoxygenation permeabilizes sickle cell anaemia red cells to magnesium and reverses its gradient in the dense cells. J Physiol 427:211-226.
312. Noguchi K, Ishii S, Shimizu T (2003) Identification of p2y9/GPR23 as a novel G protein-coupled receptor for lysophosphatidic acid, structurally distant from the Edg family. J Biol Chem 278 (28):25600-25606.
313. Yanagida K, Ishii S, Hamano F, Noguchi K, Shimizu T (2007) LPA4/p2y9/GPR23 mediates rho-dependent morphological changes in a rat neuronal cell line. J Biol Chem 282 (8):5814-5824.
314. Abbracchio MP, Burnstock G, Boeynaems JM, Barnard EA, Boyer JL, Kennedy C, Knight GE, Fumagalli M, Gachet C, Jacobson KA, Weisman GA (2006) International Union of Pharmacology LVIII: update on the P2Y G protein-coupled nucleotide receptors: from molecular mechanisms and pathophysiology to therapy. Pharmacol Rev 58 (3):281-341.
315. Auth T, Safran SA, Gov NS (2007) Fluctuations of coupled fluid and solid membranes with application to red blood cells. Physical review. E, Statistical, nonlinear, and soft matter physics 76 (5 Pt 1):051910.
316. Manno S, Takakuwa Y, Mohandas N (2002) Identification of a functional role for lipid asymmetry in biological membranes: Phosphatidylserine-skeletal protein interactions modulate membrane stability. Proc Natl Acad Sci U S A 99 (4):1943-1948.
317. Betz T, Lenz M, Joanny JF, Sykes C (2009) ATP-dependent mechanics of red blood cells. Proc Natl Acad Sci U S A 106 (36):15320-15325.

6. Publications

During PhD

- **Jue Wang,** Lisa Wagner-Britz, Anna Bogdanova, Kathrina Wiesen, Qinghai Tian, Ingolf Bernhardt, Peter Lipp, Stephan E. Philipp and Lars Kaestner. Morphologically homogeneous red blood cells present a heterogeneous response tohormonal stimulation. *PLoS ONE.* 2013 8(6): e67697. doi:10.1371/journal.pone.0067697.
- Lisa Wagner-Britz[*], **Jue Wang**[*], Lars Kaestner, Ingolf Bernhardt. Protein kinase Cα and P-type Ca^{2+} channel Cav2.1 in red blood cell calcium signalling. *Cellular Physiology and Biochemistry*. 2013 Jun 12;31(6):883-891. ([*] **Equal contribution)**
- Asya Makhro, Pascal Hanggi, Jeroen Goede, **Jue Wang**, Andrea Brüggemann, Max Gassmann, Lars Kaestner, Oliver Speer, Anna Bogdanova. N-methyl D-aspartate (NMDA) receptors in erythroid precursor cells and in circulating human red blood cells contribute to the regulation of intracellular calcium levels. Articles in Press. *Am J Physiol Cell Physiol* (September 18, 2013). doi:10.1152/ajpcell.00031.2013.
- Giampaolo Minetti, Stephane Egeé, Daniel Mörsdorf, Patrick Steffen, Asya Makhro, Cesare Achilli, Annarita Ciana, **Jue Wang**, Guillaume Bouyer, Ingolf Bernhardt, Christian Wagner, Serge Thomas, Anna Bogdanova, Lars Kaestner. Red cell investigations: Art and artefacts. *Blood review*. 2013 Mar;27(2):91-101. Epub 2013 Feb 18.
- Anna Bogdanova, Asya Makhro, **Jue Wang**, Peter Lipp and Lars Kaestner.Calcium in red blood cells - a perilous balance. *Int. J. Mol. Sci.* 2013, *14*(5), 9848-9872
- Lars Kaestner, Patrick Steffen, Duc Bach Nguyen, **Jue Wang**, Lisa Wagner-Britz, Achim Jung, Christian Wagner, Ingolf Bernhardt. Lysophosphatidic acid induced red blood cell aggregation in vitro. *Bioelectrochemistry*. 2012 Oct;87:89-95. Epub 2011 Aug 17.

- Makhro A, **Wang J,** Vogel J, Boldyrev AA, Gassmann M, Kaestner L, Bogdanova A. Functional NMDA receptors in rat erythrocytes. *Am J Physiol Cell Physiol*. 2010 Jun;298(6):C1315-25. Epub 2010 Mar 24.
- Peter Lipp, Martin Oberhofer, Qinghai Tian, **Jue Wang**, Karin Hammer, Jan Reil, Hans-Ruprecht Neuberger, Lars Kaestner. Remodelling of Calcium Handling, Ion Currents and Contraction in Rac1 Overexpressing Mouse Ventricle. *Biophysical Journal.* 01/2010; 98(3). DOI:10.1016/j.bpj.2009.12.2981
- Peter Lipp, Martin Oberhofer, Qinghai Tian, **Jue Wang**, Karin Hammer, Jan Reil, Hans-Ruprecht Neuberger, Lars Kaestner. Rac1-Induced Remodelling is Different in the Left and Right Atrium of RacET Mice. *Biophysical Journal.* 01/2010; 98(3). DOI:10.1016/j.bpj.2009.12.2983

Submitted paper

- **Jue Wang,** Kai van Bentum, Urban Sester, Lars Kaestner. Calcium homeostasis in red blood cells of dialysis patients in dependence of erythropoietin treatment. Submitted to Frontiers in Physiology.

Before PhD

- **Wang J** and Xie X. Development of a quantitative, cell-based, high-content screening assay for epidermal growth factor receptor modulators. *Acta Pharmacol Sin.* 2007 Oct;28(10):1698-704
- Xing He, Liyan Fang, **Jue Wang**, Yanghua Yi, Shuyu Zhang, Xin Xie. Bryostatin-5 blocks SDF-1 induced chemotaxis via desensitization and down-regulation of cell surface CXCR4 receptors. *Cancer Research*. 2008 Nov 1;68(21):8678-86.
- Meng T, **Wang J**, Peng H, Fang G, Li M, Xiong B, Xie X, Zhang Y, Wang X, Shen J. Discovery of benzhydrylpiperazine derivatives as CB1 receptor inverse agonists via privileged structure-based approach. *Eur J Med Chem*. 2010 Mar;45(3):1133-9. Epub 2009 Dec 16.

7. Acknowledgment

First of all, I would like to express my special gratitude to my supervisor Prof. Dr. Peter Lipp for giving me the precious opportunity to be a PhD candidate in his institute. He not only provided excellent scientific facilities and friendly working conditions, but also gave me inestimable proposals and advices for all the projects, which helped me a lot. Furthermore, he also helped me very much in my daily life.

Then I would like to thank my tutor Dr. Lars Kaestner for planning experiments, maintaining instruments and assisting in paper writing. He was patient in teaching me experimental techniques, kindly supported me, gave me constructive suggestions and critics, and was always available for questions and discussions. Without his help, I could not finish the project.

I am grateful to Dr. Martin Oberhofer, Dr. Sandra Ruppenthal and Dr. Anke Scholz for their help in experiments and daily life.

I am also thankful to Ms Kathrina Wiesen, Ms Elisabeth Kaise, Ms Laura Schröder and Ms Sabrina Hennig for their help in the animal experiments. Thanks to Ms Tanja Kuhn, Mr Xin Hui, Dr. Sara Pahlavan, Mr Benjamin Sauer, Dr. Oliver Müller, Dr. Qinghai Tian, and Ms Anne Veceredea-we had very good cooperation experiences with each other.

I would like to thank our secretary, Ms Karin Schumacher. She helped me so much with my daily life, which ensured me to concentrate on scientific research.

I am also grateful to Prof. Marc Freichel and Prof. Veit Flockerzi for providing TRP knock out mice and useful suggestions.

Now I would like to present my sincere gratitude to those people mentioned above. I would also like to present my appreciation for those people who had helped me but not listed here.

Finally, I would like to give my deep thanks to my wife, Mao Li, for her understanding, for her love and for her support. I also have to be deeply grateful to my parents and my family members who despite the distance gave me their unconditional support and love through these years.

Thank you all!

8. Curriculum Vitae

Personal Information

- Gender:Male
- Nationality: People's Republic of China
- Date of Birth: October 10th, 1981
- Major: Biology
- Mailing Address: Institute for molecular cell biology, Building 61, Saarland university, D-66421 Homburg/Saar, Germany
- Email: anjwan@googlemail.com
- Phone: 49 0176 45174184

Education

- **Oct. 2008-Present: Institute for molecular cell biology, Saarland university, Ph.D.**
- **Sep. 2004-Jun. 2007: The National Center for Drug Screening, Shanghai Institute of Materia Medica, Chinese Academy of Sciences, M.S.**
  - Biochemistry,Cell Biology, Molecular Biology, Pharmacology
- **Sep. 1999-Jun. 2003: College of Life Science, Hunan Normal University, B.A.**
  - Biochemistry,Cell Biology, Molecular Biology, Immunology, Cell Engineering, Molecular Genetics

Research Experience

- **Oct. 2008-Present: Ph.D.**
  - Research work on transient receptor potential (TRP) channel on erythrocytes and sickle cell disease.
  - Research work on N-methyl-d-aspartate (NMDA) receptors on erythrocytes.
  - Research work on human erythrocytes aggregation during blood transfusion.

- **Jul. 2007-Aug. 2008: ResearchAssistant**
  - Worked with Dr. Xie Xin at the National Center for Drug Screening.
  - Research work on cannabinoid Recptor 1 and 2. Successful screening out a novel cannabinoid recptor 1 antagonistsand animal test for further research. Systemic development of a whole cell binding assay for GPCR.
  - Research work on interaction between glucagon receptor and beta-Arrestins.
  - Research work on metabotropic glutamate receptors 2 and 3.
- **Sep.2004-Jun.2007: Master Student**
  - Research work on epidermal growth factor receptor. Systemic development of a quantitative cell-based high-content screening assay (receptor internalization assay) for epidermal growth factor receptor modulators.
  - Research work on glucagon like peptide receptor. Development of a report gene assay for glucagon like peptide-1 receptor agonist.
- **Mar.2003-Jun.2003: Lab Assistant**
  - In department of biochemistry and molecule biology, College of Life Science, Hunan Normal University
- **Jun.2002-Dec.2002:Lab Assistant**
  - In department of microbiology, College of Life Science, Hunan Normal University
  - Successful separation ofa new kind of lactobacillus and measurement of its activation

9. Attachments

A compact disk containing publications and programs mentioned in this thesis is attached.

Publication list:

1. Plos One 2013 (LPA paper) .pdf
2. Cell Physiol Biochem 2013 (PKC paper) .pdf
3. Am J Physiol Cell Physiol 2013 (NMDA paper) .pdf
4. Blood Reviews 2013.pdf
5. Int. J. Mol. Sci 2013.pdf
6. Bioelectrochemistry 2011 (LPA and Aggregation paper) .pdf
7. Am J Physiol Cell Physiol 2010 (NMDA paper) .pdf
8. Biophysical Journal.pdf
9. Biophysical Journal 2.pdf

Program/Macro list:

1. Import Raw Data.txt (Need ImageJ 1.44o or above)
2. Z projection.txt (Need ImageJ 1.44o or above)
3. PKH26 analysis.txt (Need ImageJ 1.44o or above)
4. Single cell analysis.ipf (Need Igor Pro 6.0 or above)
5. Waves Average.ipf (Need Igor Pro 6.0 or above)
6. Analysis.bas (Need Excel: Mac 2011 or above)